



<https://theses.gla.ac.uk/>

Theses Digitisation:

<https://www.gla.ac.uk/myglasgow/research/enlighten/theses/digitisation/>

This is a digitised version of the original print thesis.

Copyright and moral rights for this work are retained by the author

A copy can be downloaded for personal non-commercial research or study,  
without prior permission or charge

This work cannot be reproduced or quoted extensively from without first  
obtaining permission in writing from the author

The content must not be changed in any way or sold commercially in any  
format or medium without the formal permission of the author

When referring to this work, full bibliographic details including the author,  
title, awarding institution and date of the thesis must be given

Enlighten: Theses

<https://theses.gla.ac.uk/>  
[research-enlighten@glasgow.ac.uk](mailto:research-enlighten@glasgow.ac.uk)

THE INFLUENCE OF THE SUPPORT ON THE BEHAVIOUR OF SUPPORTED  
METAL CATALYSTS IN HYDROCARBON HYDROGENATION REACTIONS

Being a Thesis

Submitted for the Degree

of

MASTER OF SCIENCE (RESEARCH)

of the

UNIVERSITY OF GLASGOW

By

BELKACEM BOUMARAFI, D.E.S.

September, 1986

ProQuest Number: 10991870

All rights reserved

INFORMATION TO ALL USERS

The quality of this reproduction is dependent upon the quality of the copy submitted.

In the unlikely event that the author did not send a complete manuscript and there are missing pages, these will be noted. Also, if material had to be removed, a note will indicate the deletion.



ProQuest 10991870

Published by ProQuest LLC (2018). Copyright of the Dissertation is held by the Author.

All rights reserved.

This work is protected against unauthorized copying under Title 17, United States Code  
Microform Edition © ProQuest LLC.

ProQuest LLC.  
789 East Eisenhower Parkway  
P.O. Box 1346  
Ann Arbor, MI 48106 – 1346

*To my parents*

## ACKNOWLEDGEMENTS

My special gratitude goes to my supervisor, Dr. G. Webb, who encouraged me and gave me all the support during the research and all the assistance I could ask for and urged me to finish this dissertation.

I am deeply grateful to Mr. T. Boyle for all his help in the maintenance of the equipment in the Surface Chemistry laboratory at Glasgow University and to the staff of the Glassblowing Workshop for their help.

I should also like to thank my colleagues in the Surface Chemistry Group for their helpful comments.

Special thanks and appreciation go to the Algerian Government and the Ministry of High Education for the financial support.

Finally, I would like to thank Miss Betty Forbes for her patience and excellent work in the typing of this thesis.

## Summary

Platinum and rhodium metal catalysts supported on a transition metal oxide titania, and on the non-transition metal oxides alumina and silica have been used to determine the possible effects of Metal-Support Interactions on metal surface areas and the catalytic hydrogenation of buta-1:3-diene.

The adsorption of [ $^{14}\text{C}$ ]carbon monoxide on platinum and rhodium metal surfaces has been used to determine the metal surface area for each catalyst. The results of these determinations have shown that metal-support interactions are extant, particularly in the platinum and rhodium supported on titania catalysts, as revealed by a decrease in metal area following high-temperature reduction in hydrogen.

Temperature-programmed reduction, has been used and the shapes of the reduction profiles determined for each catalyst. Comparisons have been made between platinum and rhodium supported on various oxides with regard to the structure of the reduction profiles, which vary from support to support particularly with regard to the temperature at which the main peak in the profile occurs.

The hydrogenation of buta-1:3-diene over these catalysts has been found to occur in two distinct stages. In the first stage of the reaction buta-1:3-diene was predominantly hydrogenated to n-butenes, together with small amounts of n-butane, whilst in the second stage which was accompanied by an increase in rate, the n-butenes were further

hydrogenated to n-butane. All three isomeric n-butenes are observed as initial products, but-1-ene being the major product over each catalyst and cis-but-2-ene being only a minor product. The selectivities for butene formation are relatively high over all catalysts studied.

The variation of reduction temperatures of the catalysts, which causes a variation in surface area does not affect either the initial butene distributions or selectivities over any of the catalysts. Each catalyst underwent a change in activity with usage. With the platinum catalysts this was of the form of a straight deactivation to a steady state activity. However, with the rhodium catalysts the activity at first increased with usage passing through a maximum before following a normal deactivation curve to a steady state activity.

Activation energies were determined for each catalyst. With most catalysts the variation of reduction temperatures did not affect the activation energy values except with Pt on  $TiO_2$ , which gave a significantly higher value of activation energies when reduced at high temperature, suggesting the possibility that, in this case, metal-support interactions may have some effect on the activation energy.

## CONTENTS

	Page
Acknowledgements	i
Summary	ii
<u>CHAPTER ONE : INTRODUCTION</u>	1
1.1. Metal Support Interactions	1
1.2 The Hydrogenation of Buta-1:3-diene	15
<u>CHAPTER TWO : OBJECTIVES OF THE PRESENT WORK</u>	27
<u>CHAPTER THREE : EXPERIMENTAL</u>	28
3.1 The Preparation of Catalysts	28
3.2 Materials	28
3.2.1 Hydrogen	28
3.2.2 Carbon Monoxide	28
3.2.3 Radioactive Carbon Monoxide	29
3.2.4 Buta-1:3-diene	29
3.3. Apparatus	29
3.3.1 Carbon Monoxide Chemisorption	29
3.3.1.1 The Adsorption System	29
3.3.1.2 Experimental Procedure	30
3.3.1.3 Determination of Plateau of Geiger-Müller Counter	32
3.3.2 Buta-1:3-diene Hydrogenation	33
3.3.2.1 The Vacuum System	33
3.3.2.2 Experimental Procedure	34
3.3.3. The Gas Chromatography System	35
3.3.3.1 The Apparatus	35
3.3.3.2 Procedure for the Gas Chromatographic Analysis	36
3.3.4 Temperature Programmed Reduction Profiles	37
3.3.4.1 Apparatus	37
3.3.4.2 Experimental Procedure	38

CHAPTER FOUR : RESULTS

4.1	Temperature Programmed Reduction Profiles	40
4.2	[14-C]Carbon Monoxide Chemisorption and Desorption	43
4.2.1	Calculation Method of Metal Surface Area	43
4.2.2	[14-C]Carbon Monoxide Chemisorption and Desorption Results	46
4.3	Buta-1:3-diene Hydrogenation	51
4.3.1	The Reaction of Buta-1:3-diene with Hydrogen over 5% of Pt on SiO <sub>2</sub>	53
4.3.2	The Reaction of Buta-1:3-diene with Hydrogen over 5% of Pt on Al <sub>2</sub> O <sub>3</sub>	55
4.3.3	The Reaction of Buta-1:3-diene with Hydrogen over 5% of Pt on TiO <sub>2</sub>	57
4.3.4	The Reaction of Buta-1:3-diene with Hydrogen over 5% of Rh on SiO <sub>2</sub>	59
4.3.5	The Reaction of Buta-1:3-diene with Hydrogen over 5% of Rh on Al <sub>2</sub> O <sub>3</sub>	61
4.3.6	The Reaction of Buta-1:3-diene with Hydrogen over 5% of Rh on TiO <sub>2</sub>	63
4.4	Electron Microscopic Examination of Catalysts	65

CHAPTER FIVE : DISCUSSION

5.1	Temperature Programmed Reduction Profiles	66
5.2	Determination of the Surface Metal Area	68
5.3	Effects of the Support on the Behaviour of the Metal Catalysts in the Hydrogenation of Buta-1:3-diene	74
5.4	General Conclusions	82
	References	83

## CHAPTER 1

## CHAPTER 1.

### INTRODUCTION

#### 1.1 Metal Support Interactions

For many years, the context of the supported metal catalysts were as catalysts which contained one or more components other than metal. The majority of supported metal catalysts are of interest because they are employed in the petroleum and the chemical industry. The metal is supported on a carrier, which itself is catalytically inactive and which undergoes little or no chemical interaction with the metal. Bond and Burch (1) have considered the role of the support and concluded that in many cases, it has generally been considered to act simply as an inert carrier of the active component, the metal. Probably the most important practical type of catalyst is one in which the metal is supported on an inert material such as silica or alumina.

Generally, it has previously been thought that there is no chemical carrier-metal interaction. However, there is a growing body of evidence which suggests that this view may be incorrect (2). In the recent literature on supported metal catalysts, when the catalytic metals are supported on certain oxides, the support exerts a major influence on the behaviour of the metal as revealed by the size distribution of the metallic particles, metal surface areas, based on selective gas chemisorption measurements, and their

behaviour in catalytic reactions.

In such catalyts the metal exists as very small crystallites dispersed on the surface of carriers, which for convenience have been classified in terms of their porosity. For example refractory oxides, such as alumina or silica are porous whereas transition metal oxides, such as titania or zinc oxide, are generally non-porous. In the supported form, the metal is more resistant to sintering than an unsupported metal and has a high surface area i.e.  $> 1\text{m}^2 \text{g}^{-1}$  (2).

The disadvantage of supported catalysts is that they often exhibit variable activity, which affects the determination of kinetics and activation energies and, in consequence, different observations may be due to method and condition of preparation of the catalyst. However, some observations reported in the literature have suggested that certain variations in catalytic activity may be correlated with the nature of the support (1).

Sinfelt (3) reviewed some considerations of the nature of supported metal catalysts, such as methods of preparation, size of the metal crystallites and the determination of surface areas. For the catalyst preparation, a simple impregnation method was preferred from the other distinct methods (deposition, co-precipitation) and impregnation is probably the most common method. A variety of physical methods, such as electron microscopy, X-ray diffraction line broadening and low-angle X-ray scattering can be employed in the determination of size of the metal crystallites. An

important feature in studies of supported metal catalysts is the determination of the surface area of the catalysts. The most effective method of obtaining metal surface areas is by gas chemisorption. In this method, it is necessary to choose a gas which adsorbs selectively on the metal rather than on the support. The selective gas chemisorption of hydrogen or carbon monoxide has been used by many investigators (20,21, 22).

Certain support effects have been observed by Briggs et al. (4) in studies of ethene-deuteration using platinum supported on either titania or magnesia. These have shown that there is an interaction between titania or magnesia with platinum and this causes a reduction in the strength of ethene adsorption on platinum. These studies also included various other supports, such as alumina or silica, which behave as relatively inert supports and, as a result, the adsorption of ethene over platinum supported on alumina or on silica was deduced to be relatively strong.

Solymosi (5) suggested that the carrier effect was not fully understood. He suggested that the effect of the support is to stabilise the state of the active metal or to increase the degree of dispersion and, in consequence, the surface area of the catalyst.

The same author also suggested that a chemical interaction between the metal and the support, which may play an important role in producing the carrier effect, could be interpreted by considering the possibility of an electronic

interaction at the metal-support interface.

An investigation of formic acid decomposition has been reported by Solymosi (5) in his studies of a possible role of the electronic interaction at the metal-support interface. Over nickel supported on either aluminium oxide or titanium oxide, the author noticed that the activation energy for formic acid decomposition varied with the electrical conductivity and depended on the extent of doping of the support. He deduced that this change in activation energy for formic acid decomposition was a result of electronic interactions between the metal catalyst and the support.

Schwab (6) considered two kinds of influence of a carrier on the catalyst activity; a structural promotion and a synergetic promotion. The former can stabilise a high surface area of the metal catalyst, but does not alter the activation energy. The second, in which the support interacts energetically with the catalyst, is characterised by an increased reaction rate, accompanied by a decreased activation energy compared with the unsupported catalyst.

The investigation of support effects has shown that, with rhodium supported on either silica, alumina or titania catalysts (7), the nature of the support material is quite important in determining their behaviour in carbon monoxide chemisorption. Silica and titania supports provide more of the carbon monoxide species characteristic of reduction of a rhodium precursor material to rhodium metal, but rhodium on alumina catalysts appears to contain some Rh(I) sites.

Electron paramagnetic resonance (EPR) techniques have been used by Katzer et al. (8) to determine the effect of the support on the formation of such species. They suggested that the formation of the paramagnetic platinum centres involves a specific interaction with the surface of the alumina and the type of the interaction was a result of contact with a Lewis acid centre on the surface of the calcined alumina which could occur;



They concluded that the EPR signal observed for reduced Pt/Al<sub>2</sub>O<sub>3</sub> is due to a direct involvement of platinum with the alumina.

It has been suggested that the involvement of the support activity in a catalytic reaction could appear as a metal-support interaction, which may arise through the operation of specific particle size effects or the operation of bifunctional catalysis (1). The specific particle size effects were considered to be of most importance with small metal particle, highly dispersed.

By using Transmission Electron Microscopic (TEM) techniques, Yacaman (9) showed that the relative number of icosahedral non-face-centred cubic and face-centred cubic cubo-octahedral particles change with metal content.

The bifunctional catalysis has been considered in recent literature regarding petroleum reforming reactions, although the component providing the acidic function should be

regarded as a second active phase, as well as a support.

Solymosi et al. (10,11) have studied the hydrogenation of carbon dioxide on supported rhodium catalysts. It has been suggested that the important steps in methane formation are the dissociation of carbon dioxide promoted by adsorbed hydrogen, the subsequent dissociation of carbon monoxide into carbon followed by carbon hydrogenation. In their view the methanation selectivity observed in the hydrogenation of carbon dioxide was considered to be higher than in the case of the hydrogenation of carbon monoxide. The variation of the supports can also influence the specific methanation activity of the rhodium catalyst, as titania gives rise to much greater effects than alumina or silica. The effect of the support can be attributed to different extents of electronic interaction between the rhodium and the support, which can thereby influence the bonding and the reactivity of the chemisorbed species.

An important feature in studies of most metals on most supports is the size of the metal particles. Application of a number of physical methods including X-ray diffraction and Transmission Electron Microscopy (TEM) has resulted in the acquisition of more extensive data regarding particle size distributions (1). At the present time, transmission electron microscopy is the most predominantly used technique to give information on both the particle morphology and particle size. Some metal particles are smaller than about 2.5 nm and show very low contrast, in fact the particles are very thin (12).

In an investigation of hydrogen and carbon monoxide chemisorption on platinum supported on various titania powders, Baker et al. (13) observed that, after reduction in hydrogen at high temperature (875K), the reduced catalyst did not adsorb either hydrogen or carbon monoxide. This suppression of the hydrogen and carbon monoxide chemisorption was considered to be evidence for a metal-support interaction. The same catalyst was examined by Transmission Electron Microscopy (TEM) and this analysis showed that the  $\text{TiO}_2$  support was reduced to  $\text{Ti}_4\text{O}_7$ . The authors concluded that the reduction of  $\text{TiO}_2$  to  $\text{Ti}_4\text{O}_7$  was catalysed by platinum and the metal particles of platinum were predominantly hexagonal and thin, indicating a pillbox structure. Den Otter and Dautzenberg (14) examined platinum on alumina after high temperature reduction (>700K) in hydrogen. They observed that the capacity for hydrogen chemisorption was decreased, but metal particles of platinum were still present in a highly dispersed state. The authors suggested that the decrease of hydrogen chemisorption may be a consequence of the catalyst being poisoned by contaminants originating from the support. The available literature (15) indicates that the method of catalyst preparation, drying and temperature of calcination, including the choice of metallic salt and the choice of support can affect the oxidation state of the dispersed metal.

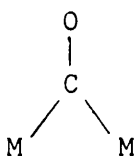
Temperature-programmed reduction (TPR) techniques offer the possibility of determining the oxidation state of the

catalyst. Robertson et al. (16) have examined copper, nickel, and copper-nickel supported on silica catalysts, using temperature-programmed reduction techniques and observed that the method of catalyst drying and temperature of calcination may affect the oxidation state of the catalysts. The reducibility of nickel oxide supported on silica was such that it was difficult to reduce to zero-valent state, this could be because of a nickel oxide on silica interaction; copper oxide on silica was more easily reduced to zero-valent state and, in this case, it was concluded that the support appeared to act simply as a dispersing agent. An assessment of the use of temperature-programmed reduction of dried and non-calcined silica-supported bimetallic catalysts proved to be very difficult, although the absence of a high temperature reduction peak was taken as an indication that both metals had been reduced to the zero-valent state.

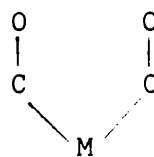
In order to obtain detailed information regarding the areas of Group VIII metals dispersed on various support materials, it is necessary to have a detailed knowledge of the nature of the adsorbed states of carbon monoxide on the various metallic substrates. Three types of adsorbed carbon monoxide on metals have been identified (20):-



I



II



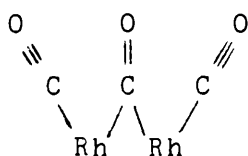
III

where the linear form (I) predominates with copper, iron and platinum. The bridge form (II) is most important with nickel and palladium, whilst with rhodium all three forms can be observed.

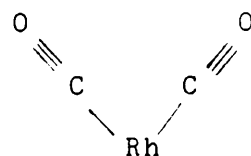
The adsorption of carbon monoxide on supported Group VIII metals has been extensively studied by infrared spectroscopy and has been the subject of many investigations (17,18,19). Carbon monoxide chemisorption on rhodium supported on alumina has been studied by Yang and Garland (18), who proposed three types of surface species, consisting of a linear species (A) with one carbon monoxide resident on one rhodium atom, giving rise to a band at  $2050\text{ cm}^{-1}$ ; a bridged species (B) consisting of a carbon monoxide bonded to two rhodium atoms with an observed band at  $1925\text{ cm}^{-1}$ , with each of the two rhodium atoms being bonded to a single "linear" carbon monoxide; and two linear carbon monoxide molecules bonded to a single rhodium atom species (C) giving rise to bands observed at  $2027$  and  $2095\text{ cm}^{-1}$ .



Species (A)



Species (B)



Species (C)

Sinfelt et al. (23) reported that the adsorption of carbon monoxide on rhodium metal supported on silica can give rise to two different forms of adsorbed species, a linear structure (A) and a bridged structure (B). In the

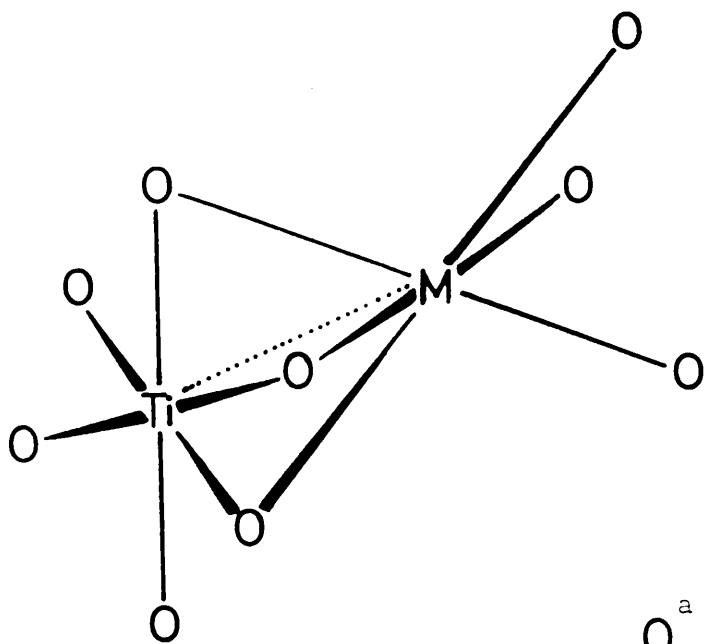
case of the linear structure, each adsorbed carbon monoxide molecule is attached to one metal atom at the surface, whereas with the bridged structure, each adsorbed molecule is considered to be attached to two surface metal atoms. Eischens and Pliskin (21) showed that the species adsorbed in the linear form gives rise to bands above  $2000\text{ cm}^{-1}$ , whilst the bridged form gives bands below  $2000\text{ cm}^{-1}$ . Recent studies by Blyholder (22) have suggested that, when both linear and bridged sites are available, bridged sites are likely to be more stable for the bonding of carbon monoxide to a nickel surface.

The adsorption of carbon monoxide on platinum supported on alumina or on silica has been investigated by Bain et al. (24), using a [ $^{14}\text{C}$ ]carbon monoxide radiotracer method. The results of this study were interpreted in terms of the existence of two adsorbed states of carbon monoxide on each of the catalysts. It was further suggested that the weakly bound species corresponded to linearly bound carbon monoxide, whilst the strongly bound species was adsorbed as a bridged species.

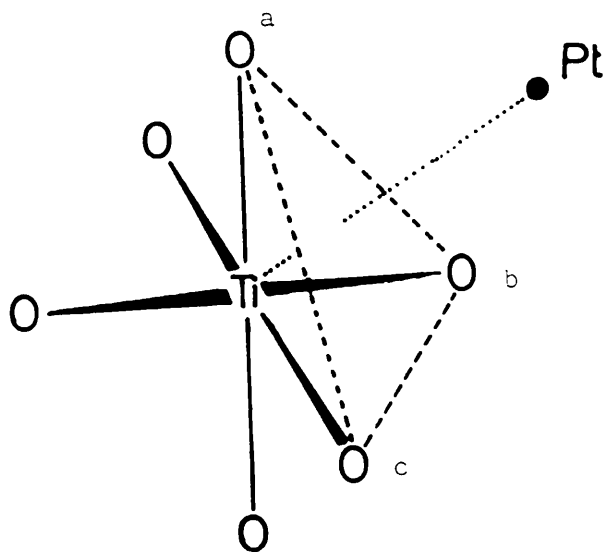
In the last few years considerable effort has been directed towards finding an explanation of the interaction between Group VIII metals and titanium dioxide. This kind of interaction has been termed Strong Metal-Support Interaction (SMSI), as first used by the Exxon group (25). The origins of SMSI effects are still the subject of considerable debate.

There are essentially three types of explanation

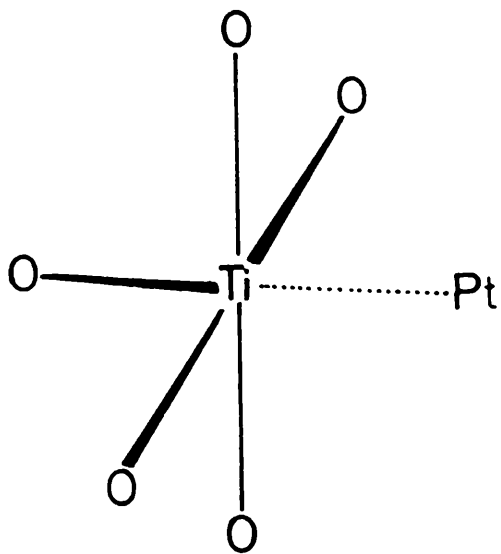
suggested in the literature to define the origins of these Strong Metal-Support Interactions. First, an explanation given by Tauster et al. (26), who considered that the origin of the strong metal-support interactions could be established by consideration of two known classes of compounds. One is the so-called hexagonal barium titanates (27) whose molecular structure is  $\text{Ba}(\text{MTi})\text{O}_3$ , where M is a metal, which can be  $\text{Ti}^{3+}$ , V, Cr, Mn, Fe, Co, Ru, Rh, Ir and Pt, and whose phases probably have a composition close to  $\text{BaM}_{\frac{1}{3}}\text{T}_{\frac{2}{3}}\text{O}_{3-x}$  being, in some cases, oxygen-deficient ( $x \neq 0$  corresponds to divalency or trivalency of the donor cationic metal M). It was suggested that one out of every two titanium ions present is directly bonded to the donor metal cation (M) (see Model A). The bonding connecting adjacent  $\text{TiO}_6$  and  $\text{MO}_6$  octahedra takes place through their shared face. If this suggestion is correct, a platinum atom on a titania surface could show a similar ability to form direct metal-metal bonds through one face of a molecular  $\text{TiO}_6$  octahedron. However, Horsley (28) described a molecular cluster model for platinum supported on a titania catalyst (see Model B). The molecular cluster that is taken to represent the system consists of a simple platinum atom interacting with an octahedral  $(\text{TiO}_6)^{8-}$  cluster. The important feature of this model is that the platinum atom is outside the  $(\text{TiO}_6)^{8-}$  cluster. Its nearest neighbours are the triangle of oxygen atoms a, b, c and any interaction of the platinum atom with the titanium ion must take place across this face. The same author also proposed an alternative model (see Model C), by removing one of the



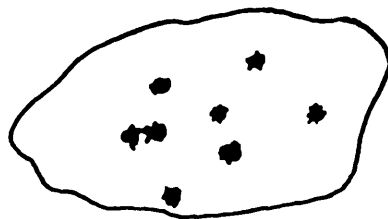
Model A



Model B



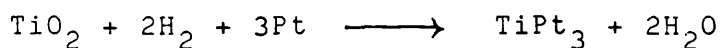
Model C



Scheme D

oxygen ions from the  $(\text{TiO}_6)^{8-}$  cluster and allowing a platinum atom to occupy the vacant site so created. The platinum atom is then close enough to the titanium ion for metal-metal bonding to occur.

A second explanation for the strong metal-support interaction involves a model in which formation of Lewis-acid-base intermetallic compounds, such as  $\text{TiPt}_3$  and  $\text{TiIr}_3$  are formed. For example,  $\text{TiPt}_3$  has been reported to form from finely ground powders of  $\text{TiO}_2$  and the noble-metal in the presence of hydrogen, but only at temperatures  $\geq 1200^\circ\text{C}$ .



Strong metal-support interaction effects have also been explained in terms of the reducibility of the support. A typical example is titania. Tauster et al. (25) discovered some years ago, that the reduction of noble-metals supported on titania at low temperatures ( $200^\circ\text{C}$ ) produced well-dispersed metals which exhibited the capacity to adsorb hydrogen and carbon monoxide. However, when reduction was carried out on the same materials at  $500^\circ\text{C}$ , hydrogen and carbon monoxide adsorption decreased to near zero. Since H/M or CO/M ratios represent the evidence for the existence of SMSI, it is important to know the range of H/M or CO/M ratios which are due to real differences in the particle size or to the suppression of hydrogen chemisorption. Some details have been obtained in studies of rhodium supported on titania which have shown large variations in the H/M or CO/M ratios may occur. In such cases the H/M and CO/M ratios represent

lower limits on the dispersions of the samples. The authors (25) observed H/M and CO/M values in excess of unity for Ir/TiO<sub>2</sub> and Rh/TiO<sub>2</sub> and for Ir/Al<sub>2</sub>O<sub>3</sub> and Ir/SiO<sub>2</sub> samples. When the reduction temperature of the same materials was increased to 500°C, a marked decrease was observed in the hydrogen and carbon monoxide uptakes, with H/M and CO/M ratios decreasing to near zero.

Ocal and Ferrer (29) used X-ray Photoelectron Spectroscopy (XPS) to investigate the state of strong metal-support interactions in platinum deposited on a titanium surface and on a thin film of titania. They observed that annealing these catalyst samples at ~500°C caused a change in the electronic structure of platinum atoms. An electron transfer between platinum and titanium atoms has been postulated to explain the observed narrowing of the Pt 4f<sub>7/2</sub> XPS line.

The third explanation of S.M.S.I. considers that the metal and the support interact to form a compound, or alternatively that there is a partial encapsulation of the metal particles by the support oxide with a consequent change in surface area and geometry of the metal surface (see Scheme D).

The effects of the strong metal-support interactions on the hydrocarbon reactions have been studied by Schepers et al. (30) over rhodium supported on either titania or silica. It has been found that the selectivity in reactions of the hydrocarbons used, such as n-hexane, neohexane (2,2-dimethylbutane) and methylcyclopentane, changes. These changes in

selectivity were concluded to arise from the effects described in the third explanation above, namely that in the strong metal-support interaction state the metal surface is covered by a blocking layer of an oxide in the form of islands.

## 1.2 The Hydrogenation of Buta-1:3-diene

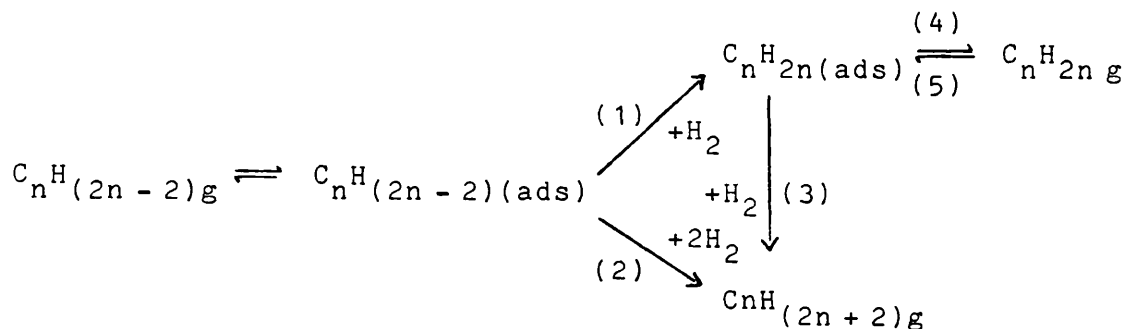
The metal-catalysed hydrogenation of multiply unsaturated hydrocarbons has been extensively reviewed by Webb (31). In general, the hydrogenation reactions of diolefins are most efficiently catalysed by the nine Group VIII metals, together with copper, gold, rhenium and tungsten. The Group VIII metals have been found to possess good hydrogenation activity; nickel, palladium and platinum have been most extensively studied (32,33).

It has been already noted (31) that one of the characteristics of catalytic hydrogenation reactions is the ability of the catalyst to encourage the formation of more than one reaction product. Thus, for example, in the hydrogenation of a diunsaturated hydrocarbon, the corresponding mono-olefin may be formed as an intermediate product along with the alkane. However, the olefin may be the major product in the initial stage of the reaction. In addition with diunsaturated olefins containing four or more carbon atoms, the mono-olefin product can be formed in more than one isomeric form.

The hydrogenation of buta-1:3-diene catalysed by the noble Group VIII metals is a good example which has been studied by Bond and Webb (34). The mono-olefin product can be expressed numerically as the yield of the mono-olefin product divided by the total product yield. This ratio is termed selectivity (S), for formation of n-butenes from buta-1:3-diene

$$\text{selectivity (S)} = \frac{\text{yield of olefin}}{\text{(yield of olefin + yield of alkane)}}$$

A general reaction scheme of diunsaturated hydrogenation may be written as follows (35):-

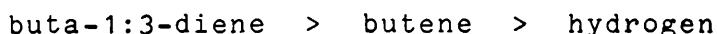


From this reaction scheme, the selectivity may be governed by two factors, a mechanistic factor and a thermodynamic factor. If the alkane is formed from the olefin, via step (3), without desorption and readsorption of olefin (step (4) and (5)), then the mechanistic factor is in operation. The thermodynamic factor arises when the strengths of adsorption of the mono-olefin and the diunsaturated olefin are different. If the latter is more strongly adsorbed, the former may be excluded from the surface and the thermodynamic selectivity will be high. Conversely, if the strengths of adsorption are approximately the same, olefin readsorption may occur and the thermodynamic selectivity will be low.

Before attempting to discuss possible reaction mechanisms, it is relevant to examine the nature of the adsorbed states. Avery (36) studied the adsorption of buta-1:3-diene on a

clean palladium-silica surface, after contacting the buta-1:3-diene with the catalyst, no infrared spectrum was observed. On addition of hydrogen, an intense infrared spectrum containing bands similar to those observed from the adsorption of straight chain mono-olefins was observed. Also, it was observed that heating to 300°C in hydrogen for a few minutes did not remove the adsorbed residues.

Phillipson et al. (32) have observed that the buta-1:3-diene is adsorbed much more strongly than hydrogen and that, in consequence, the catalytic surface is mostly covered by chemisorbed buta-1:3-diene and hydrocarbon species formed from it. Over all noble metals, except iridium and osmium, the selectivities observed in the first stage of the reaction were constant, or nearly so, until virtually all of the buta-1:3-diene had reacted, indicating that the buta-1:3-diene is more strongly adsorbed than the butenes (37). Webb (31) has considered that in hydrogenation of butene over several metals the general order with respect to hydrogen is commonly approximately unity and that for butene is zero or slightly negative. This indicates the strong adsorption of butene relative to hydrogen. The sequence for the relative strengths of adsorption may be represented as:

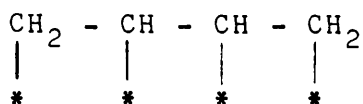


In the gas-phase hydrogenation of buta-1:3-diene over all noble metal catalysts, the selectivities for olefin formation were very pronounced; palladium is almost completely selective for olefin formation (33,41,42). For

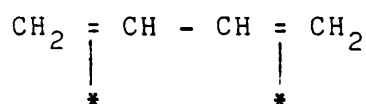
reactions carried out over these metals, the overall order of reaction, as determined from the pressure fall against time curves, was observed to be dependent upon the initial (hydrogen:buta-1:3-diene) ratio and upon the metal. The shapes <sup>of</sup> pressure fall-time curves are dependent upon the initial hydrogen:buta-1:3-diene ratio and upon the metal. With iridium and osmium, which exhibit a relatively low selectivity, the pressure fall-time curves show either an "acceleration-point" occurring very late in the reaction (iridium) or no "acceleration-point" at all (osmium) (31). Conversely, the other noble Group VIII metals, which exhibit a high selectivity for olefin formation, exhibit pressure-time curves in which the reaction is occurring in two distinct stages, the onset of the second stage being accompanied by an increase in rate (34).

One of the characteristics of the hydrogenation of buta-1:3-diene over Group VIII metal catalysts is that all three butene isomers may be formed directly from the parent hydrocarbon. It is interesting that over all alumina-supported metal catalysts, which have been studied (32,33, 38), all three isomers are formed. The reaction has also been studied in the liquid phase using nickel, palladium and platinum catalysts (39,40). Wells et al. (32,43) have observed that, with nickel or cobalt, the butene distribution depends upon the temperature of reduction of the catalyst. With both metals, supported on alumina, when reduced above  $360^{\circ}\text{C}$  (Ni) or  $440^{\circ}\text{C}$  (Co), trans-but-2-ene was the major olefinic product.

It is generally considered that, before undergoing hydrogenation, a diunsaturated hydrocarbon must be adsorbed on to the metal surface. Bond et al. (37) have considered two structures for adsorbed buta-1:3-diene.



(Structure A)



(Structure B)

Structure A has four metal-carbon  $\sigma$  bonds, and in consequence would be very strongly adsorbed. However, this structure seems unlikely, as the strain would be quite considerable.

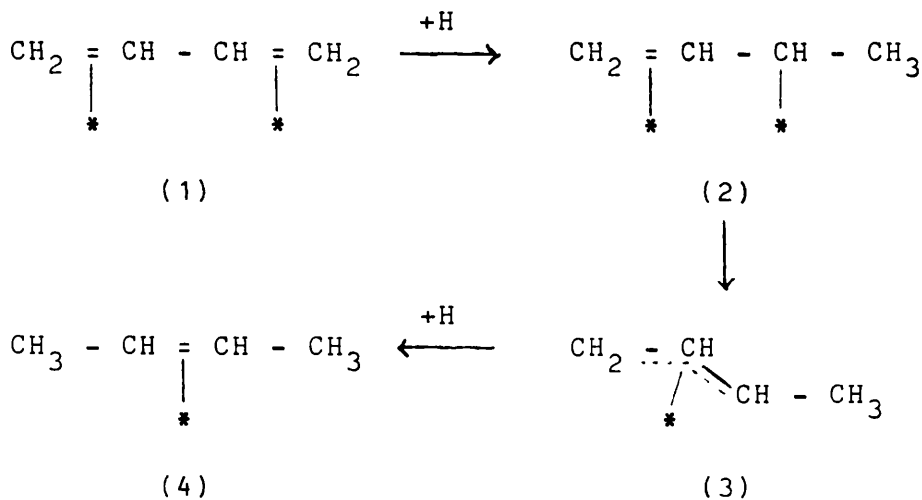
Structure B, which would also be more strongly adsorbed than a butene, assuming the latter involves one  $\pi$ -olefin-metal bond, would give an adsorbed species in which the strain would be much less than that in structure A.

Therefore, structure B can be considered as the most probable representation of the adsorbate state of buta-1:3-diene.

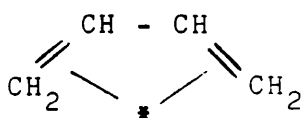
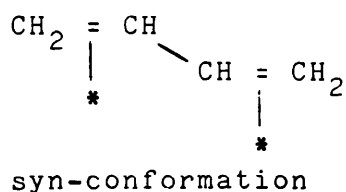
Assuming that buta-1:3-diene adsorbs as a  $\pi$ -olefin-metal, two general routes can be considered leading to the formation of but-2-ene. 1:2-addition of two hydrogen atoms to the diene as shown below, where the but-1-ene is formed directly from the adsorbed buta-1:3-diene and the but-2-ene may be produced by the subsequent isomerisation of but-1-ene with the latter first desorbing from the surface.



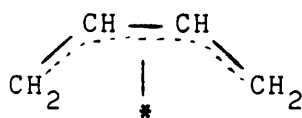
but-2-enes from adsorbed buta-1:3-diene.



In the 1:4-addition process the conformation of adsorbed  $\text{-C}_4\text{H}_7$  determines the configuration of the but-2-ene produced. The addition of the second hydrogen atom is envisaged to involve 1-methyl- $\pi$ -allylic species (3), which may represent a transition state between (2) and (4). Considering this process, the adsorbed buta-1:3-diene can be present on the surface in either of two conformations.



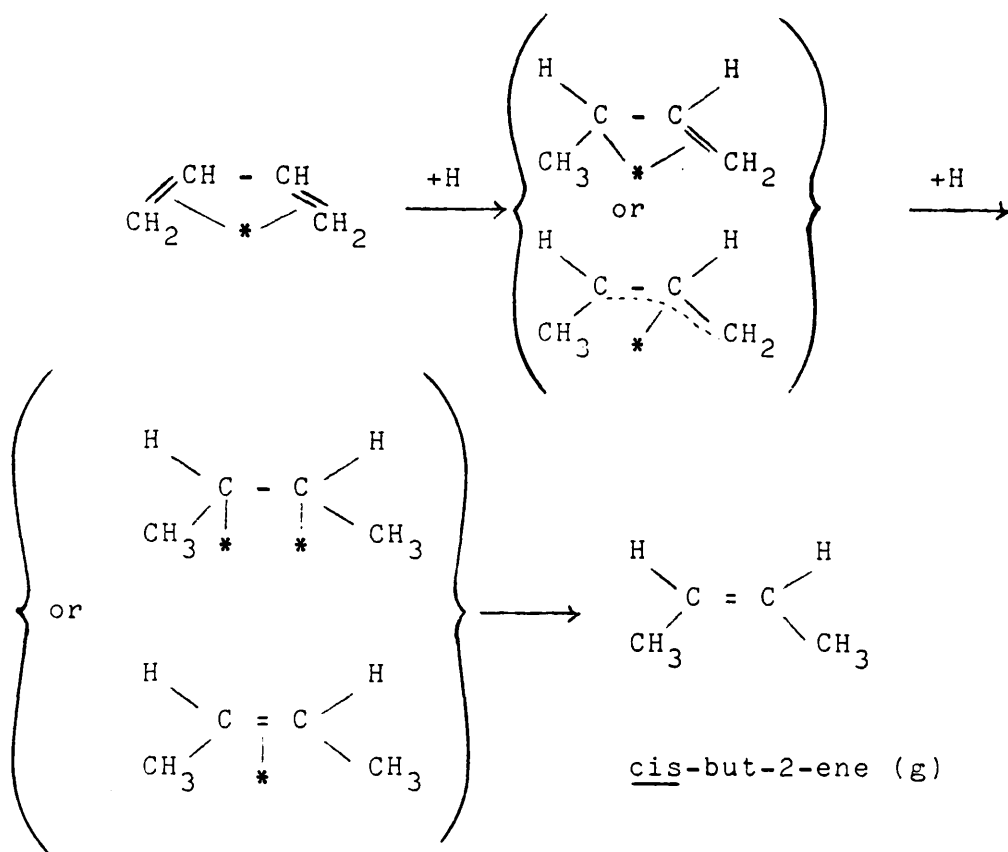
(Structure I)



(Structure II)

anti-conformation

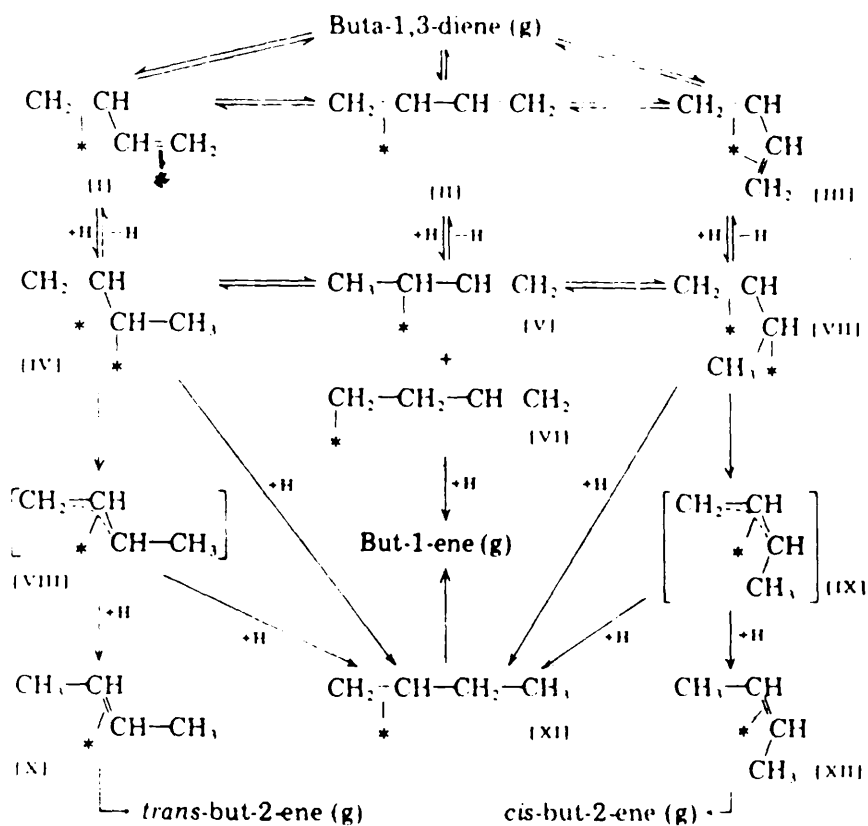




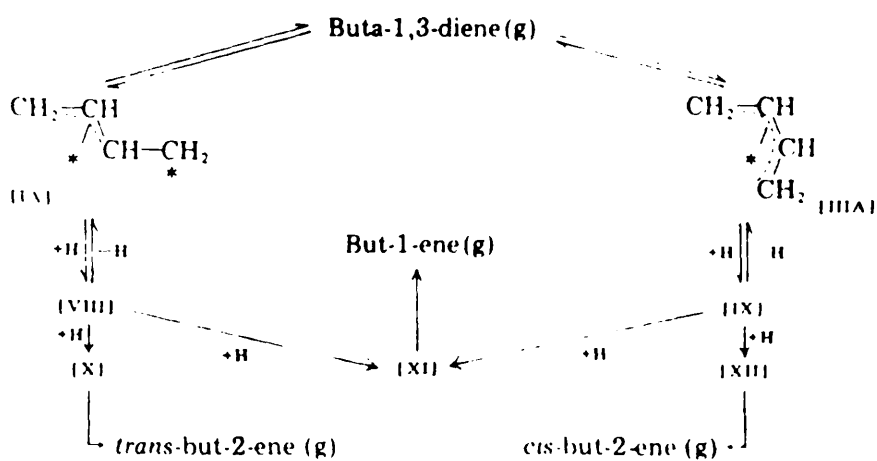
It is well established that in the gas phase, at ambient temperature, the relative proportions of the syn- and anti-conformations of buta-1:3-diene are 97% syn, 3% anti. On the assumption that these proportions of the conformers are maintained in the adsorbed state of buta-1:3-diene, it would be expected that (trans/cis) ratios in but-2-ene of around 30 would be observed, although in practice the highest (trans/cis) ratio is only  $\sim 16$ , as found with palladium catalysts.

In an attempt to rationalise the various observations made over all the nine Group VIII metals, Wells et al. (32,33) proposed the general mechanisms (A and B).

## Mechanism A



## Mechanism B



Reaction schemes for the hydrogenation of buta-1,3-diene.

According to mechanism B, which was proposed for a palladium-catalysed reaction (34), buta-1:3-diene was adsorbed in such a manner that the two conformations (1A) and (111A) are non-interconvertible, as are (VIII) and (IX), because of the nature of the metal-adsorbate bonds and the relative stabilities of the anti- and syn-conformations, as described by Webb (31). Buta-1:3-diene chemisorption as (1A) rather than as (111A) will be reflected in the high value of trans-but-2-ene:cis-but-2-ene ratio.

In general, mechanism A was proposed for metals where the trans:cis-but-2-ene ratio was around unity. Thus, for example, reactions catalysed by ruthenium, rhodium, osmium, iridium, iron and platinum as concluded from the butene distributions (32,34). This mechanism contains a variety of reversible steps. The adsorbed state of buta-1:3-diene has been considered (32) to exist as a mono- $\pi$ -bonded species (II) and as di- $\pi$ -adsorbed species, the latter of which can exist in the two conformations (I) and (III). The addition of a hydrogen atom converts chemisorbed buta-1:3-diene into the half-hydrogenated states (IV), (V), (VI) and (VII), together with a further species  $\text{CH}_2 - \text{CH}_2 - \text{CH} = \text{CH}_2$  (XIII) which is not shown in the scheme.

Each of these species may give but-1-ene after the addition of a further hydrogen atom, and this completes the 1:2-addition of two hydrogen atoms to adsorbed buta-1:3-diene process. 1:4-addition is achieved when (IV) and (VII) are converted, via the  $\pi$ -allylic species (VIII) and (IX)

respectively into trans- and cis-but-2-ene respectively by adding a further hydrogen atom. It was suggested that the relative importance of the various steps in mechanism A may be different for different metals.

CHAPTER 2

## 2. OBJECTIVES OF THE PRESENT WORK

The main objective of the work described in this thesis was to examine the effects of strong metal-support interactions on the behaviour of rhodium and platinum catalysts in the hydrogenation of buta-1:3-diene. To achieve this objective a series of platinum and rhodium catalysts supported on silica, alumina and titania have been prepared and characterised.

Catalyst characterisation of the various supported metals has been carried out using temperature-programmed reduction and, after reduction in hydrogen at either low (200°C) or high (450°C) temperature, determination of metal surface areas by [<sup>14</sup>C]carbon monoxide chemisorption.

The activity, selectivity and product distributions given by the various catalysts in the hydrogenation of buta-1:3-diene have been determined with respect to (a) the nature of the catalyst support and (b) the influence of hydrogen pretreatment of the catalysts.

## CHAPTER 3

### 3.1 The Preparation of Catalysts

#### Catalyst Supports

Three different supports were employed.

Condea  $\gamma$ -alumina ( $\text{Al}_2\text{O}_3$ ) was supplied by I.C.I. plc.

Aerosil silica ( $\text{SiO}_2$ ) was supplied by Degussa Ltd.

P-25-titania ( $\text{TiO}_2$ ) was supplied by Degussa Ltd.

#### Procedure

In each preparation, similar weights of the support were used (about 9.5g). Each support was slurried in distilled water. 5 grams chloroplatinic acid ( $\text{H}_2\text{PtCl}_6$ ) was dissolved in 100ml distilled water. The aqueous solution was stirred and was distributed to three different supports. The distribution of the aqueous solution was calculated to give 5% weight by the weight of the platinum metal on each support. The measured volumes of the chloroplatinic acid solution were added to the previously wetted supports with continuous stirring. The excess water was evaporated off and the supported salt was dried in an air oven for several hours. Each dry sample was crushed and sieved and then stored in a sample bottle until required.

### 3.2 Materials

#### 3.2.1 Hydrogen

Cylinder Hydrogen was supplied by British Oxygen Company and was used without further purification.

#### 3.2.2 Carbon Monoxide

Carbon Monoxide (Special Gas Grade) was used as supplied by British Oxygen Company.

### 3.2.3 Radioactive Carbon Monoxide

This was prepared by the reduction of  $^{14}\text{CO}_2$  with metallic zinc. The apparatus consisted of a Pyrex loop with a cold finger and B14 socket for attachment of the [ $^{14}\text{C}$ ]  $\text{CO}_2$  ampoule (figure 3.1). A portion of the loop had a furnace around it.

[ $^{14}\text{C}$ ] labelled Carbon Dioxide was supplied by the Radiochemical Centre, Amersham, with specific activity of 1 mci. It was reduced to Carbon Monoxide using metallic zinc supported on silica at a reduction temperature  $360^\circ\text{C}$  for 72 hours (44). Any unconverted carbon dioxide was frozen out before the [ $^{14}\text{C}$ ] labelled Carbon Monoxide was transferred to an evacuated storage vessel, where it was diluted to the required specific activity with non-radioactive carbon monoxide before use.

### 3.2.4 Buta-1:3-diene

Buta-1:3-diene (BDH Laboratory Chemical Ltd.) was found to contain no impurities detectable by gas chromatography and was used after degassing several times.

## 3.3 Apparatus

### 3.3.1 Carbon Monoxide Chemisorption

#### 3.3.1.1 The adsorption system

The diagram of the carbon monoxide chemisorption is shown schematically in (figure 3.2). It consisted of a conventional glass vacuum system maintained at a pressure of  $10^{-4}$  torr or better. By means of a mercury diffusion pump (P2) backed by oil rotary pump (P1). The inlet and outlet to the diffusion

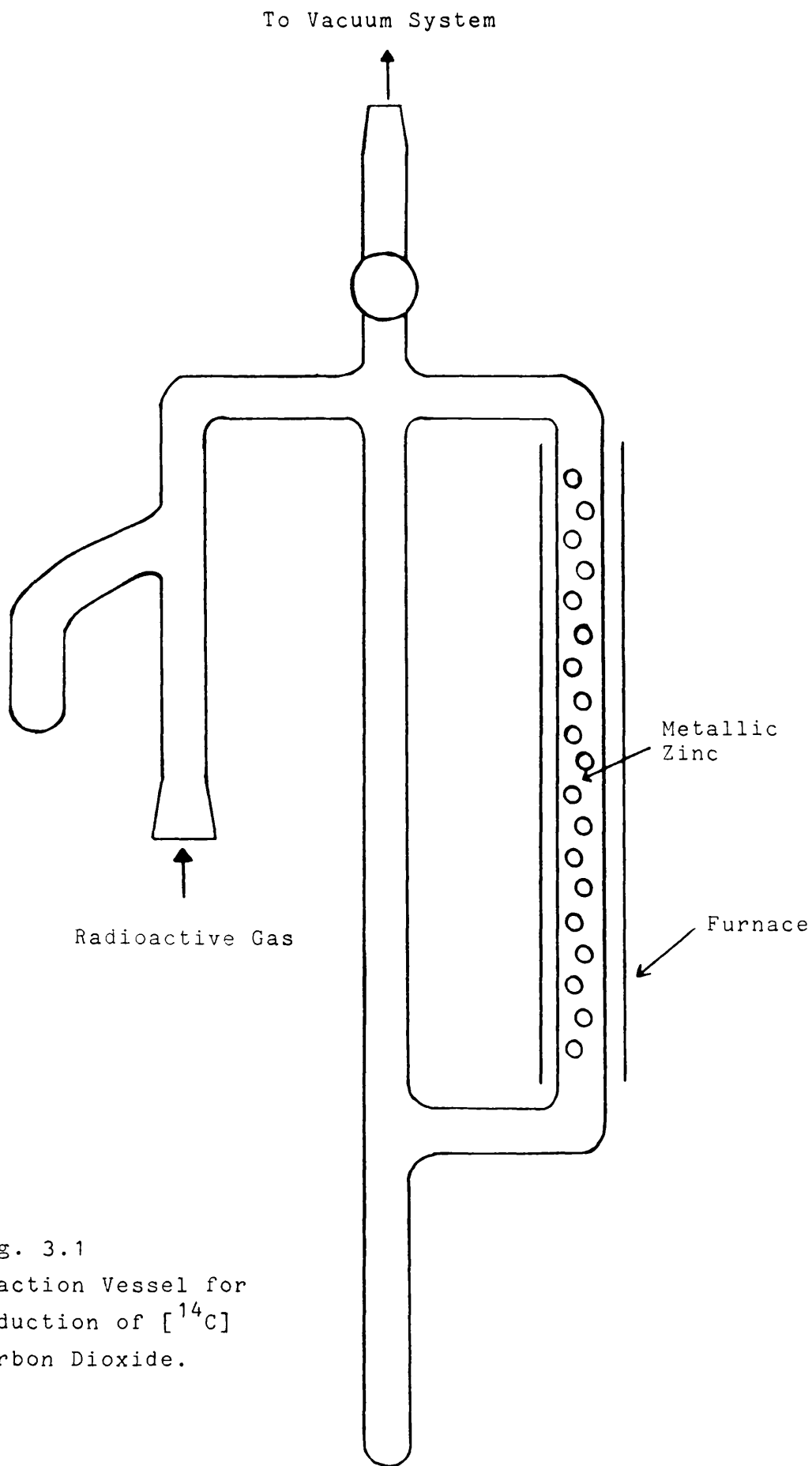


Fig. 3.1  
Reaction Vessel for  
Reduction of  $[^{14}\text{C}]$   
Carbon Dioxide.

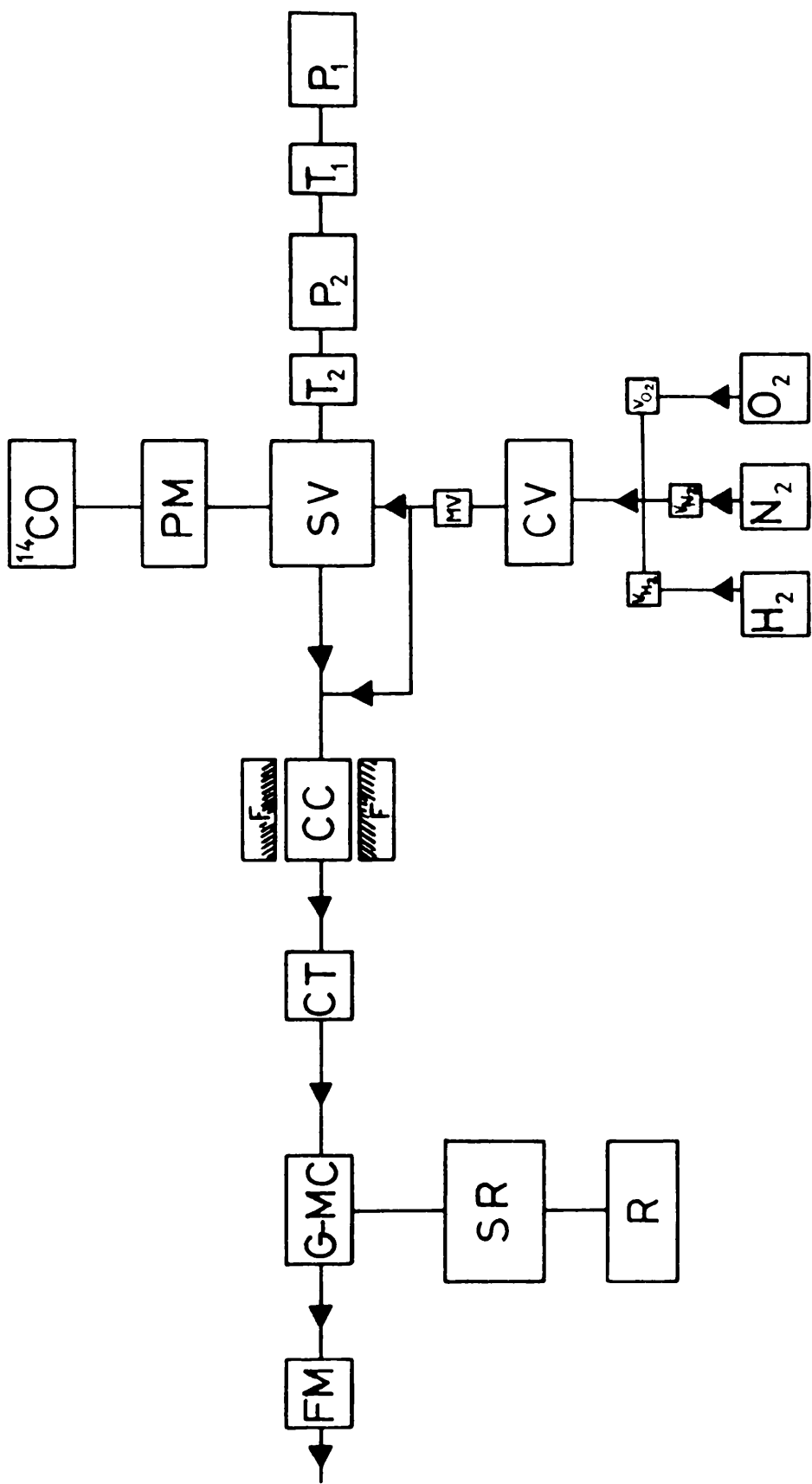


Fig. 3.2 Scheme of determination of carbon monoxide - area.

pump was protected by liquid nitrogen trap (T1, T2). A standard volume (SV) was connected to the vacuum line, a pressure measuring device (PM) and the  $^{14}\text{CO}$  storage vessel. The carrier gas stream could be directed through the sample volume or via a by-pass into the catalyst chamber (CC). A mercury manometer (M) was used for measuring the pressure in the standard volume.

Three different gases (namely, hydrogen, oxygen and nitrogen) could be passed over the catalyst. The flow rate of each gas was controlled by means of needle valves ( $V_{\text{H}_2}$ ,  $V_{\text{O}_2}$  and  $V_{\text{N}_2}$ ), a control valve (CV, Precision air pressure regular, Negretti Zombra) and a Nupro precision fine metering valve (MV). The gas flow could be directed through the standard volume, to sweep the carbon monoxide pulses into the catalyst chamber, or through the by-pass and then over the catalyst.

The catalyst sample was contained in a Pyrex U-tube (see figure 3.3) surrounded by a cylindrical electrical furnace (F). A cold trap (CT), cooled by liquid nitrogen, was placed in the outlet line from the U-tube before the gases entered the counting chamber. A Geiger-Müller Counter (G-M C) was used to count the radioactivity in the outlet flow gases. The counter was connected to a Scaler-Ratemeter (N.E. SR5), which recorded the total integrated counts in the carbon monoxide pulse. The radioactivity in each pulse was also recorded on a potentiometric chart recorder.

### 3.3.1.2 Experimental Procedure

An amount of the catalyst (usually from 20 to 200 mg) was placed on the sintered glass frit in the U-tube (see figure 3.3). Nitrogen gas was passed through the catalyst sample for 30 minutes to remove air. The flow rate of the gas was stabilised

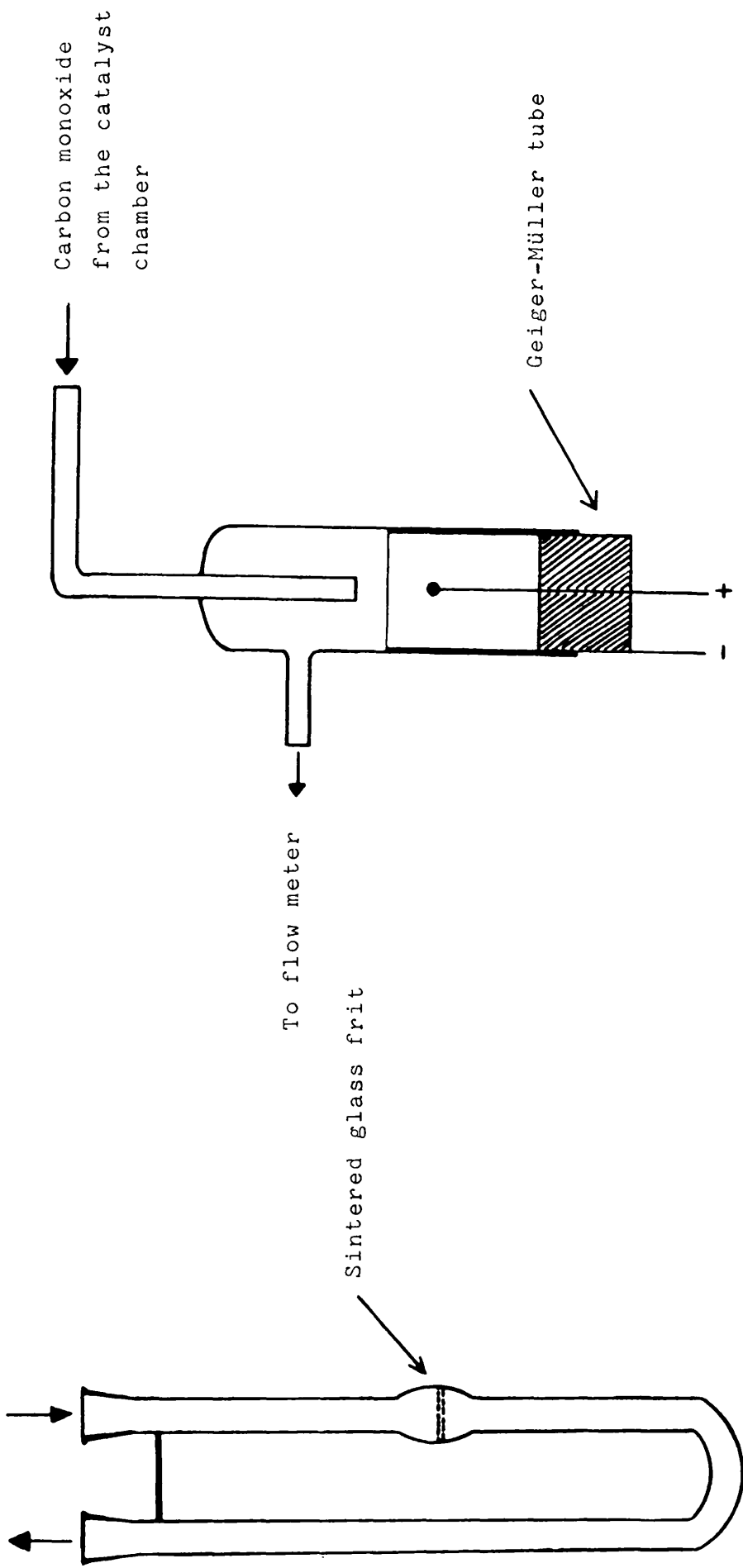


Fig. 3.3 Pyrex U-tube

Fig. 3.4 Counting chamber

by a Nupro precision fine metering valve and it was measured at the outlet end by a bubble flowmeter (FM). The operating conditions for carbon monoxide chemisorption are shown in (Table 3.1).

The current was supplied to the furnace and was controlled by the use of a Variac transformer. The temperatures were measured using a "Comark" electronic thermometer with a chromel/alumel thermocouple placed in contact with the U-tube. When the required reduction temperature was achieved, the flowing nitrogen was replaced by hydrogen, which was flowed over the catalyst for 1 hour. The U-tube was cooled in flowing nitrogen to ambient temperature to remove any residual hydrogen.

A successive number of pulses of carbon monoxide were passed over the catalyst in the nitrogen carrier gas stream. An amount of carbon monoxide was adsorbed onto the active surface of the catalyst; the remainder passed via a liquid nitrogen trap where any carbon dioxide was condensed into the counting chamber, see figure 3.4, where it was detected by the Geiger-Müller counter. The sample loop of the standard volume was evacuated between pulses.

In a series of pulses, the peaks, on the recorder increased in size to a maximum, and, thereafter decreased in (figure 3.5). The decrease was due to the decreasing pressure of the carbon monoxide in each pulse as measured using the mercury manometer. Any carbon dioxide which had been found to condense in cold trap was measured by removing the liquid nitrogen trap and counting the evolved gas. The liquid nitrogen trap was then replaced. The U-tube was heated in stages to various pre-determined temperatures and the temperature held steady. In

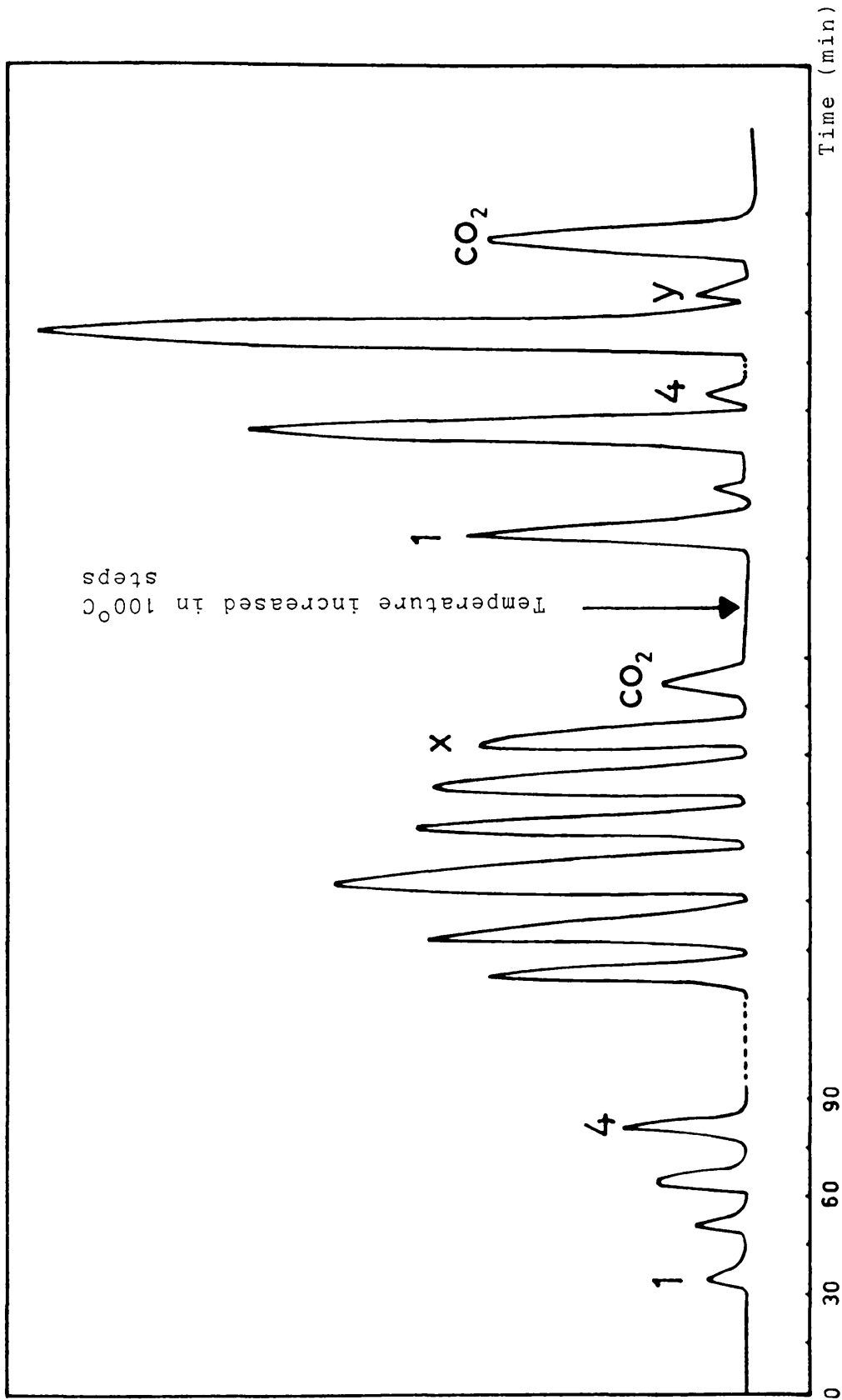


Fig. 3.5 Counts from successive pulses of  $^{14}\text{C}$  CO passed over reduced catalyst  
 significant adsorption (from 1 to x peaks + CO<sub>2</sub> peak)  
 desorption (from 1 to y peaks + CO<sub>2</sub> peak)

order to count the carbon dioxide evolved up to that temperature, the liquid nitrogen trap was removed and carbon dioxide allowed to flow through the counting chamber. The liquid nitrogen trap was again replaced and further heating continued, the carbon monoxide and carbon dioxide evolved being measured after each temperature was reached. Without replacing the trap, the gas flow was changed from nitrogen to oxygen to remove any strongly bonded carbon monoxide or carbonaceous material left on the catalyst.

#### 3.3.1.3 Determination of Plateau of Geiger-Müller Counter

The Geiger-Müller tube (Mullard MX 168/01) was mounted vertically. A [60-Co] source was placed close to the G-M counter and the count rate determined as a function of the applied voltage. A typical graph is shown in Figure 3.6.

The count rate rose rapidly until a plateau was reached, where count rate increased slowly with voltage. At the end of the plateau the count rate began to rise rapidly again. The working voltage was determined as the mid-point of the plateau region. This voltage was used for all measurements. The sensitivity of the Geiger-Müller counter varied slightly from day to day and, in consequence, a calibration was carried out before each experiment.

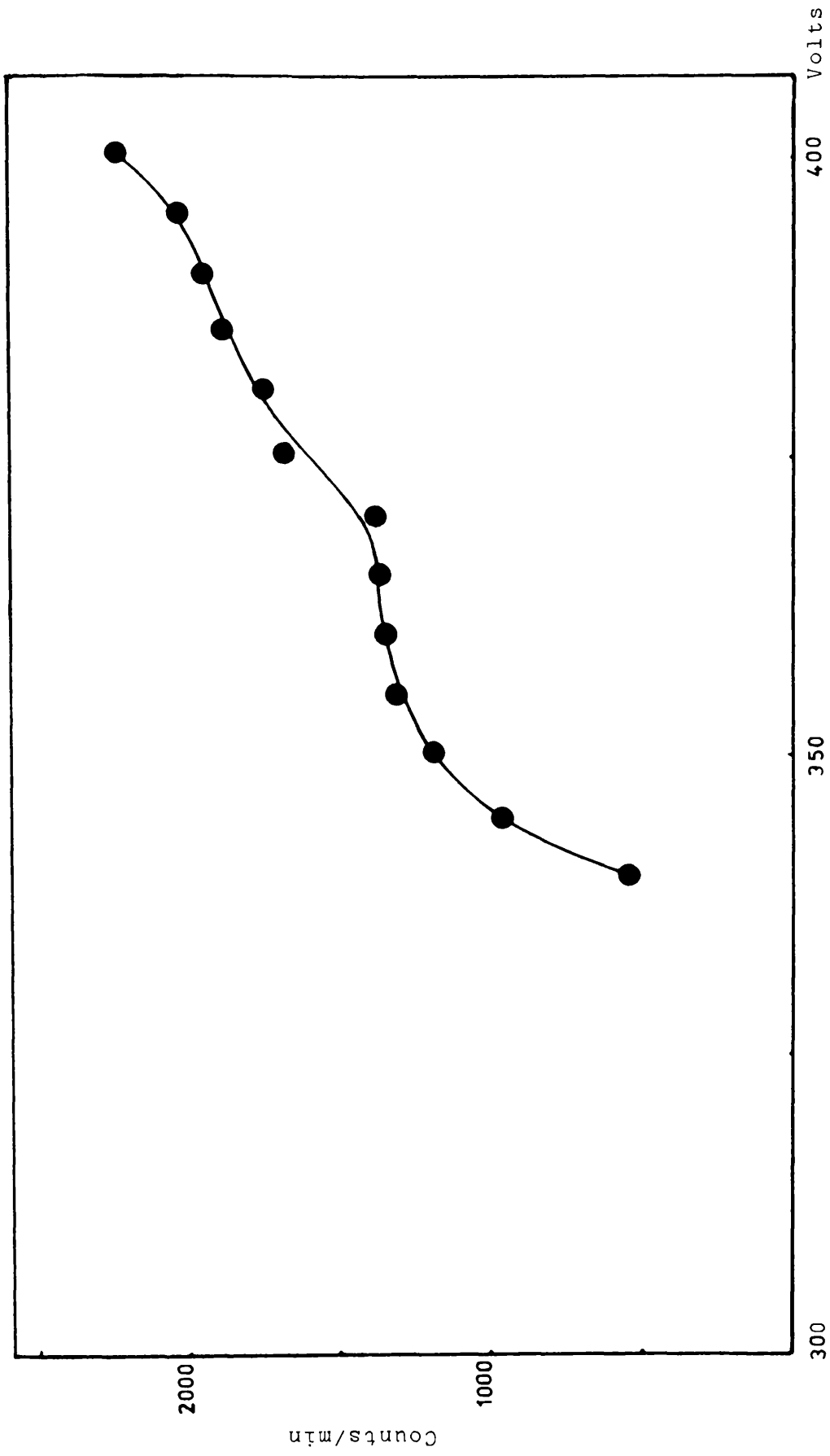


Fig. 3.6 Geiger-Müller tube plateau

Table 3.1Operating Conditions for Carbon Monoxide Chemisorption

Temperature	20 ± 2°C
Carrier gas	Nitrogen
Flow rate	30 ml/min
Oxidising gas	Oxygen
Flow rate	30 ml per minute
Reducing gas	Hydrogen
Flow rate	30 ml per minute
Chart speed	0.2 cm per minute
Sample loop	1 ml
Integral counting time	15 minutes

3.3.2 Buta-1:3-diene Hydrogenation3.3.2.1 The Vacuum System (see figure 3.7)

The apparatus consisted of a conventional vacuum system. It was evacuated by a combination of oil rotary pump ( $P_1$ ) and mercury diffusion pump ( $P_2$ ), which was protected by inlet and outlet liquid nitrogen traps ( $T_1$ ,  $T_2$ ) respectively. Three storage vessels ( $V_1$ ,  $V_2$  and  $V_3$ ) contained hydrogen, buta-1:3-diene and a 1:3 mixture of buta-1:3-diene and hydrogen respectively. Reactions were carried out in a 'Pyrex' flat-bottomed reaction vessel (RV) (Volume ca. 100 cm<sup>3</sup>) surrounded by an electric furnace (F). Reactions were followed by the pressure fall recorded using a pressure transducer (PT) (N.E. type SE/V/10D), the output from which was fed to a potentiometric recorder (R). This enabled pressure changes of 0.01 torr to be accurately measured.

The pressures of reactants in the storage vessels were measured using a mercury manometer (M), which was kept remote

from the reaction vessel to minimise the possibility of poisoning of the catalyst by mercury vapour. An expansion vessel (EV) was used for the extraction of the reaction mixture from the reaction vessel before passage through a spiral trap (ST), cooled in liquid nitrogen, to separate the hydrocarbon products from unreacted hydrogen. The hydrocarbon products were then distilled from the spiral trap into a liquid nitrogen cooled sample vessel (SV) for transfer to the gas chromatographic apparatus for analysis.

### 3.3.2.2 Experimental Procedure

The weighed catalyst sample (usually from 3 to 17 mg) was sealed into the reaction vessel, which was connected to the vacuum system. It was evacuated for twenty minutes at room temperature. The temperature was raised to the required reduction temperature, using a "Comark" electronic thermometer which utilised a chromel/alumel thermocouple. This was placed in contact with the base of the reaction vessel. The catalyst sample was reduced in hydrogen gas for sixteen hours at the required temperature and was then evacuated for fifteen minutes before being cooled to room temperature in vacuum.

A premixed sample of buta-1:3-diene (2.5 torr) and hydrogen (75 torr) was admitted to the reaction vessel to a total pressure of  $100 \pm 2$  torr. The progress of hydrogenation was observed by the pressure fall observed with pressure transducer, the output from which was recorded on a potentiometric recorder. With each freshly reduced catalyst sample, a series of five standard buta-1:3-diene hydrogenation reactions were carried out at room temperature before the catalyst was used to determine the variation of rates, product distribution and selectivity with

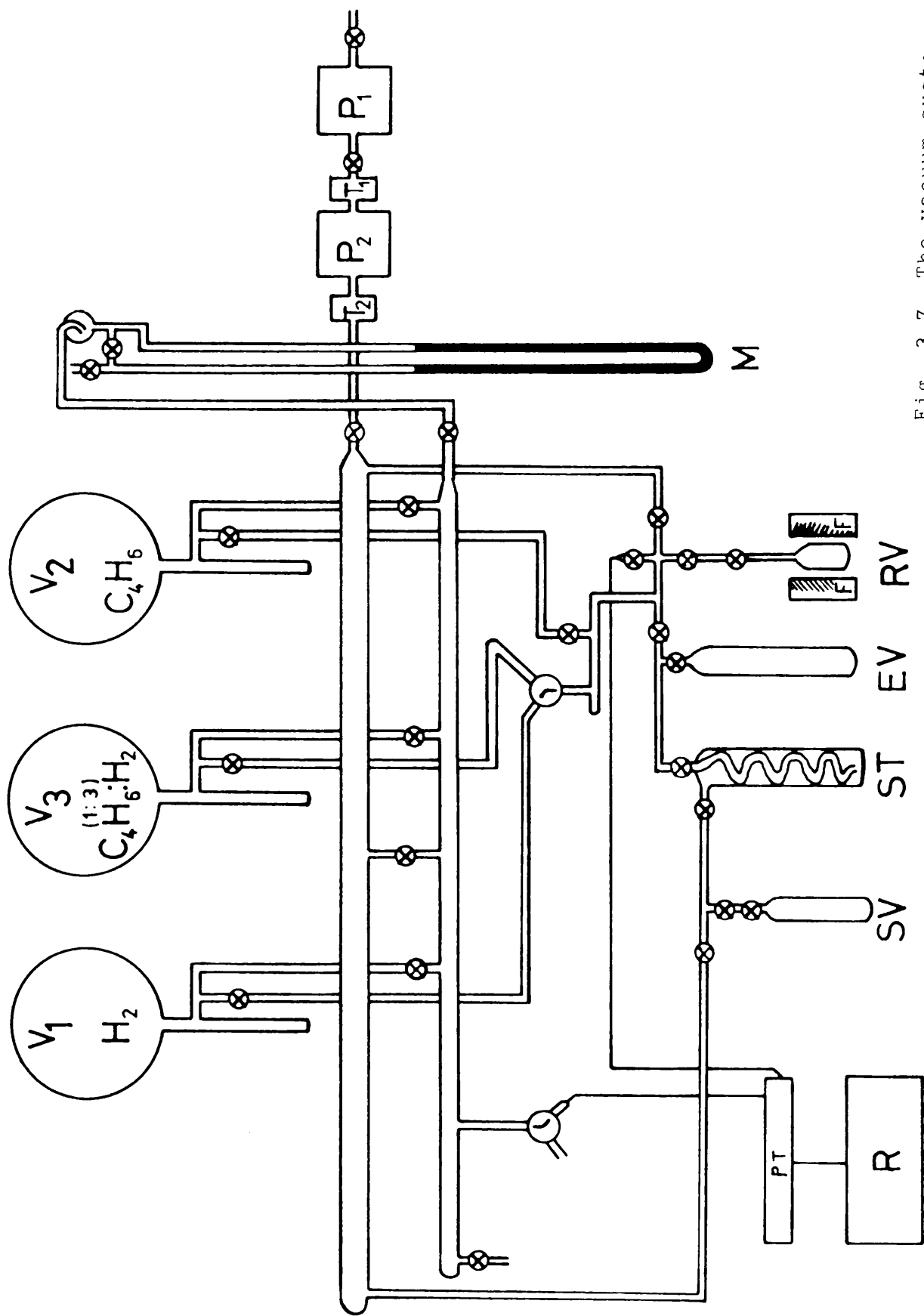


Fig. 3.7 The vacuum system

the experimental variables. This procedure was necessary to ensure that reproducible behaviour of the catalyst under standard conditions was achieved.

### 3.3.3 The Gas Chromatography System

#### 3.3.3.1 The Apparatus

The gas chromatography system is shown schematically in figure 3.8. It consisted of a chromatography column, 12 m long, 6 mm i.d. "Pyrex" glass tubing, packed with 33% dimethylsulpholane supported on 30 - 60 mesh firebrick. Using this column, effective separation of the products of buta-1:3-diene hydrogenation, namely n-butane, but-1-ene, trans-but-2-ene, cis-but-2-ene and buta-1:3-diene could be satisfactorily achieved.

Helium was used as carrier gas, the flow rate being controlled by a control valve (CV) (Precision air pressure regular). The flowing gas was passed through one arm of the thermal conductivity cell (Gow Mac model 10 - 285) via the sample inlet system (as described below) then through the chromatography column and finally through the other arm of the thermal conductivity cell. The operating conditions and the relevant retention data are summarised in Table 3.2.

#### Sample Inlet System

A diagram of the sample inlet system is shown in figure 3.9. It consisted of a U-tube sealed at each end by a spring-loaded tap ( $S_1$ ,  $S_2$ ). The carrier gas flow was directed either through the U-tube (via  $S_1$ ) then through the chromatography column or through a by-pass (via  $S_2$ ) and then on to the column.

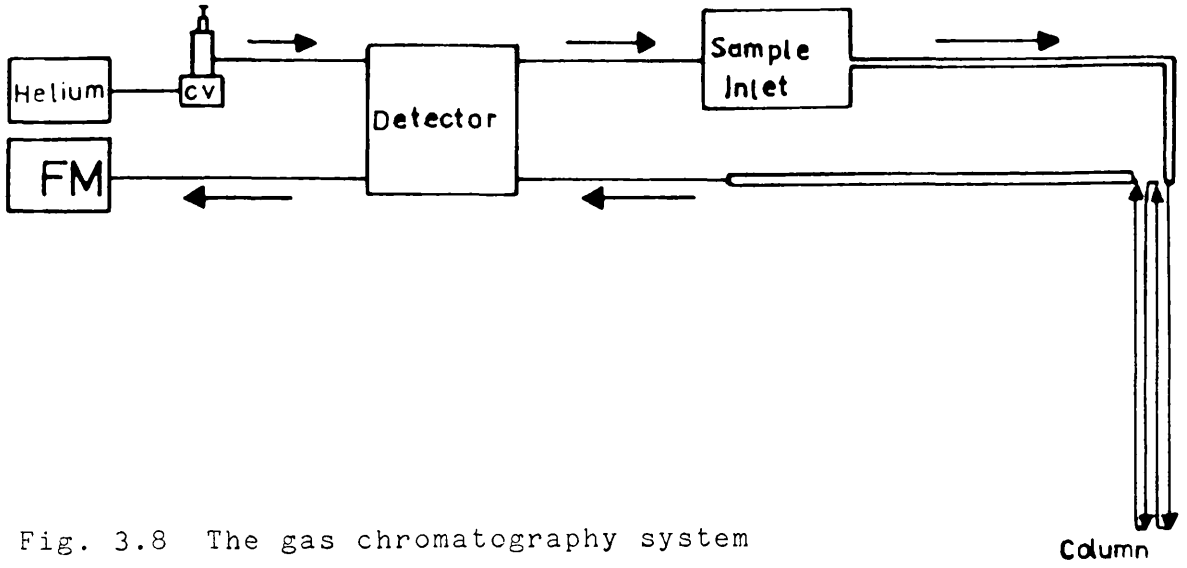


Fig. 3.8 The gas chromatography system

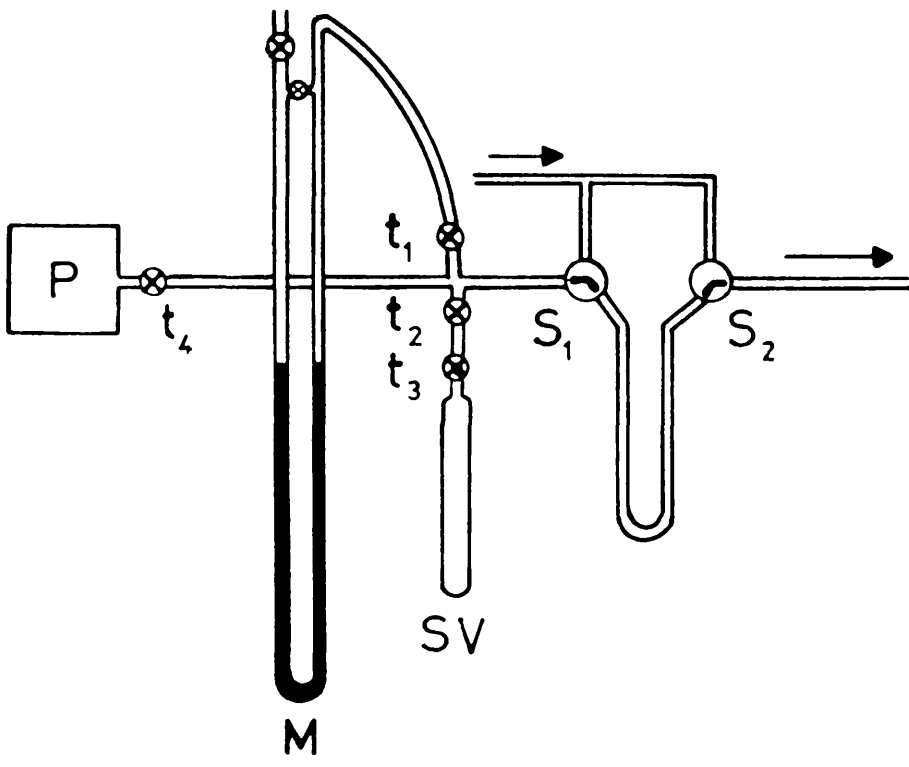


Fig. 3.9 Sample inlet system

Samples were admitted from the sample vessel (SV) into the evacuated sample loop and the sample pressure measured by means of the mercury manometer (M).

Table 3.2

Operating Conditions and Retention Data for C<sub>4</sub>-hydrocarbons  
on 33% Dimethylsulpholane on Firebrick

Temperature	20.0 ± 2°C
Carrier gas	Helium
Flow rate	40.0 ± 3 ml per minute
Counter gas inlet pressure	2.0 atm. (approx.)
Hydrocarbons	retention time (minutes)
<u>n</u> -butane	17 ± 1
But-1-ene	24 ± 1
<u>Trans</u> -but-2-ene	32 ± 1
<u>Cis</u> -but-2-ene	36 ± 1
Buta-1:3-diene	53 ± 1

3.3.3.2 Procedure for the Gas Chromatographic Analysis

The sample hydrocarbon product was transferred from the hydrogenation apparatus to the gas chromatograph in a sample vessel which was attached to the gas chromatographic sampling system. After evacuation of the sampling system (figure 3.9), the tap ( $t_4$ ) was shut. Taps ( $t_1$ ,  $t_2$ ,  $t_3$ ) and the spring-loaded tap ( $S_1$ ) were turned and the inlet pressure was measured by the mercury manometer (M). The spring-loaded taps ( $S_1$ ,  $S_2$ ) were turned simultaneously and the carrier gas was allowed to sweep the sample product from the U-tube to the column. A typical trace is shown in figure 3.10.

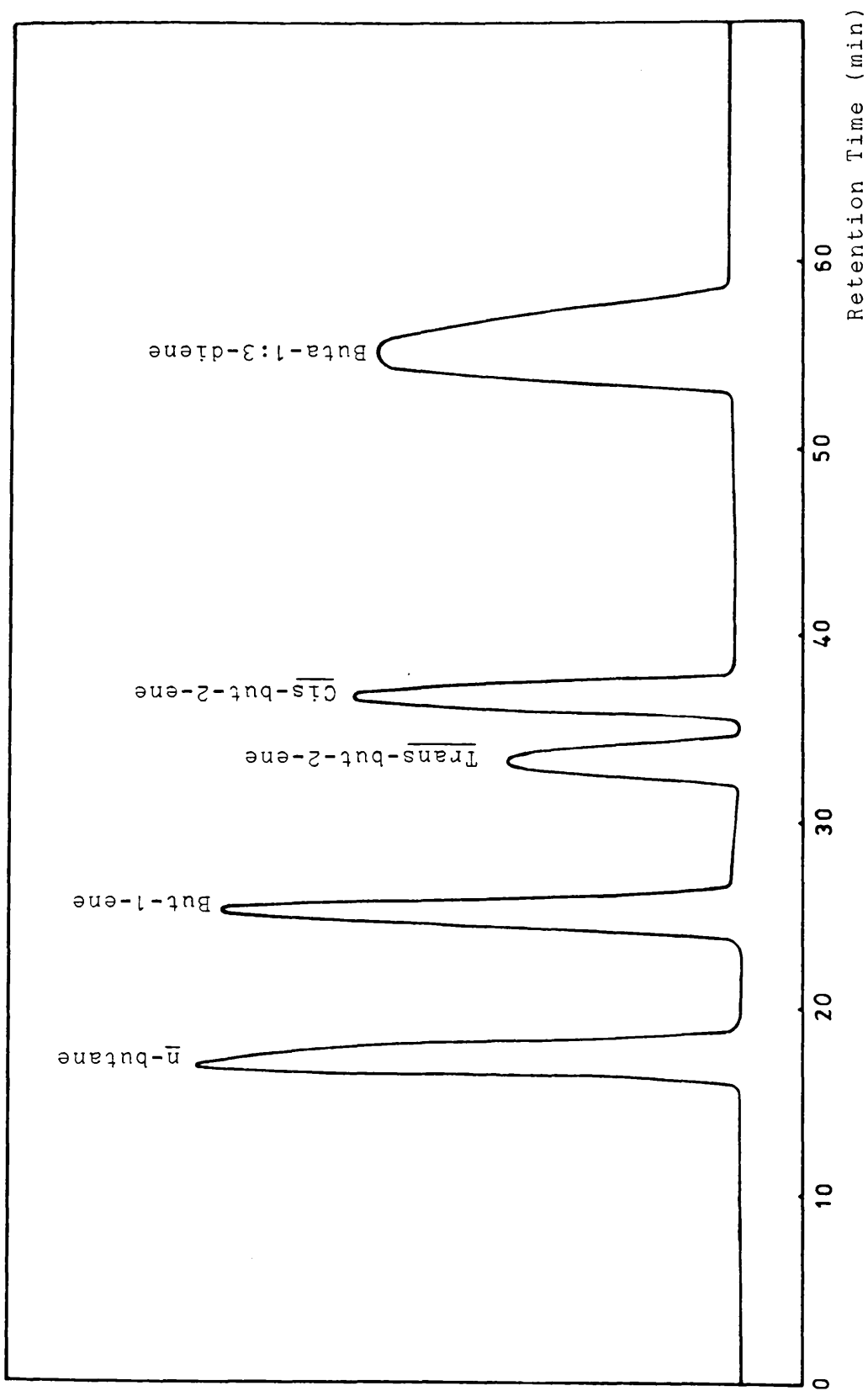


Fig. 3.10 Separation of reaction products on the dimethylsulpholane column

Before injecting any sample products into the chromatography column, the system was calibrated, using a "standard mixture" of known composition and containing all the possible reaction products. When the "standard mixture" was passed through the column, five peaks were obtained. By measuring the area under each peak, using a fixed armed planimeter, and dividing the peak area for each gas by the corresponding partial pressure, the sensitivity factor (f) for each gas was obtained.

$$f = \frac{\text{Peak area}}{\text{Partial pressure of gas}}$$

The sensitivity factors for the C<sub>4</sub>-hydrocarbons are shown in table 3.3.

Table 3.3

Factor Data for C<sub>4</sub>-hydrocarbons

Hydrocarbons	factors
<u>n</u> -butane	0.080
But-1-ene	0.086
<u>Trans</u> -but-2-ene	0.085
<u>Cis</u> -but-2-ene	0.090
Buta-1:3-diene	0.093

3.3.4 Temperature Programmed Reduction Profiles

3.3.4.1 Apparatus (see figure 3.11)

The catalyst was placed in a quartz tube which was surrounded by a cylindrical electrical furnace (F). The temperature of the furnace was controlled by a linear temperature programmer (SR) (Stanton Redcroft, model LVP/CA 40/R).

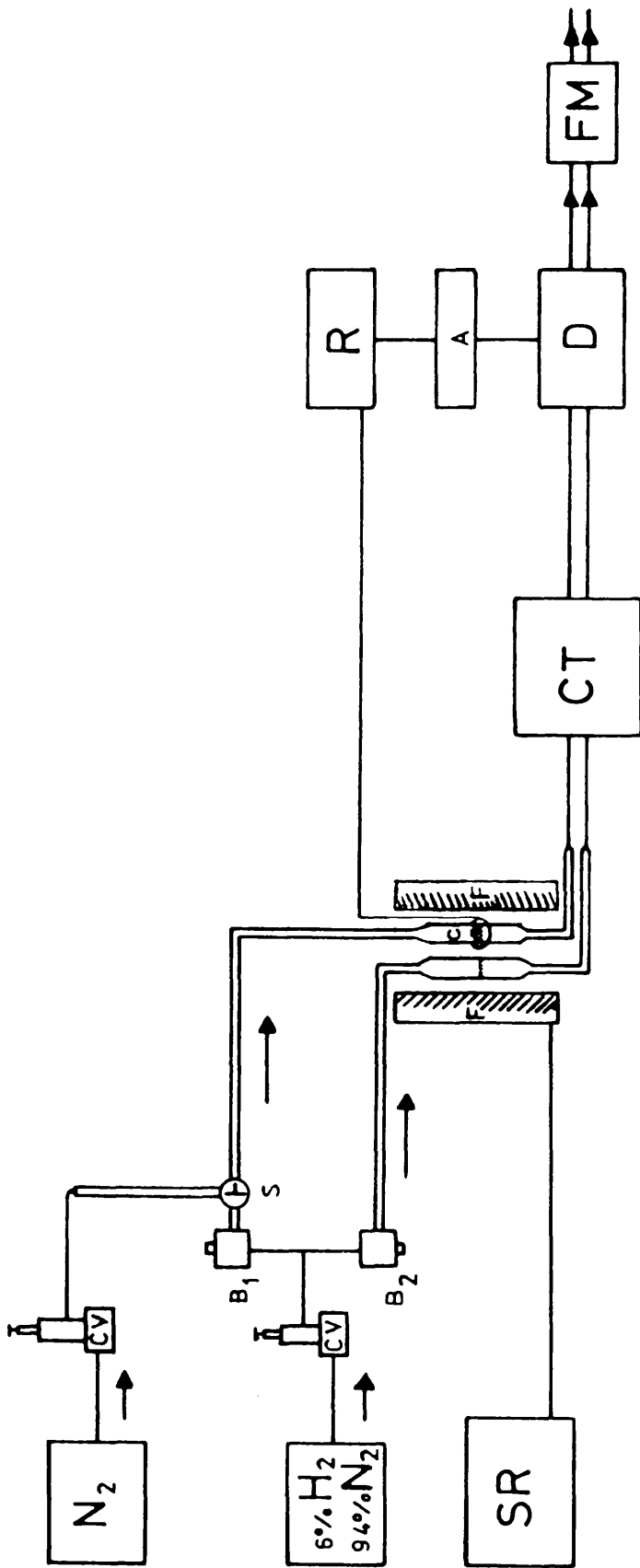


Fig. 3.11 Temperature Programmed Reductions apparatus

A chromel/alumel thermocouple was placed in contact with the catalyst tube inside the furnace and the temperature recorded on a Chart Recorder (R) (type RE 520.20).

The nitrogen gas flow, used only to degas the catalyst sample before reduction, was simply controlled by a control valve (CV) (Precision air pressure regular). Reductions were carried out using a 6% hydrogen/94% nitrogen gas stream. The flow rate of the gas stream was adjusted by means of a control valve (CV) and, after splitting into two streams, one of which flowed through the catalyst chamber, the other through an empty reduction chamber, by two Brooks (model 8744) flow controllers ( $B_1$  and  $B_2$ ). A cylindrical cold trap (CT) (methylene chloride and solid carbon dioxide) was used to remove any reduction products and the reduction process was monitored by uptake of hydrogen from the 6% hydrogen/nitrogen stream as shown by the thermal conductivity detector (D) (Gow Mac model 10.825), the output from which was recorded on the same chart as that used to record temperature changes. A linear temperature programmer enabled a steady rate of temperature rise ( $5^\circ - 10^\circ\text{C}$  per minute) to be maintained up to a maximum of  $700^\circ\text{C}$ .

#### 3.3.4.2 Experimental Procedure

Before carrying out the Temperature Programmed Reductions, the catalyst sample was purged at room temperature with nitrogen gas (British Oxygen Company) for fifteen minutes. When the catalyst sample was ready for temperature-programmed reduction measurements, the nitrogen gas was directed to the outlet and replaced by the 6% hydrogen/94% nitrogen stream (flow rate =  $30\text{ ml min}^{-1}$ ). A hot wire detector was used for measuring the

thermal conductivity differences between the gas, the detector (D) output was fed to an amplifier and the results were observed and potentiometric chart recorder.

CHAPTER 4

#### 4.1 Temperature Programmed Reduction Profiles

Temperature programmed reduction was carried out to examine the reduction profiles of the various catalysts. When each of the catalysts was heated from room temperature to 700°C reduction peaks were observed in the temperature range 127°-500°C. The temperature corresponding to each peak maximum was noted.

The T.P.R. results for each catalyst are presented below.

##### 4.1.1 5% Pt on SiO<sub>2</sub>

A sample (0.2026g) of catalyst was heated at the rate of 6°C per minute. Five distinct reduction peaks were observed as shown in Figure 4.1.1. The temperatures corresponding to the peak maxima were:

$T_{\max}$ (a)	$T_{\max}$ (b)	$T_{\max}$ (c)	$T_{\max}$ (d)	$T_{\max}$ (e)	unit
130	150	202	384	450	°C

$T_{\max}$  (a),  $T_{\max}$  (b) and  $T_{\max}$  (c) were resolved and  $T_{\max}$  (c) was the main sharp reduction peak.  $T_{\max}$  (d) and  $T_{\max}$  (e) were unresolved.

##### 4.1.2 5% Pt on Al<sub>2</sub>O<sub>3</sub>

A sample (0.2034g) of catalyst was heated at the rate of 5°C per minute. Four distinct reduction peaks were observed as shown in Figure 4.1.2. The temperatures corresponding to the peak maxima were:

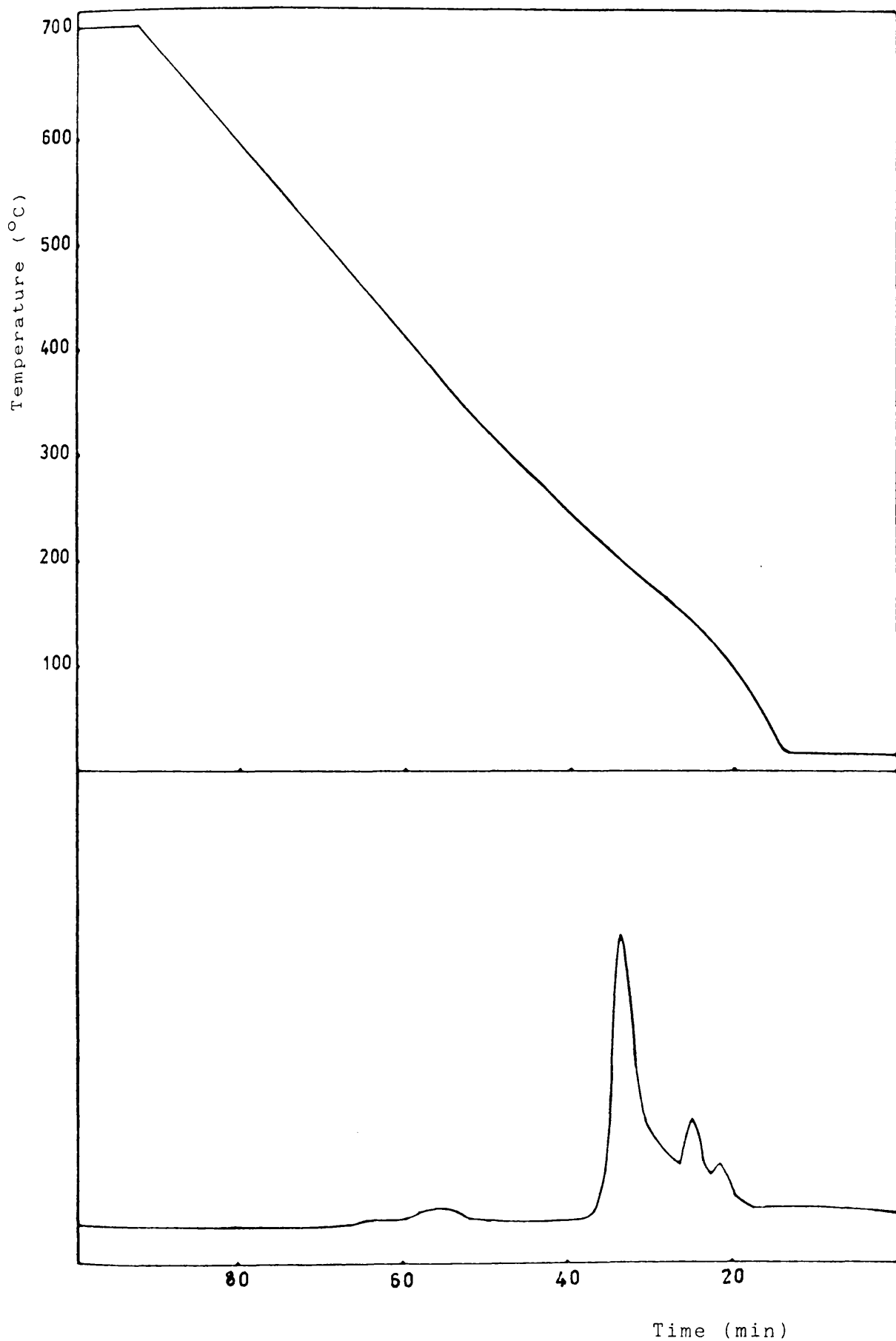


Figure 4.1.1 Temperature-programmed reduction of 5% Pt/SiO<sub>2</sub>.

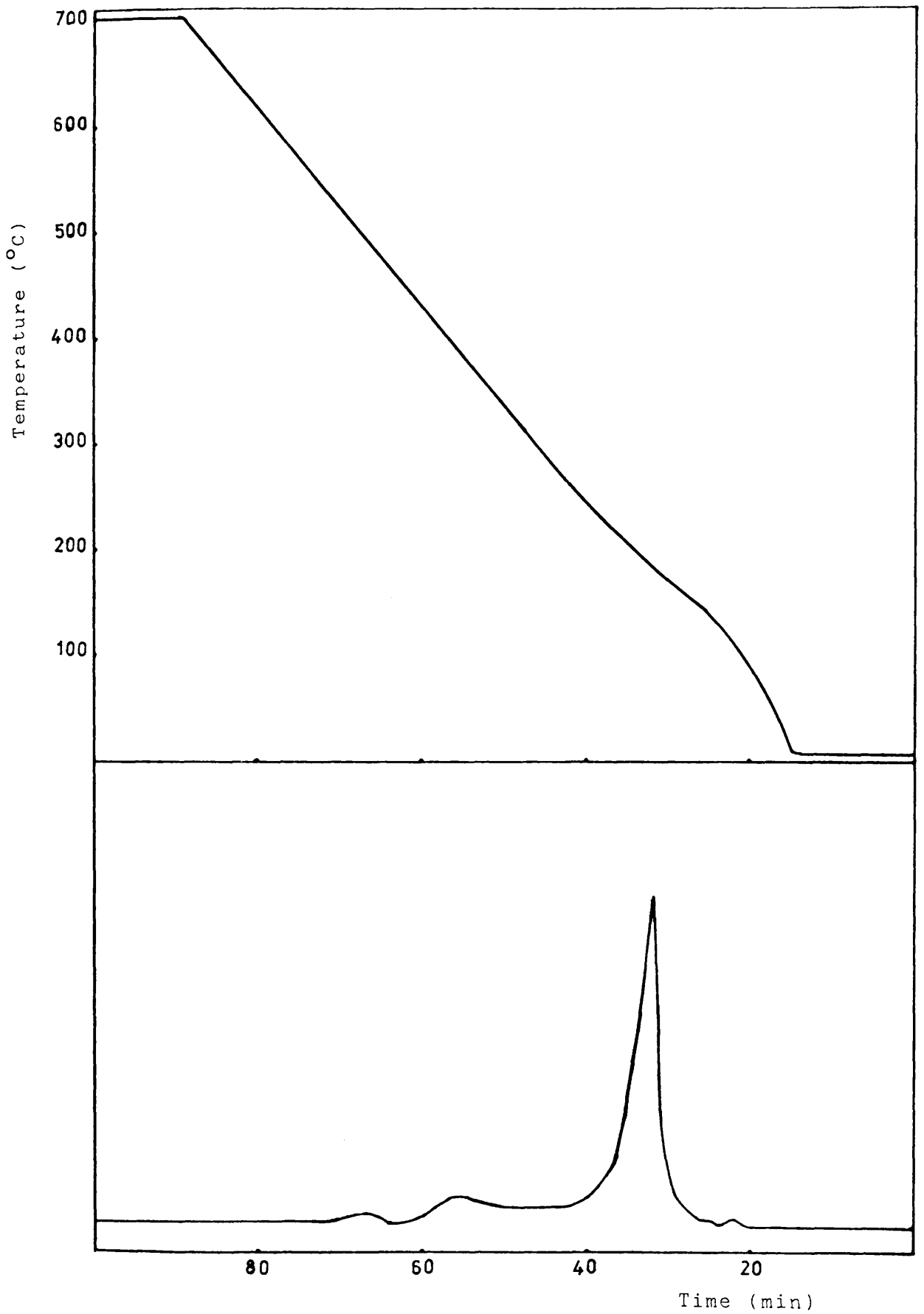


Figure 4.1.2 Temperature-programmed reduction of 5% Pt/Al<sub>2</sub>O<sub>3</sub>

$T_{\max}$ (a)	$T_{\max}$ (b)	$T_{\max}$ (c)	$T_{\max}$ (d)	unit
136	217	396	500	$^{\circ}\text{C}$

All reduction peaks were resolved,  $T_{\max}$  (b) was the only sharp reduction peak and the remainder of the peaks were small.

#### 4.1.3 5% Pt on $\text{TiO}_2$

A sample (0.2037g) of catalyst was heated at the rate of  $10^{\circ}\text{C}$  per minute. Three distinct reduction peaks were observed as shown in Figure 4.1.3. The temperatures corresponding to the peak maxima were:

$T_{\max}$ (a)	$T_{\max}$ (b)	$T_{\max}$ (c)	unit
159	209	278	$^{\circ}\text{C}$

$T_{\max}$  (a) was the major reduction peak followed by two small peaks, all reduction peaks were resolved.

#### 4.1.4 5% Rh on $\text{SiO}_2$

A sample (0.2027g) of catalyst was heated at the rate of  $5^{\circ}\text{C}$  per minute. Three distinct reduction peaks were observed as shown in Figure 4.1.4. The temperatures corresponding to the peak maxima were:

$T_{\max}$ (a)	$T_{\max}$ (b)	$T_{\max}$ (c)	unit
204	227	237	$^{\circ}\text{C}$

The first reduction peak was unresolved but the remainder of the peaks were partially resolved.

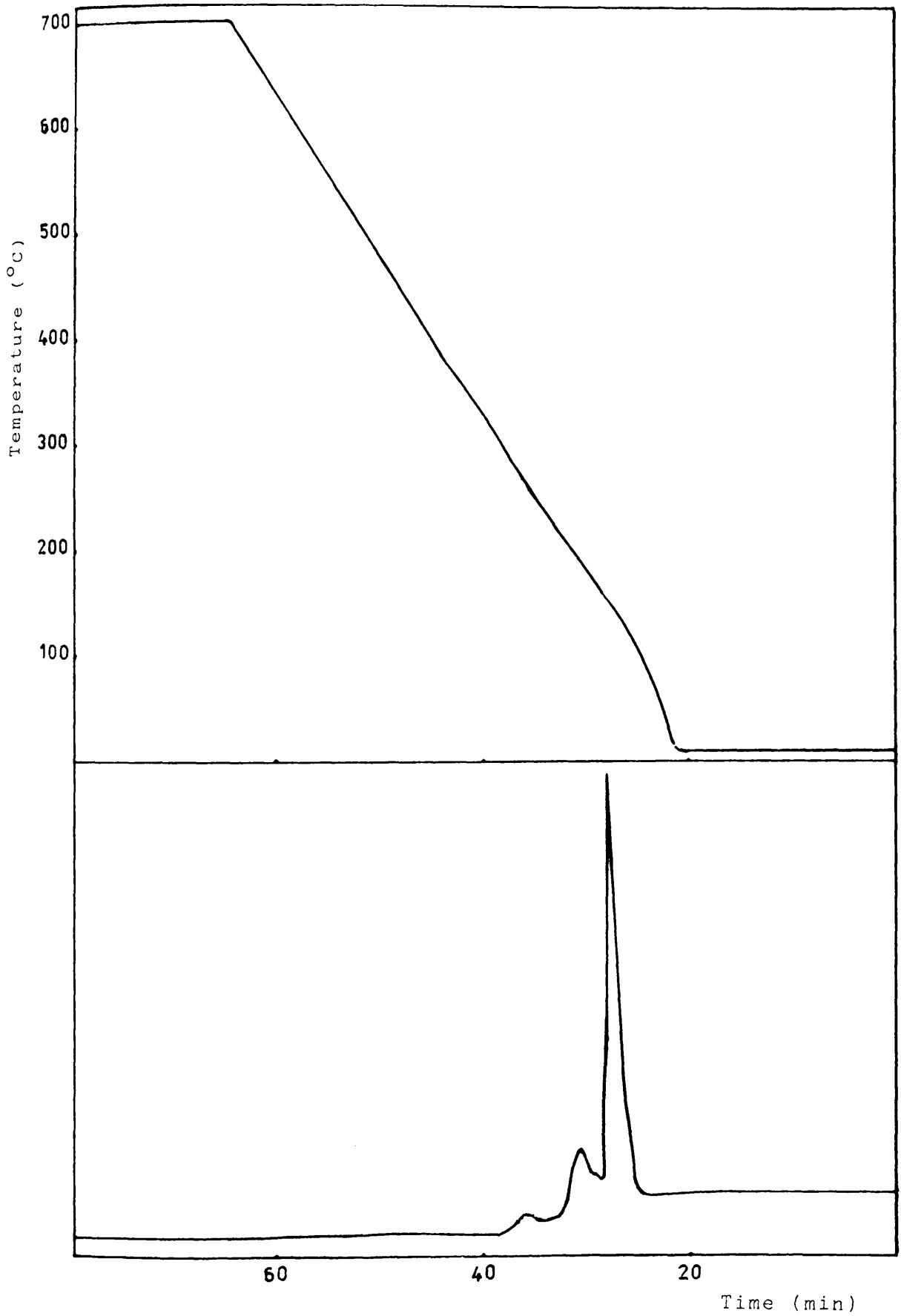


Figure 4.1.3 Temperature-programmed reduction of 5% Pt/TiO<sub>2</sub>

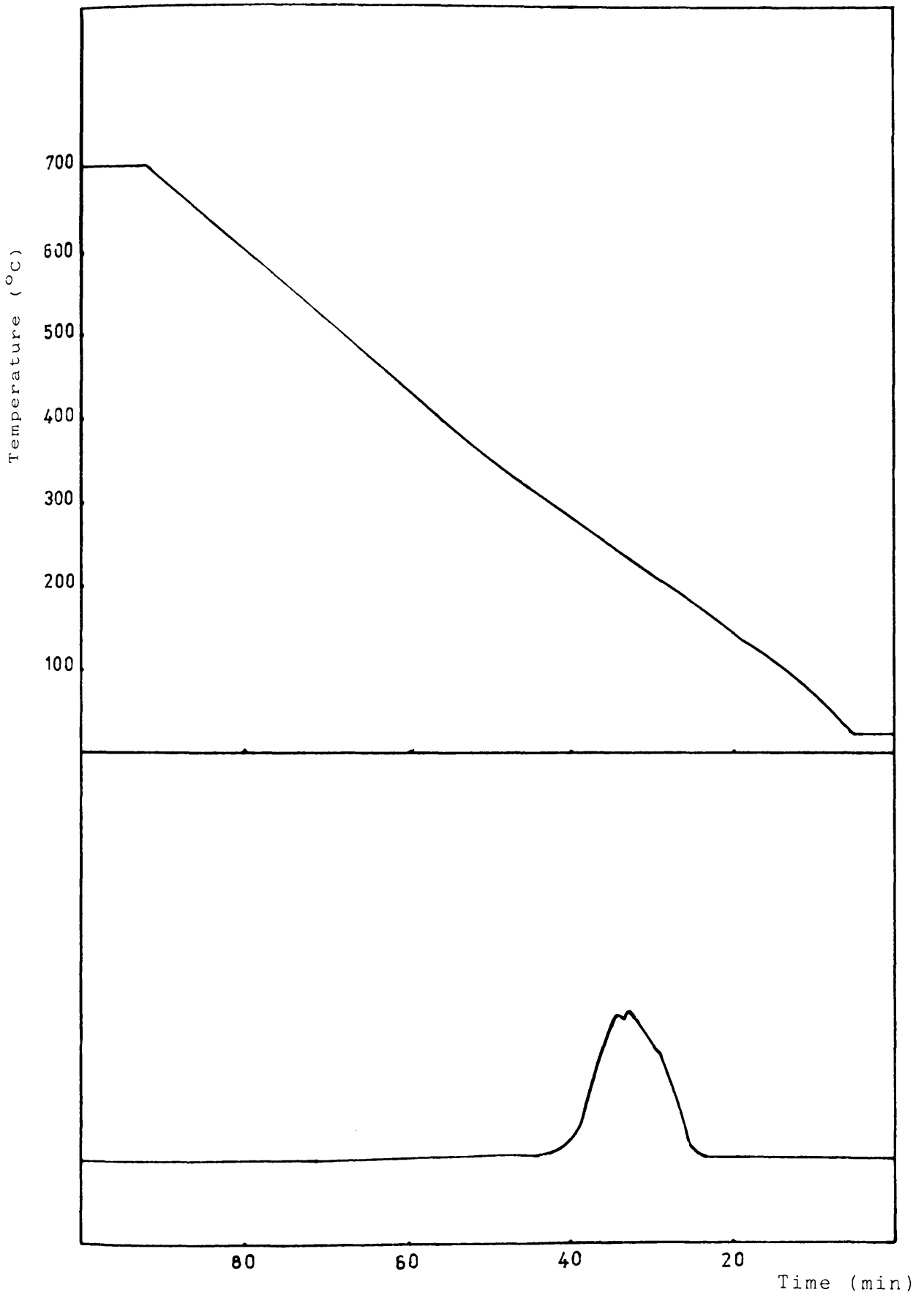


Figure 4.1.4 Temperature-programmed reduction of 5% Rh/SiO<sub>2</sub>

#### 4.1.5 5% Rh on Al<sub>2</sub>O<sub>3</sub>

A single reduction peak of sample (0.2031g) was observed in the T.P.R. profile at  $T_{\max} = 135^{\circ}\text{C}$ . The heating rate was  $6^{\circ}\text{C}$  per minute and the profile is shown in Figure 4.1.5.

#### 4.1.6 5% Rh on TiO<sub>2</sub>

A sample (0.1968g) of catalyst was heated at the rate of  $6^{\circ}\text{C}$  per minute. Three reduction peaks were observed as shown in Figure 4.1.6. The temperatures corresponding to the peak maxima were:

$T_{\max}$ (a)	$T_{\max}$ (b)	$T_{\max}$ (c)	unit
127	150	178	$^{\circ}\text{C}$

The T.P.R. profile shows only one large reduction peak at  $150^{\circ}\text{C}$  with the other two peaks as small shoulders to the main peak.

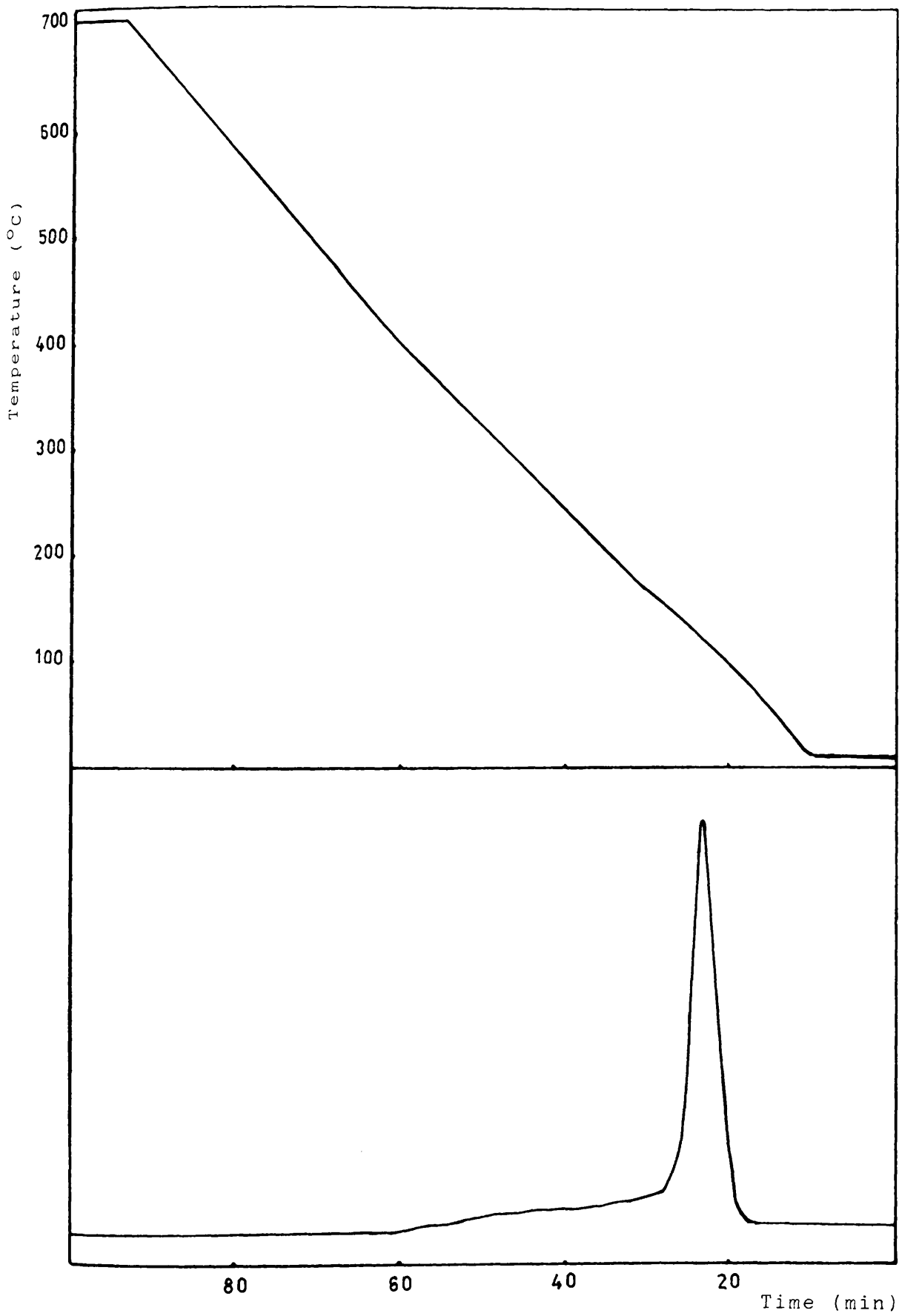


Figure 4.1.5 Temperature-programmed reduction of 5% Rh/Al<sub>2</sub>O<sub>3</sub>

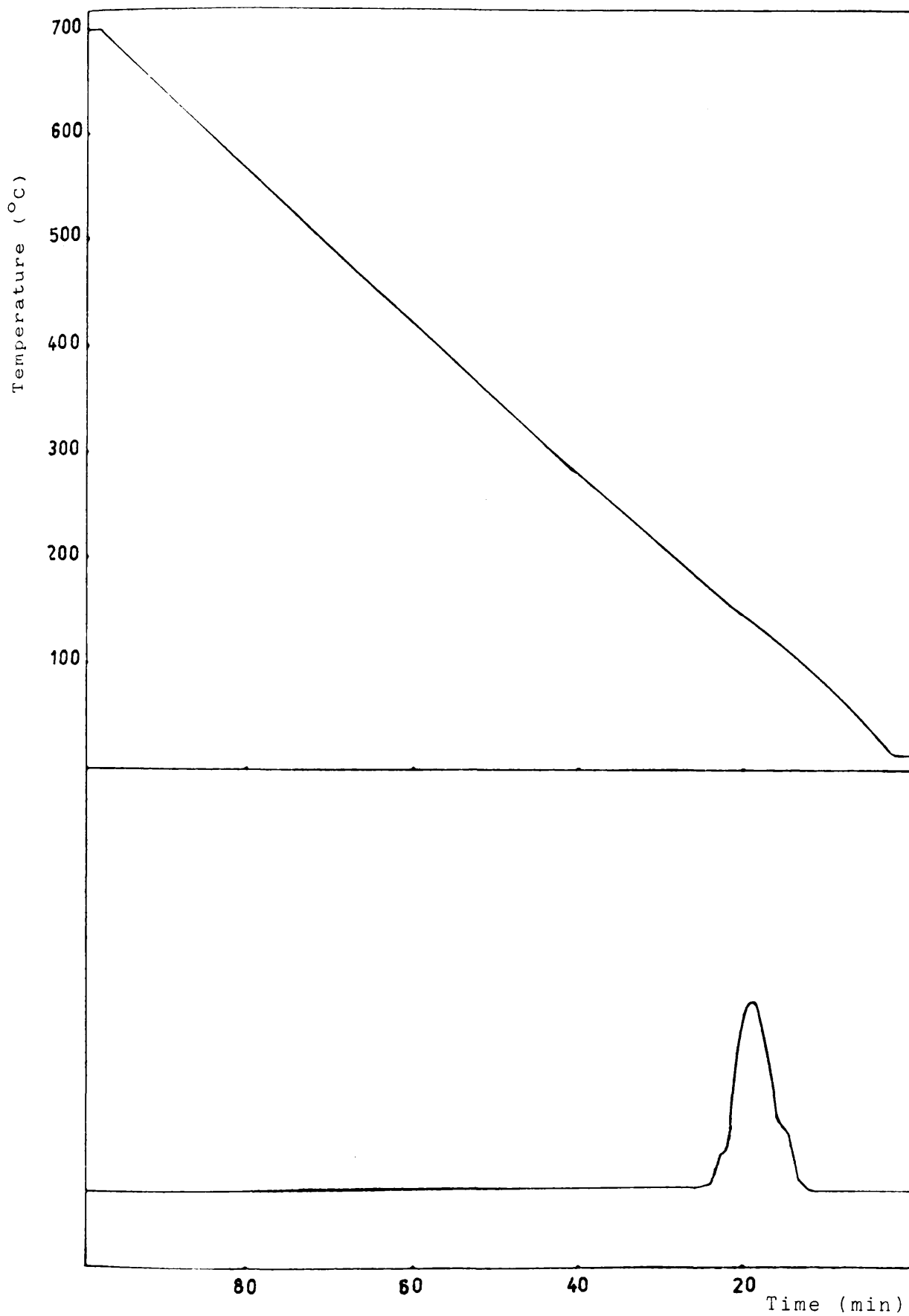


Figure 4.1.6 Temperature-programmed reduction of 5% Rh/TiO<sub>2</sub>

## 4.2 [<sup>14</sup>C]Carbon Monoxide Chemisorption and Desorption

### 4.2.1 Method of Calculation of Metal Surface Areas

The specific metal surface area of the catalyst can be determined as:

$$A = (Na_m)/m_{cat} \quad (a)$$

where  $A$  = Metal area ( $m^2 g^{-1}$ )

$N$  = Number of CO molecules adsorbed by sample

$a_m$  = Average area occupied by each CO molecule ( $16.2 \times 10^{-20} m^2$ )

$m_{cat}$  = Weight of catalyst used (g)

Using the pulsed flow technique described in Section 3, the total number of carbon monoxide molecules adsorbed by the catalyst sample was calculated as follows:

Following each pulse, the total integrated count ( $N_i$ ) in the reactor eluant was determined when adsorption was complete, as shown by a constant value for the radioactive count in the eluant, the total eluted radioactivity was calculated as

$$N_T = \sum_0^n Ni, \quad (\text{where } n = \text{no. of pulses}).$$

The quantity  $N_T$  was then converted to an equivalent pressure ( $P_x$ ) in the sample loop using an appropriate factor  $f$  (counts  $\text{torr}^{-1}$ ):-

$$P_x = (N_T/f).$$

The factor,  $f$ , was determined in one of two ways. When

adsorption was complete, a further three pulses of  $^{14}\text{CO}$  were passed, at a known pressure ( $P_A$ ) in the sample loop, over the catalyst and the average count from these three pulses determined. Thus,

$$f = (\sum_0^3 N_i / \sum P_A)$$

Alternatively, values of  $f$  were determined directly by passing pulses of known size through an empty reactor tube and determining the total radioactive counts in the eluant, as shown in Table 4.2.1

The total amount of carbon monoxide adsorbed by the catalyst was then calculated as a difference in pressure between the total pressure pulsed over the catalyst ( $P_T$ ) and the pressure in the reactor eluant:

$$\begin{aligned} P_S &= (P_T - P_x) \\ &= [P_T - (N_T/f)] \end{aligned}$$

and hence, by use of the ideal gas equation, the number of molecules of CO adsorbed was calculated as:

$$N = (N_A P_S V / R.T) \quad (b)$$

where  $N_A =$  Avogadro Number ( $6.023 \times 10^{23} \text{ mol}^{-1}$ )  
 $V =$  Volume of Sample Loop ( $1 \text{ cm}^3$ ).

As an alternative, the total amount of radioactive CO desorbed from the catalyst at temperatures up to  $200^\circ\text{C}$  was determined and this value used to calculate the corresponding sample pressure ( $P'_S$ ) and hence the number of molecules originally adsorbed.

In general, good agreement was obtained between the values of  $P_s$  and  $P'_s$  as shown in the succeeding tables.

Table 4.2.1

Calibration of [ $^{14}\text{C}$ ]Carbon Monoxide

Pulse	Time (sec)	Pressure (torr)	Counts	Corrected Counts
(CO) 1	1000	48	15796	14967
2	"	46	15976	15147
3	"	43	15779	14950
4	"	40.5	14643	13814
5	"	39	13790	12961
6	"	36.5	13616	12787
7	"	35	12500	11671
$\text{CO}_2$	"		2236	1407

#### 4.2.2 Metal Areas as Determined by [<sup>14</sup>C]Carbon Monoxide Chemisorption and Desorption

As an example, the results obtained with Rh/alumina catalysts are presented below in full. The remaining results are summarised in Tables 4.2.3 and 4.2.4.

The sample catalyst (0.0302g) was reduced at 200°C in a flowing hydrogen gas for 1 hour.

Operating voltage: 364V

Range: 400 cps

Gas flow: 30 ml/min

Background: 733 counts in 1000 sec

#### Applications

$$f = 335.1 \text{ (counts/torr)}$$

$$P_T = 576 \text{ (torr)}$$

$$N_T = 92084 \text{ (counts)}$$

$P_S$  can be calculated:-

$$P_S = 576 \text{ (torr)} - \frac{92084}{335.1}$$

$$= 301.2 \text{ (torr)}$$

Then, the equation (b):-

$$N = \frac{6.023 \times 10^{23} \text{ (molecules)} \times 301.2 \text{ (torr)} \times 1 \text{ (ml)} \times 273 \text{ (K)}}{760 \text{ (torr)} \times 22.414 \times 10^3 \text{ (ml)} \times 293 \text{ (K)}}$$

$$N = 0.0992 \times 10^{20} \text{ (molecules)}$$

= number of adsorbed molecules.

And then, the equation (a)

$$A = \frac{0.0992 \times 10^{20} \times 16.2(\text{\AA}^2)}{0.0302 \text{ (grams)}}$$

$$A = 53.21 \times 10^{20} (\text{\AA}^2/\text{grams})$$

$$A = 53.21 (\text{m}^2/\text{grams})$$

$$A = \text{surface area per gram of the Rh on Al}_2\text{O}_3$$

Finally, the number of desorbed molecules ( $N'$ ) can be determined:

$$N'_T = 91463 \text{ (counts)}$$

$$P'_s = \frac{91463 \text{ (counts)}}{335.1 \text{ (counts/torr)}}$$

$$= 272.9 \text{ (torr)}$$

$$N' = \frac{6.023 \times 10^{23} \text{ (molecules)} \times 272.9 \text{ (torr)} \times 1 \text{ (ml)} \times 273 \text{ (K)}}{760 \text{ (torr)} \times 22.414 \times 10^3 \text{ (ml)} \times 293 \text{ (K)}}$$

$$N' = 0.0899 \times 10^{20} \text{ (molecules)}$$

Table 4.2.2

[<sup>14</sup>C]Carbon Monoxide Chemisorption and Desorption over Catalyst  
5% of Rh on Al<sub>2</sub>O<sub>3</sub>

Chemisorption

	Pulse	Time (sec)	Pressure (torr)	Counts	Corrected Counts
Trap on					
	1	1000	50	1244	511
	2	"	47	1473	740
	3	"	45	2624	1891
	4	"	42.5	3525	2792
	5	"	40	4353	3620
	6	"	38	5226	4493
	7	"	36.5	6192	5459
	8	"	35	6217	5484
	9	"	32.5	6687	5954
	10	"	31	7175	6442
	11	"	29	7481	6748
	12	"	28	7463	6730
	13	"	27	6543	5810
	14	"	25.5	6451	5718
	15	"	24.5	6698	5965
	16	"	23	6172	5439
	17	"	21.5	6074	5341
Trap off				13680	12947

Desorption

Trap	Time (sec)	T <sub>min</sub> (°C)	T <sub>max</sub> (°C)	Counts	Corrected Counts
on	1000	20	110	5609	4876
off	1000	110	110	21391	20658
on	2000	110	200	50096	48630
off	1000	200	200	17519	16786
O <sub>2</sub> off	700	200	200	1026	513

Table 4.2.3

[<sup>14</sup>C]Carbon Monoxide Chemisorption and Desorption on Platinum Supported on  
Three Different Supports

Catalyst	Reduction Temperature (°C)	Mass of Sample (grams)	No. of adsorbed molecules of CO (x 10 <sup>19</sup> molecules)	No. of desorbed molecules of CO (x 10 <sup>19</sup> molecules)	Area of 1 gram of catalyst (m <sup>2</sup> /grams)
5% Pt/SiO <sub>2</sub>	200	0.0393	0.186	0.151	7.67
	450	0.0385	0.234	0.212	9.85
5% Pt/Al <sub>2</sub> O <sub>3</sub>	200	0.0437	0.214	0.208	7.93
	450	0.0442	0.172	0.161	6.30
5% Pt/TiO <sub>2</sub>	200	0.0445	0.057	0.048	2.08
	450	0.0449	0.024	0.022	0.87

Table 4.2.4

[<sup>14</sup>C]Carbon Monoxide Chemisorption and Desorption on Rhodium Supported on  
Three Different Supports

Catalyst	Reduction Temperature (°C)	Mass of Sample (grams)	No. of adsorbed molecules of CO (x 10 <sup>19</sup> molecules)	No. of desorbed molecules of CO (x 10 <sup>19</sup> molecules)	Area of 1 gram of catalyst (m <sup>2</sup> grams)
5% Rh/SiO <sub>2</sub>	200	0.202	0.200	0.194	16.04
	450	0.201	0.284	0.247	22.89
5% Rh/Al <sub>2</sub> O <sub>3</sub>	200	0.0302	0.992	0.899	53.21
	450	0.0293	0.465	0.448	25.71
5% Rh/TiO <sub>2</sub>	200	0.0205	0.082	0.077	6.48
	450	0.0203	0.049	0.046	3.91

### 4.3 Buta-1:3-diene Hydrogenation

Throughout this section, the terms but-1-ene, trans-but-2-ene, cis-but-2-ene, low reduction temperature and high reduction temperature are abbreviated to 1-B, t-2-B, c-2-B, LRT and HRT respectively.

Butadiene will be used to refer to buta-1:3-diene, since buta-1:2-diene has not been used in this work.

#### Calculation of Initial Rates

The initial rates of reactions were calculated from pressure fall against time curves using the gradient of the tangent to the curve at zero time.

#### Calculation of Activation Energies

The initial rates were measured as a function of temperature in a series of reactions. The activation energies were then determined from the Arrhenius equation;

$$k = A \exp(- E_a/RT)$$

where

k = rate constant

A = pre-exponential factor

$E_a$  = activation energy

R = gas constant (8.314 J/mole °K)

T = temperature (°K)

using plots of  $\log_{10} k$  against  $1/T$ .

#### Calculations of Selectivity and Extent of Reaction

The Selectivity, S, for the olefin formation is defined as

$$S = \frac{\text{yield of olefin}}{\text{yield of olefin} + \text{yield of alkane}}$$

where the yield of olefin represents the total yield of 1-B, t-2-B and C-2-B, and the yield of alkane represents the yield of n-butane.

The percentage conversion may be calculated from the product distribution as determined by gas chromatography. It can be defined as the number of moles of hydrogen consumed per mole of hydrocarbon present in the reaction mixture, calculated as follows:

$$\% \text{ Conversion} = (2 \times \% \text{ n-butane yield}) + \% \text{ olefin yield}$$

#### 4.3.1 The Reaction of Butadiene with Hydrogen over 5% Pt/SiO<sub>2</sub>

##### 4.3.1.1 The Pressure Fall against Time Curves for LRT and HRT Catalysts

(0.0095g) and (0.0106g) samples of catalyst were reduced, respectively, at low reduction temperature and at high reduction temperature. Figure 4.3.1.1 shows the pressure fall-time curves observed with each catalyst, from which it can be seen that the reaction occurred in two distinct stages. In each case the onset of the second stage was accompanied by an increase in rate. The acceleration point, denoted as  $-\Delta_{Pa}$ , was obtained by extrapolating the first and the second stages of each reaction and finding the point of intersection. The acceleration occurred at a pressure fall of 31.5 torr and 30.0 torr respectively for the LRT and HRT catalysts.

##### 4.3.1.2 Deactivation Phenomena

A sample (0.0095g) of catalyst was reduced at 220°C. A series of hydrogenations were carried out consecutively at room temperature on the same catalyst sample. Between each reaction, the reaction vessel was evacuated for ten minutes to remove all the products of the previous hydrogenation. The variation of initial rate with reaction number is shown in figure 4.3.1.2.

##### 4.3.1.3 The Variation of Selectivity and Butene Distribution with Conversion at LRT and at HRT

Five successive hydrogenations, using a hydrogen:butadiene ratio of approximately 3 to 1 were carried out on two samples

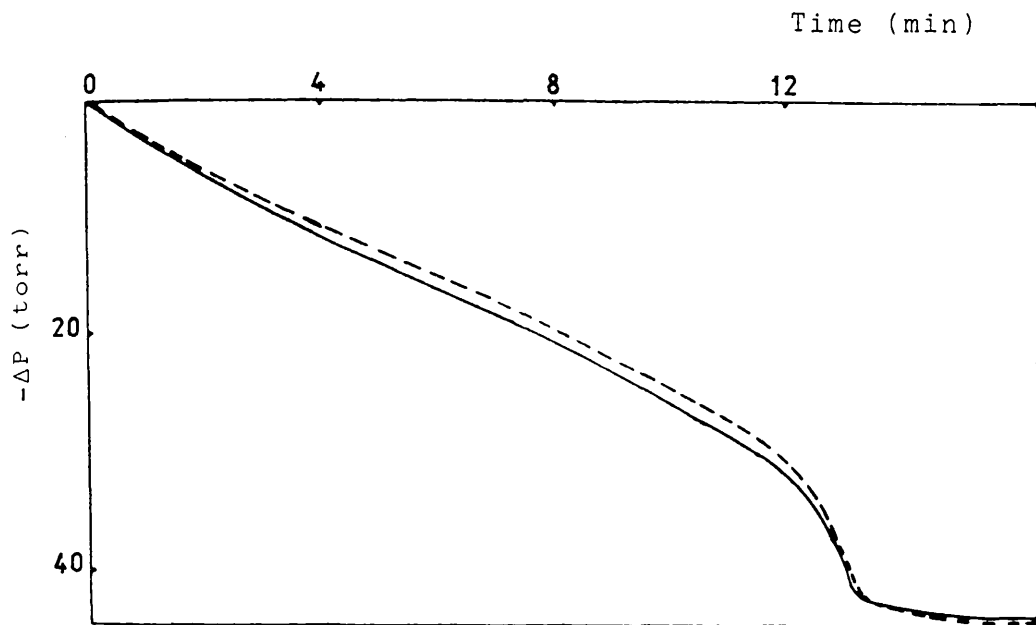


Figure 4.3.1.1 A typical pressure fall against time curve for the reaction of 25 torr of butadiene with 75 torr of hydrogen at  $20 \pm 2^\circ\text{C}$  over 5% Pt/SiO<sub>2</sub>. (Legend; LRT (220°C) ----- ; HRT (450°C) ——— )

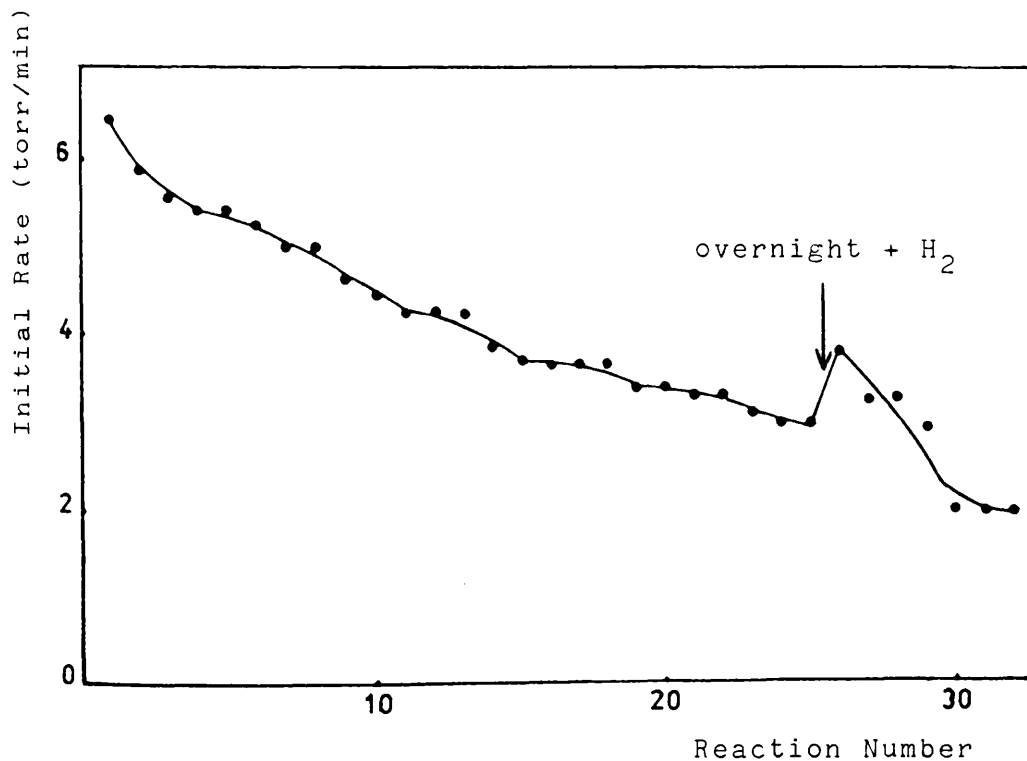


Figure 4.3.1.2 The Variation of Initial Rate with Reaction Number for the reaction of 25 torr of butadiene with 75 torr of hydrogen at  $20 \pm 2^\circ\text{C}$  over 5% Pt/SiO<sub>2</sub> reduced at low temperature (220°C).

of catalyst. The results are shown in Table 4.3.1.1. From these results, the selectivity and the initial distribution of butenes are obtained by extrapolation of figure 4.3.1.3. to zero conversion. The results are presented in Table 4.3.1.2.

Table 4.3.1.2

Catalyst Reduction Temperature (°C)	Initial Butene Distribution (%)			Selectivity
	1-B	<u>t</u> -2-B	<u>C</u> -2-B	
220	71.0	19.7	9.3	0.720
450	73.8	17.6	8.6	0.751

#### 4.3.1.4 Dependence of Butene Distribution upon Temperature and the Activation Energies for LRT and HRT Catalysts

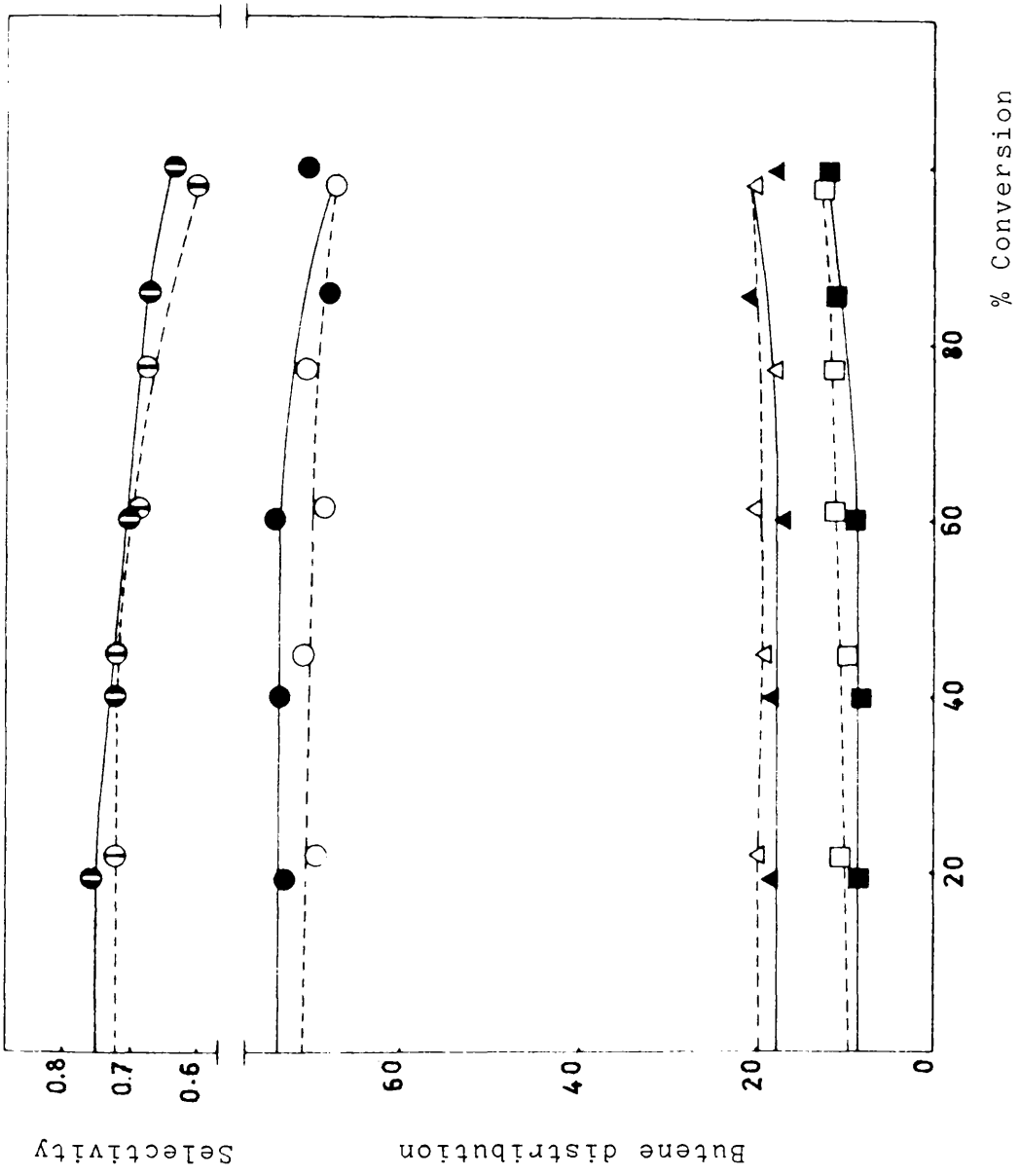
A series of reactions were carried out in the range 0° to 90°C (LRT) and 20° to 120°C (HRT) respectively using a standard 1:3::butadiene:hydrogen mixture. Each reaction was allowed to proceed to a percentage conversion of 40 ± 5% and then analysed. The results are shown in Table 4.3.1.3.

The activation energies were determined from the log (initial rate) versus (1/T) plots (figure 4.3.1.4) and were found to be 58.61 KJ mole<sup>-1</sup> and 57.84 KJ mole<sup>-1</sup> respectively, for catalyst samples reduced at low and high temperature.

Figure 4.3.1.3 The Variation of Selectivity and Butene distribution with Conversion (%) at  $20 \pm 2^\circ\text{C}$  over 5% Pt/SiO<sub>2</sub>.

(Legend; LRT (220°C))

- Selectivity; ---○--- 1-B;
  - △--- t-2-B; ---□--- c-2-B;
- HRT (450°C)
- Selectivity —●— 1-B
  - ▲— t-2-B; —■— c-2-B)



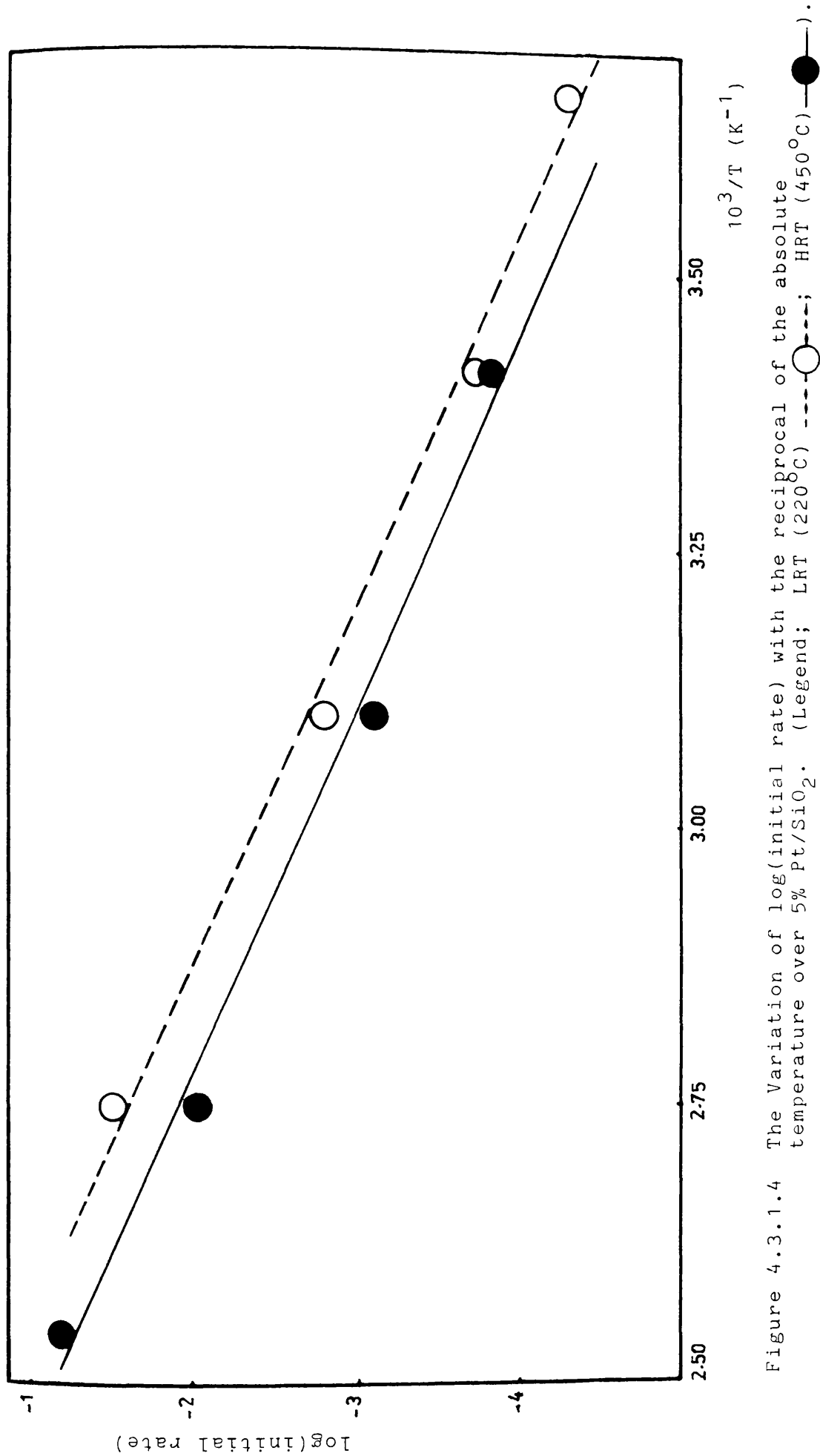


Figure 4.3.1.4 The Variation of log(initial rate) with the reciprocal of the absolute temperature over 5% Pt/SiO<sub>2</sub>. (Legend; LRT (220°C) ---○---; HRT (450°C) ---●---).

Table 4.3.1.1

Dependence of Butene Distribution and Selectivity upon Conversion over 5% Pt/SiO<sub>2</sub> reduced at LRT and at HRT at a reaction temperature of 20 ± 2°C; initial butadiene pressure 25 torr; initial hydrogen pressure 75 torr.

Reaction	Conversion (%)	Reduction Temperature (°C)	Butene Distribution			Selectivity
			1-B	<u>t</u> -2-B	<u>C</u> -2-B	
3	22.1	220	69.6	20.0	10.4	0.723
5	44.6	"	71.0	19.1	9.9	0.722
2	60.8	"	68.6	20.4	11.0	0.687
4	76.5	"	70.7	18.1	11.2	0.679
1	96.8	"	67.4	20.2	12.4	0.605
3	19.5	450	73.1	18.5	8.4	0.758
5	39.9	"	73.8	18.2	8.0	0.721
2	59.7	"	74.3	17.0	8.7	0.702
4	84.9	"	68.0	21.1	10.9	0.673
1	98.8	"	70.5	17.9	11.6	0.639

Table 4.3.1.3

The Variation of Initial Rate and Butene Distribution with  
Increasing Temperature over 5% Pt/SiO<sub>2</sub>

Reaction	Temperature (°C)	Butene Distribution			Initial Rate (torr/min)
		1-B	<u>t</u> -2-B	<u>C</u> -2-B	
Catalyst Reduction Temperature = 220°C					
5	0	66.4	21.0	12.6	0.03
1	20	65.3	20.8	13.9	0.11
3	50	67.6	21.4	11.0	0.97
2	90	56.5	27.2	16.3	18.18
Catalyst Reduction Temperature = 450°C					
1	20	68.0	21.3	10.7	0.09
3	50	70.8	17.7	11.5	0.49
2	90	58.0	24.4	17.6	5.61
4	120	55.1	27.5	17.4	38.34

#### 4.3.2 The Reaction of Butadiene with Hydrogen over 5% Pt/Al<sub>2</sub>O<sub>3</sub>

##### 4.3.2.1 The Pressure Fall against Time Curves for LRT and HRT Catalysts

(0.0105g) and (0.0080g) samples of catalyst were reduced respectively at low reduction temperature and high reduction temperature. Figure 4.3.2.1 shows the pressure fall-time curves observed with each catalyst, from which it can be seen that the reaction occurred in two distinct stages. In each case the onset of the second stage was accompanied by an increase in rate. The acceleration point, denoted as  $-\Delta P_a$ , was obtained by extrapolating the first and the second stages of each reaction and finding the point of intersection. The acceleration occurred at a pressure fall of 33.7 torr and 27.5 torr respectively for the LRT and HRT catalysts.

##### 4.3.2.2 Deactivation Phenomena

A sample (0.0105g) of catalyst was reduced at 230°C. A series of hydrogenations were carried out consecutively at room temperature on the same catalyst sample. Between each reaction, the reaction vessel was evacuated for ten minutes to remove all the products of the previous hydrogenation. The variation of initial rate with reaction number is shown in figure 4.3.2.2

##### 4.3.2.3 The Variation of Selectivity and Butene Distribution with Conversion at LRT and at HRT

Five successive hydrogenations, using a hydrogen:butadiene

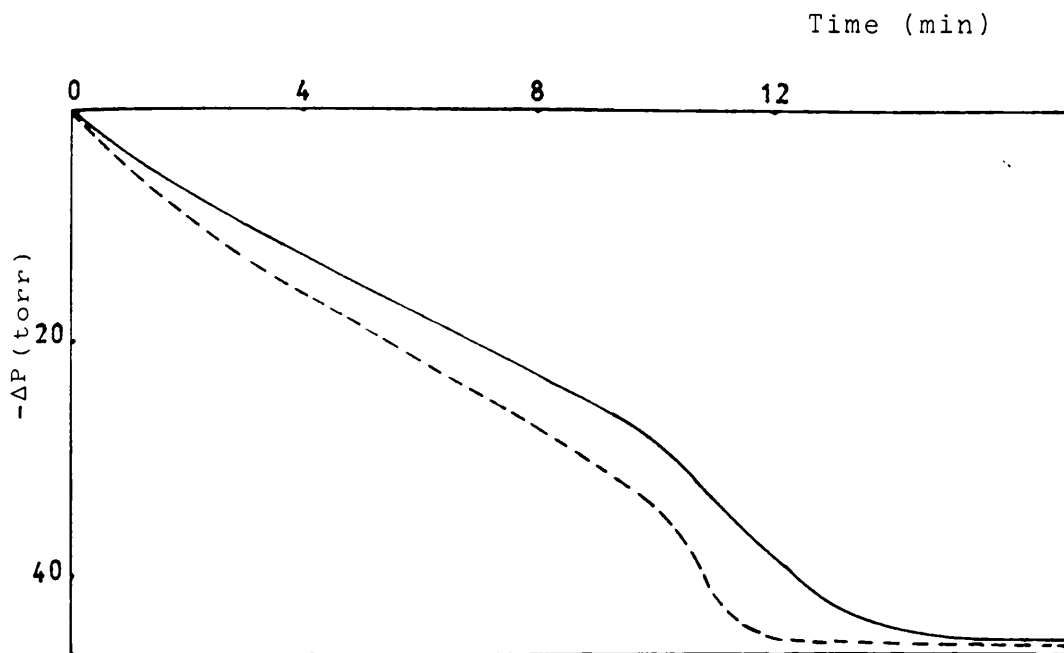


Figure 4.3.2.1 A typical pressure fall against time curve for the reaction of 25 torr of butadiene with 75 torr of hydrogen at  $20 \pm 2^\circ\text{C}$  over 5% Pt/Al<sub>2</sub>O<sub>3</sub>. (Legend; LRT (230°C) ----- ; HRT (449°C) ————— )

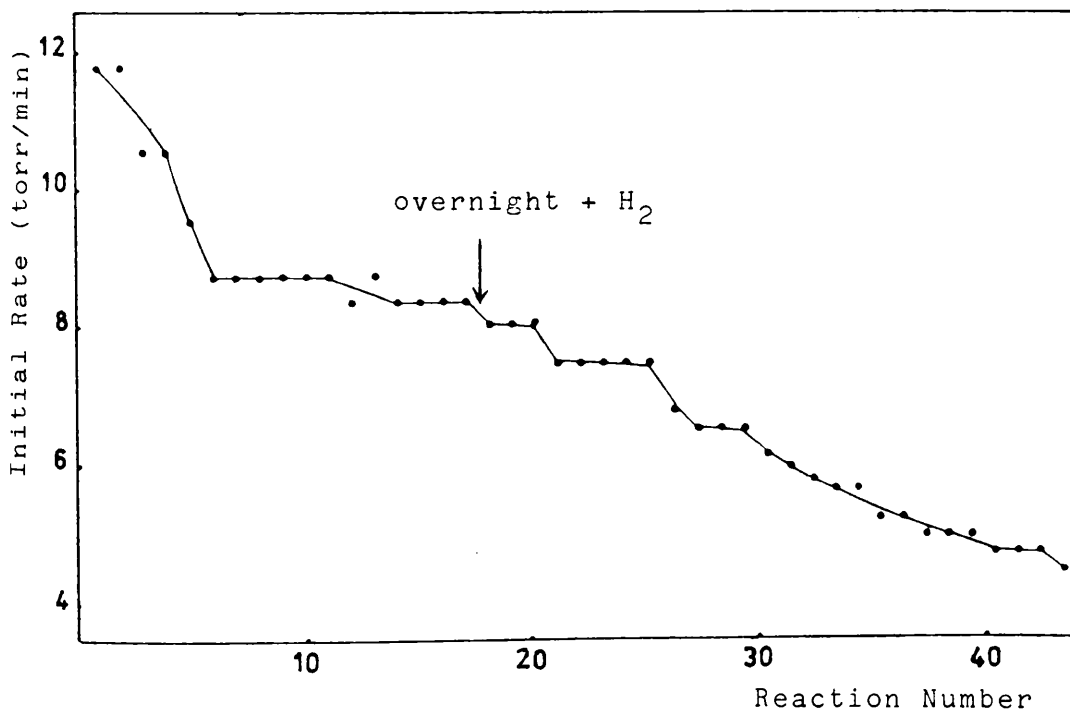


Figure 4.3.2.2 The Variation of Initial Rate with Reaction Number for the reaction of 25 torr of butadiene with 75 torr of hydrogen at  $20 \pm 2^\circ\text{C}$  over 5% Pt/Al<sub>2</sub>O<sub>3</sub> reduced at low temperature (230°C).

ratio of approximately 3 to 1 were carried out on two samples of catalyst. The results are shown in Table 4.3.2.1. From these results, the selectivity and the initial distribution of butenes are obtained by extrapolation of figure 4.3.2.3 to zero conversion. The results are presented in Table 4.3.2.2.

Table 4.3.2.2

Catalyst Reduction Temperature ( $^{\circ}\text{C}$ )	Initial Butene Distribution (%)			Selectivity
	1-B	<u>t</u> -2-B	<u>C</u> -2-B	
230	73.0	18.4	8.6	0.710
449	70.0	19.5	10.5	0.746

#### 4.3.2.4 Dependence of Butene Distribution upon Temperature and the Activation Energies for LRT and HRT Catalysts

A series of reactions were carried out in the range  $0^{\circ}$  to  $90^{\circ}\text{C}$  (LRT) and  $20^{\circ}$  to  $120^{\circ}\text{C}$  (HRT) respectively using a standard 1:3::butadiene:hydrogen mixture. Each reaction was allowed to proceed to a percentage conversion of  $40 \pm 5\%$  and then analysed. The results are shown in Table 4.3.2.3. The activation energies were determined from the log (initial rate) versus ( $1/T$ ) plots (figure 4.3.2.4) and were found to be  $49.19 \text{ KJ mole}^{-1}$  and  $50.49 \text{ KJ mole}^{-1}$  respectively for catalyst samples reduced at low and high temperature.

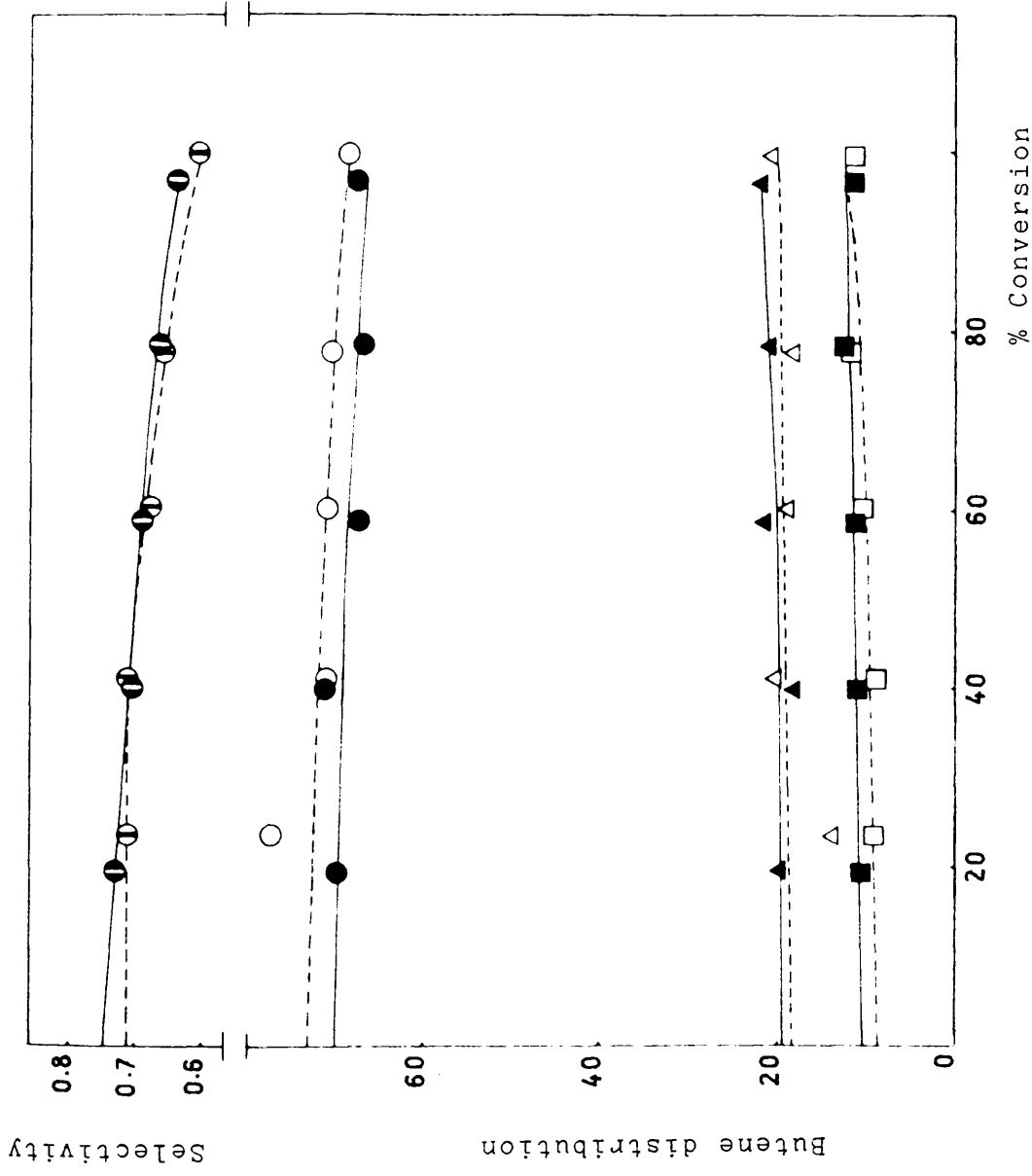


Figure 4.3.2.3 The Variation of Selectivity and Butene distribution with Conversion (%) at  $20 \pm 2^\circ\text{C}$  over 5% Pt/Al<sub>2</sub>O<sub>3</sub>.

(Legend; LRT (230°C)  
 ---○--- Selectivity; ---○--- 1-B;  
 ---△--- t-2-B; ---□--- c-2-B;  
 HRT (449°C)  
 ---●--- Selectivity; ---●--- 1-B;  
 ---▲--- t-2-B; ---■--- c-2-B).

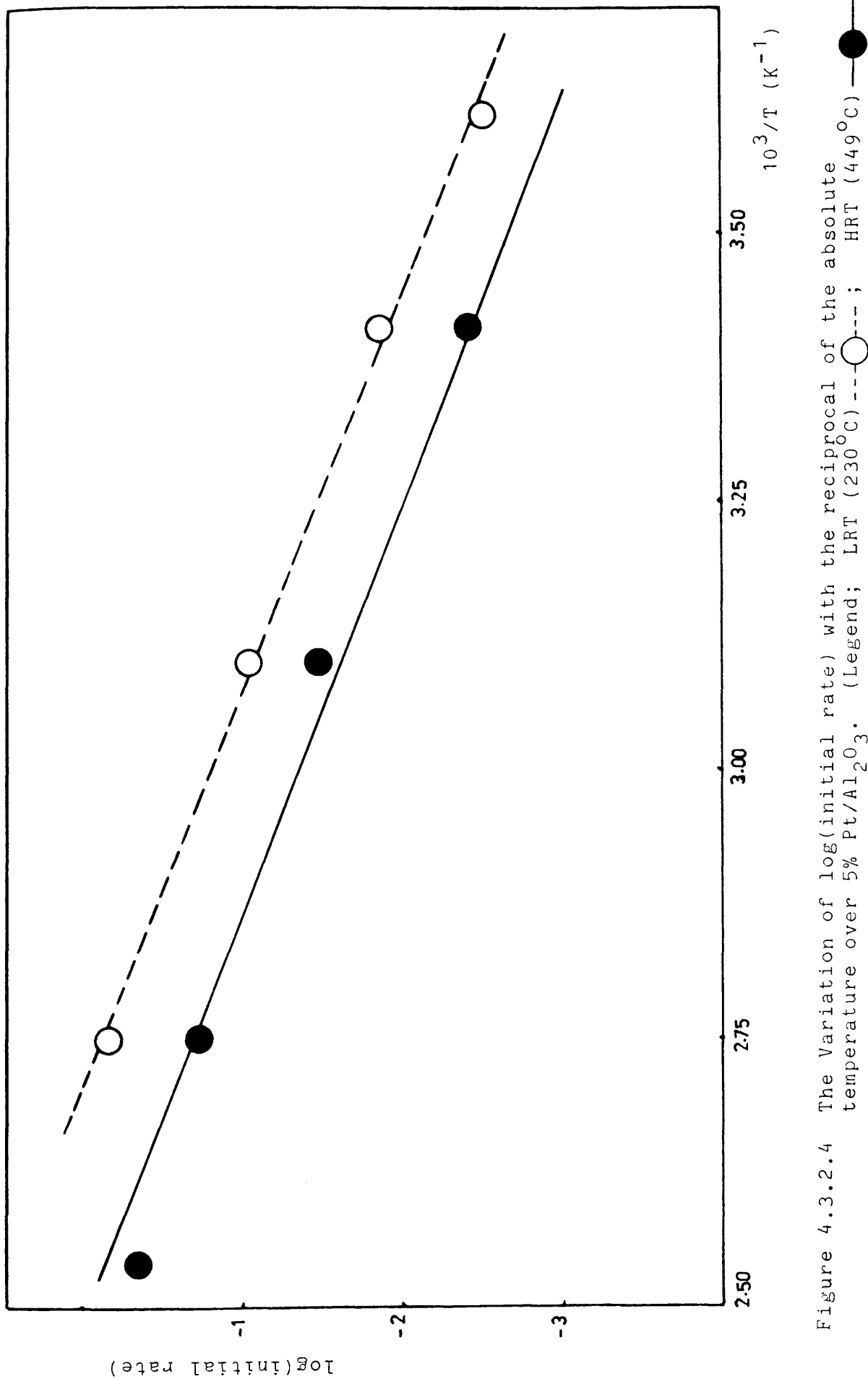


Figure 4.3.2.4 The Variation of  $\log(\text{initial rate})$  with the reciprocal of the absolute temperature over 5% Pt/Al<sub>2</sub>O<sub>3</sub>. (Legend; LRT (230°C) ---○---; HRT (449°C) —●—).

Table 4.3.2.1

The Variation of Butene Distribution and Selectivity with Conversion over 5% Pt/Al<sub>2</sub>O<sub>3</sub> reduced at LRT and at HRT at a reaction temperature of 20 ± 2°C; initial buta-1:3-diene pressure 25 torr; initial hydrogen pressure 75 torr.

Reaction	Conversion (%)	Reduction Temperature (°C)	Butene Distribution			Selectivity
			1-B	<u>t</u> -2-B	<u>C</u> -2-B	
3	23.7	230	77.1	13.7	9.2	0.712
5	41.2	"	71.0	20.2	8.8	0.712
2	60.3	"	70.7	18.9	10.4	0.675
4	77.7	"	70.2	18.2	11.6	0.656
1	99.8	"	68.4	20.5	11.1	0.606
3	19.6	449	69.6	19.7	10.7	0.727
5	40.1	"	71.0	18.0	11.0	0.702
2	58.9	"	67.3	21.4	11.3	0.688
4	78.5	"	66.7	20.9	12.4	0.660
1	96.8	"	67.1	21.6	11.3	0.635

Table 4.3.2.3

The Variation of Initial Rate and Butene Distribution with increasing Temperature over 5% Pt/Al<sub>2</sub>O<sub>3</sub>

Reaction	Temperature (°C)	Butene Distribution			Initial Rate (torr/min)
		1-B	<u>t</u> -2-B	<u>C</u> -2-B	
Catalyst Reduction Temperature = 230°C					
5	0	69.0	19.4	11.6	0.18
1	20	71.1	19.7	9.2	0.81
3	50	68.4	19.3	12.3	5.26
2	90	60.9	23.2	15.9	40.00
Catalyst Reduction Temperature = 449°C					
1	20	66.9	21.0	12.1	0.23
3	50	66.5	20.6	12.9	1.93
2	90	63.0	21.3	15.7	11.06
4	120	53.7	28.0	18.3	26.89

### 4.3.3 The Reaction of Butadiene with Hydrogen over 5% Pt/TiO<sub>2</sub>

#### 4.3.3.1 The Pressure Fall against Time Curves for LTR and HRT Catalysts

(0.0100g) and (0.0104g) samples of catalyst were reduced respectively at low reduction temperature and high reduction temperature. Figure 4.3.3.1 shows the pressure fall-time curves observed with each catalyst, from which it can be seen that the reaction occurred in two distinct stages. In each case the onset of the second stage was accompanied by an increase in rate. The acceleration point, denoted as  $-\Delta P_a$ , was obtained by extrapolating the first and the second stages of each reaction and finding the point of intersection. The acceleration occurred at a pressure fall of 33.2 torr and 32.2 torr respectively for the LRT and HRT catalysts.

#### 4.3.3.2 Deactivation Phenomena

A sample (0.0103g) of catalyst was reduced at 200°C. A series of hydrogenations were carried out consecutively at room temperature on the same catalyst sample. Between each reaction, the reaction vessel was evacuated for ten minutes to remove all the products of the previous hydrogenation. The variation of initial rate with reaction number is shown in figure 4.3.3.2

#### 4.3.3.3 The Variation of Selectivity and Butene Distribution with Conversion at LRT and at HRT

Five successive hydrogenations, using a hydrogen:butadiene ratio of approximately 3 to 1 were carried out on two samples

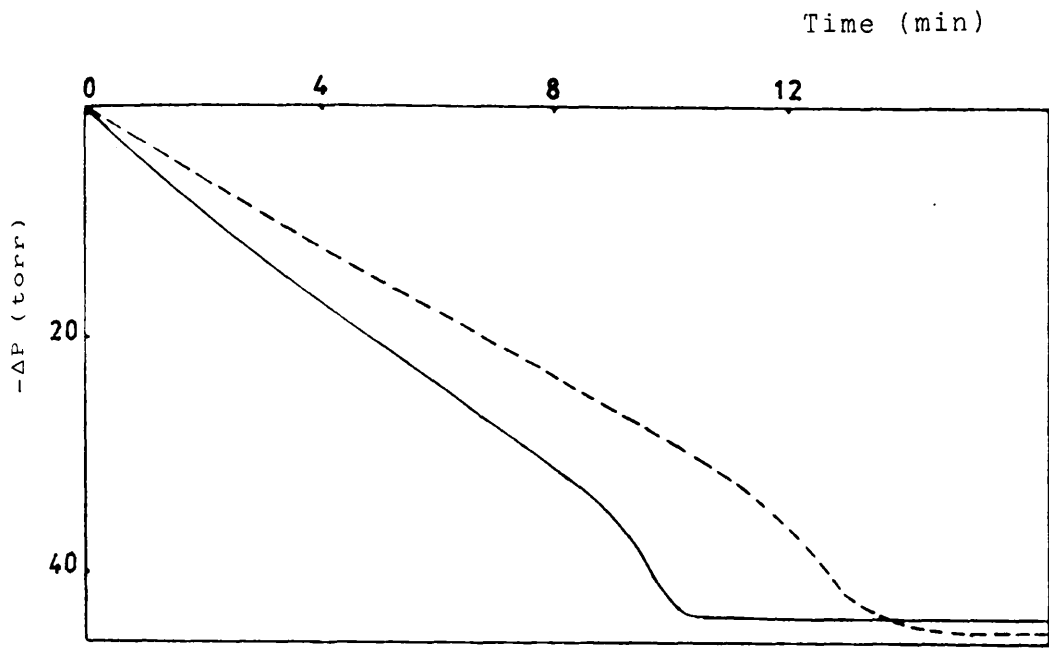


Figure 4.3.3.1 A typical pressure fall against time curve for the reaction of 25 torr of butadiene with 75 torr of hydrogen at  $20 \pm 2^\circ\text{C}$  over 5% Pt/TiO<sub>2</sub>. (Legend; LRT (200°C) ----- ; HRT (450°C) ——— ).

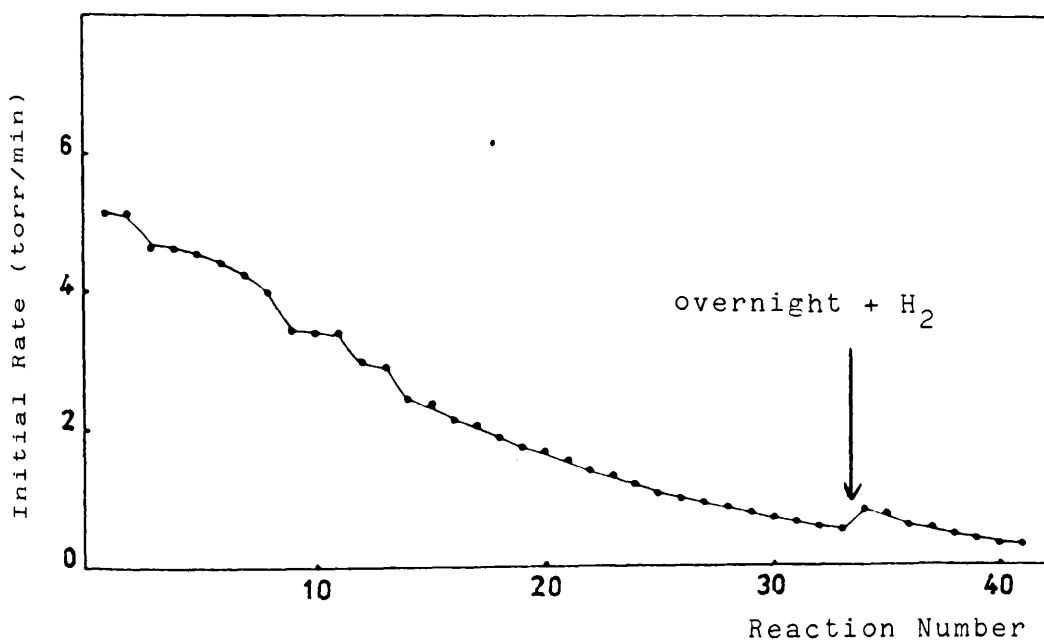


Figure 4.3.3.2 The Variation of Initial Rate with Reaction Number for the reaction of 25 torr of butadiene with 75 torr of hydrogen at  $20 \pm 2^\circ\text{C}$  over 5% Pt/TiO<sub>2</sub> reduced at low temperature (200°C).

of catalyst. The results are shown in Table 4.3.3.1. From these results, the selectivity and the initial distribution of butenes are obtained by extrapolation of figure 4.3.3.3 to zero conversion. The results are presented in Table 4.3.3.2.

Table 4.3.3.2

Catalyst Reduction Temperature ( $^{\circ}\text{C}$ )	Initial Butene Distribution (%)			Selectivity
	1-B	<u>t</u> -2-B	<u>C</u> -2-B	
200	77.3	12.6	10.1	0.698
450	75.0	14.0	11.0	0.667

4.3.3.4 Dependence of Butene Distribution upon Temperature and the Activation Energies for LRT and HRT catalysts

A series of reactions were carried out in the range  $20^{\circ}$  to  $90^{\circ}\text{C}$  (LRT) and  $20^{\circ}$  to  $120^{\circ}\text{C}$  (HRT) respectively using a standard 1:3::butadiene:hydrogen mixture. Each reaction was allowed to proceed to a percentage conversion of  $40 \pm 5\%$  and then analysed. The results are shown in Table 4.3.3.3. The activation energies were determined from the log (initial rate) versus  $(1/T)$  plots (figure 4.3.3.4) and were found to be  $42.33 \text{ KJ mole}^{-1}$  and  $59.57 \text{ KJ mole}^{-1}$  respectively for catalyst samples reduced at low and high temperature.

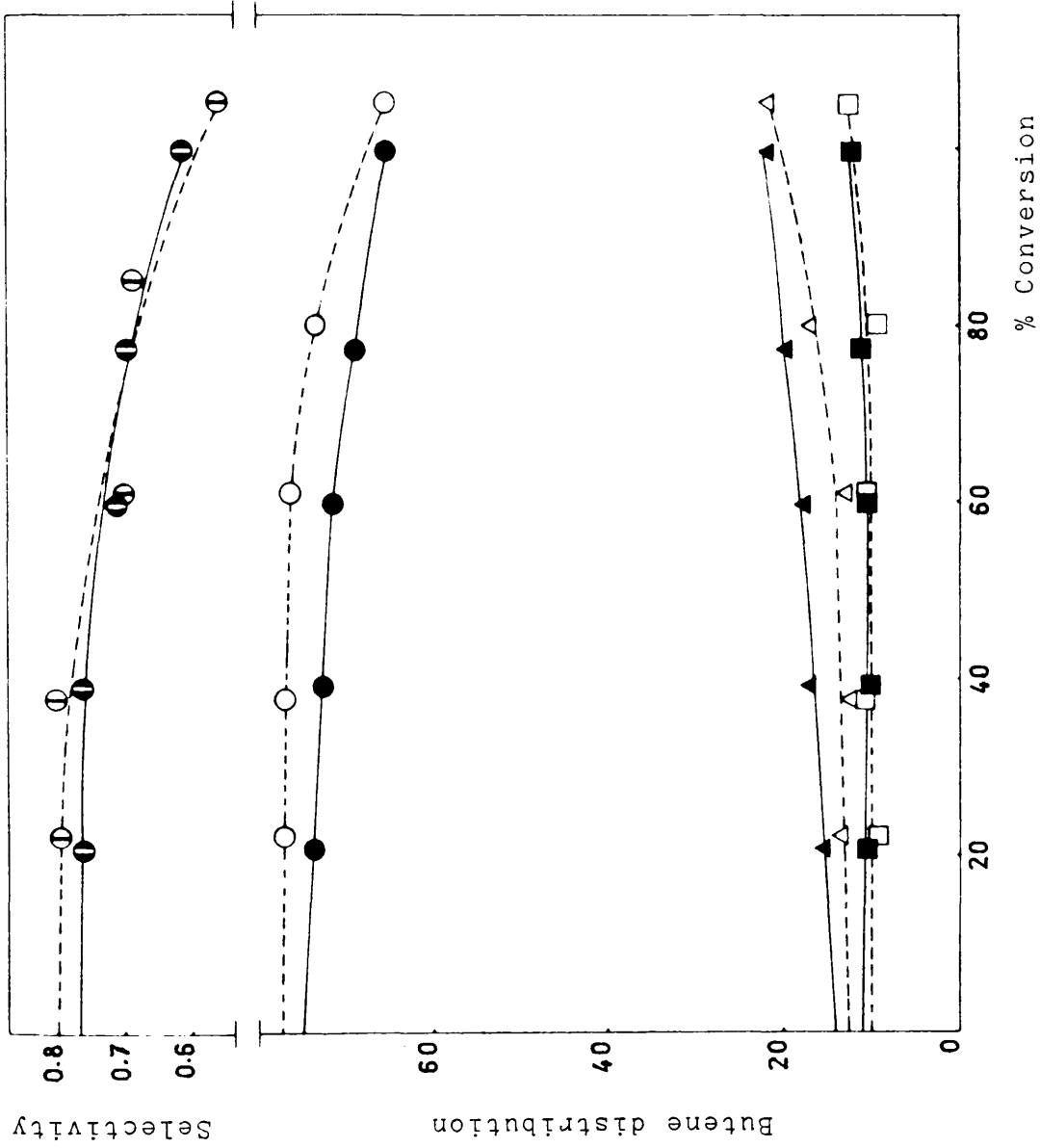
Figure 4.3.3.3 The Variation of Selectivity and Butene distribution with Conversion (%) at  $20 \pm 2^\circ\text{C}$  over 5% Pt/TiO<sub>2</sub>

(Legend; LRT (200°C)

---○--- Selectivity; ---○--- 1-B;  
 ---△--- t-2-B ---□--- c-2-B;

HRT (450°C)

—●— Selectivity —●— 1-B;  
 —▲— t-2-B —■— c-2-B)



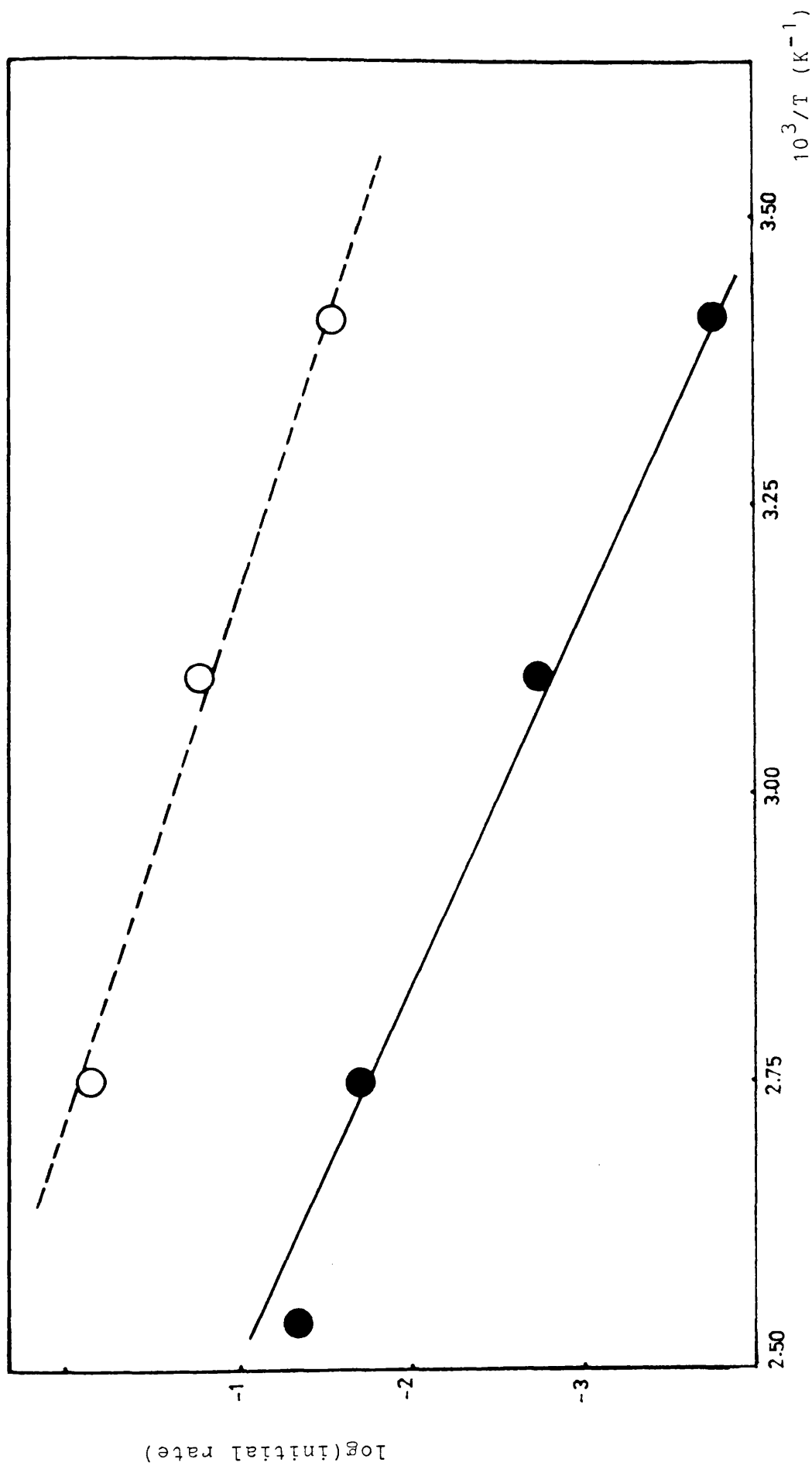


Figure 4.3.3.4 The Variation of  $\log(\text{initial rate})$  with the reciprocal of the absolute temperature over 5% Pt/TiO<sub>2</sub>. (Legend; LRT (200°C)-●-; HRT (450°C)-○-).

Table 4.3.3.1

The Variation of Butene Distribution and Selectivity with Conversion over 5% Pt/TiO<sub>2</sub> reduced at LRT and at HRT at a Reaction Temperature of 20 ± 2°C; initial buta-1:3-diene pressure 25 torr; initial hydrogen pressure 75 torr.

Reaction	Conversion (%)	Reduction Temperature (°C)	Butene Distribution			Selectivity
			1-B	<u>t</u> -2-B	<u>C</u> -2-B	
3	22.3	200	77.3	13.5	9.2	0.696
5	37.8	"	77.2	12.1	10.7	0.705
2	61.1	"	76.6	12.8	10.6	0.605
4	80.1	"	73.7	17.0	9.3	0.590
1	105.1	"	65.8	21.6	12.6	0.466
3	20.9	450	73.8	15.5	10.7	0.660
5	39.2	"	72.7	17.0	10.3	0.620
2	59.9	"	71.7	17.7	10.6	0.613
4	77.4	"	69.0	19.6	11.4	0.600
1	99.8	"	65.8	21.8	12.4	0.517

Table 4.3.3.3

The Variation of Initial Rate and Butene Distribution with  
increasing Temperature over 5% Pt/TiO<sub>2</sub>

Reaction	Temperature (°C)	Butene Distribution			Initial Rate (torr/min)
		1-B	<u>t</u> -2-B	<u>C</u> -2-B	
Catalyst Reduction Temperature = 200°C					
1	20	75.2	14.8	10.0	1.71
3	50	68.9	18.5	12.6	10.00
2	90	53.3	28.9	17.8	43.48
Catalyst Reduction Temperature = 450°C					
1	20	71.3	17.8	10.9	0.01
3	50	65.9	21.2	12.9	0.11
2	90	63.4	22.4	14.2	1.21
4	120	60.4	24.2	15.4	2.78

#### 4.3.4 The Reaction of Butadiene with Hydrogen over 5% Rh/SiO<sub>2</sub>

##### 4.3.4.1 The Pressure Fall against Time Curves for LRT and HRT Catalysts

(0.0091g) and (0.0079g) samples of catalyst were reduced respectively at low reduction temperature and at high reduction temperature. Figure 4.3.4.1 shows the pressure fall-time curves observed with each catalyst, from which it can be seen that the reaction occurred in two distinct stages. In each case the onset of the second stage was accompanied by an increase in rate. The acceleration point, denoted as  $-\Delta P_a$ , was obtained by extrapolating the first and the second stages of each reaction and finding the point of intersection. The acceleration occurred at a pressure fall of 25.2 torr and 24.0 torr respectively for the LRT and HRT catalysts.

##### 4.3.4.2 Deactivation Phenomena

A sample (0.0091g) of catalyst was reduced at 250°C. A series of hydrogenations were carried out consecutively at room temperature on the same catalyst sample. Between each reaction, the reaction vessel was evacuated for ten minutes to remove all the products of the previous hydrogenation. The variation of initial rate with reaction number is shown in figure 4.3.4.2.

##### 4.3.4.3 The Variation of Selectivity and Butene Distribution with Conversion at LRT and at HRT

Five successive hydrogenations, using a hydrogen:butadiene ratio of approximately 3 to 1 were carried out on two samples of catalyst. The results are shown in Table 4.3.4.1. From these

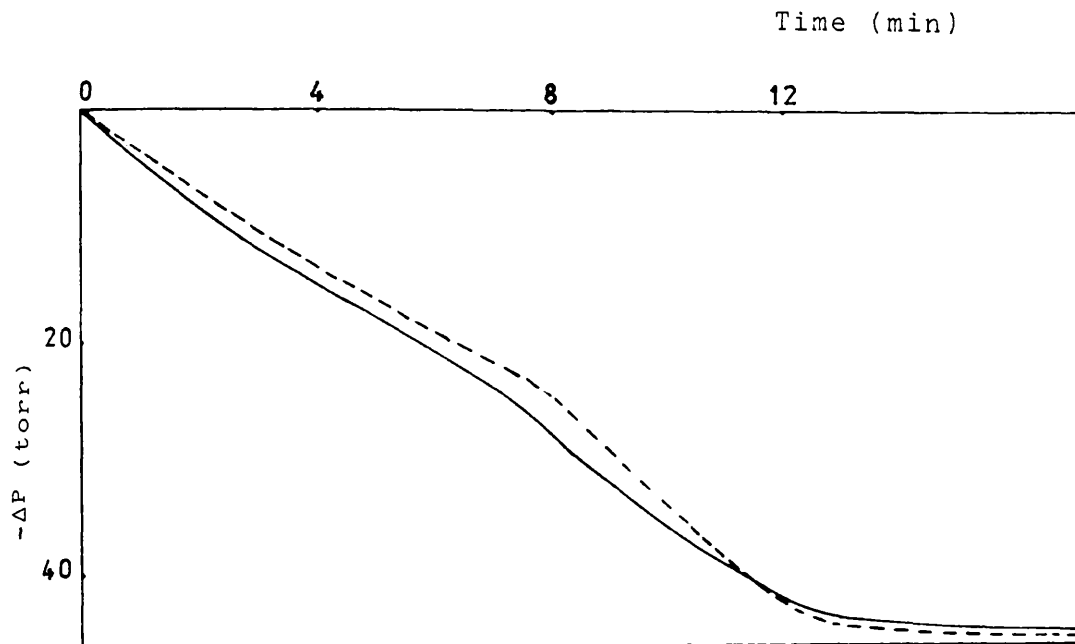


Figure 4.3.4.1 A typical pressure fall against time curve for the reaction of 25 torr of butadiene with 75 torr of hydrogen at  $20 \pm 2^\circ\text{C}$  over 5% Rh/SiO<sub>2</sub>. (Legend; LRT (250°C) ----- ; HRT (450°C) ————— ).

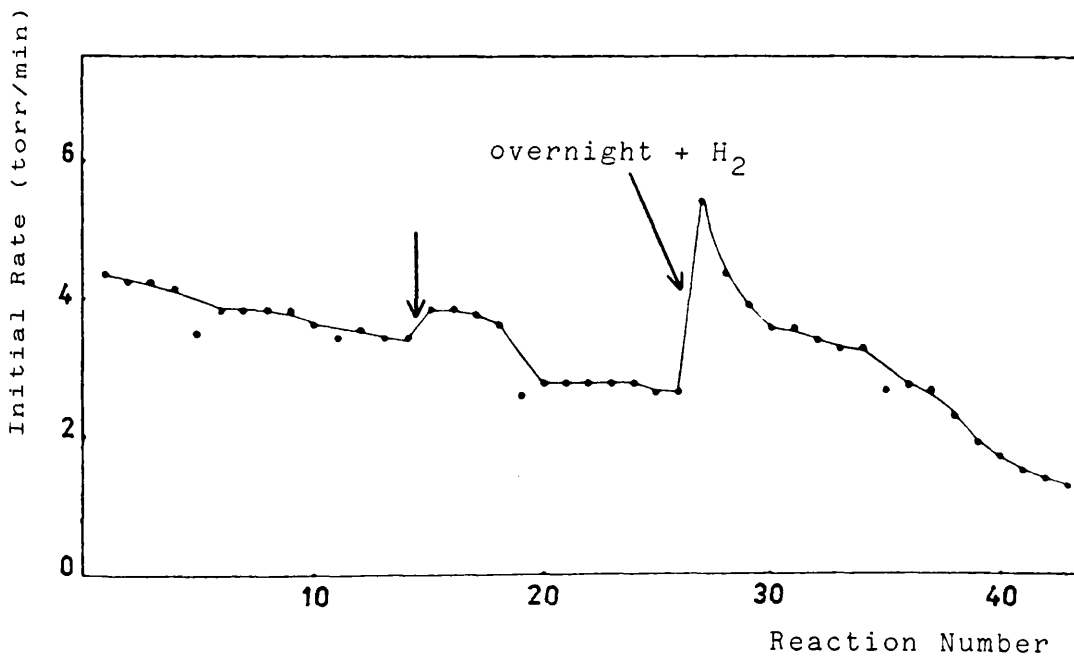


Figure 4.3.4.2 The Variation of Initial Rate with Reaction Number for the reaction of 25 torr of butadiene with 75 torr of hydrogen at  $20 \pm 2^\circ\text{C}$  over 5% Rh/SiO<sub>2</sub> reduced at low temperature (250°C).

results, the selectivity and the initial distribution of butenes are obtained by extrapolation of figure 4.3.4.3 to zero conversion. The results are presented in Table 4.3.4.2.

Table 4.3.4.2

Catalyst Reduction Temperature ( $^{\circ}\text{C}$ )	Initial Butene Distribution (%)			Selectivity
	1-B	<u>t</u> -2-B	<u>C</u> -2-B	
250	58.4	25.7	15.9	0.920
450	56.5	27.6	15.9	0.905

4.3.4.4 Dependence of Butene Distribution upon Temperature and the Activation Energies for LRT and HRT Catalysts

A series of reactions were carried out in the range  $20^{\circ}$  to  $90^{\circ}\text{C}$  (LRT) and  $0^{\circ}$  to  $50^{\circ}\text{C}$  (HRT) respectively using a standard 1:3::butadiene:hydrogen mixture. Each reaction was allowed to proceed to a percentage conversion of  $40 \pm 5\%$  and then analysed. The results are shown in Table 4.3.4.3. The activation energies were determined from the log (initial rate) versus  $(1/T)$  plots (figure 4.3.4.4) and were found to be  $51.07 \text{ KJ mole}^{-1}$  and  $50.11 \text{ KJ mole}^{-1}$  respectively for catalyst samples reduced at low and high temperature.

Selectivity

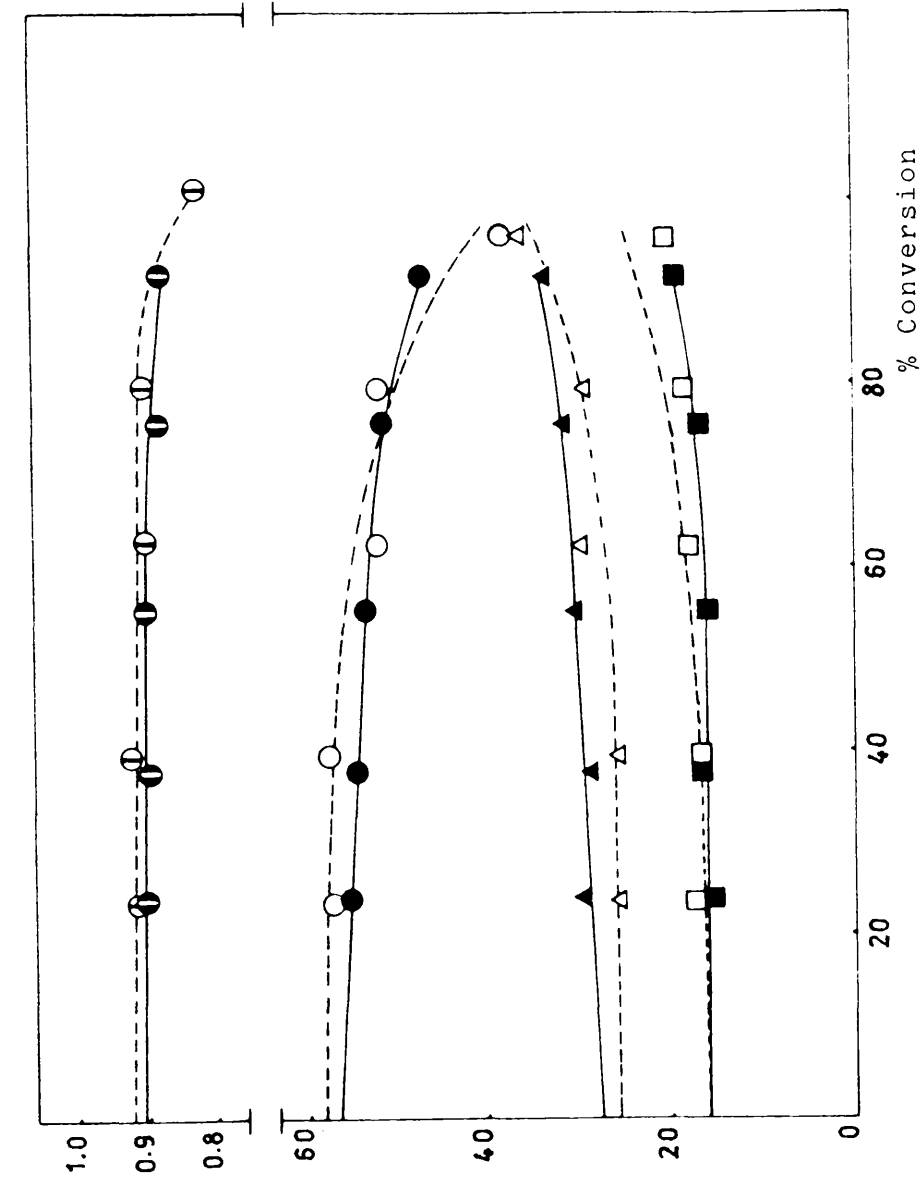


Figure 4.3.4.3 The Variation of Selectivity and Butene distribution with Conversion (%) at 20 + 20C over 5% Rh/SiO<sub>2</sub> (Legend; LRT (250°C))

- Selectivity; 1-B
  - △--- t-2-B
  - c-2-B
  - Selectivity; 1-B
  - ▲--- t-2-B
  - c-2-B
- HRT (450°C)

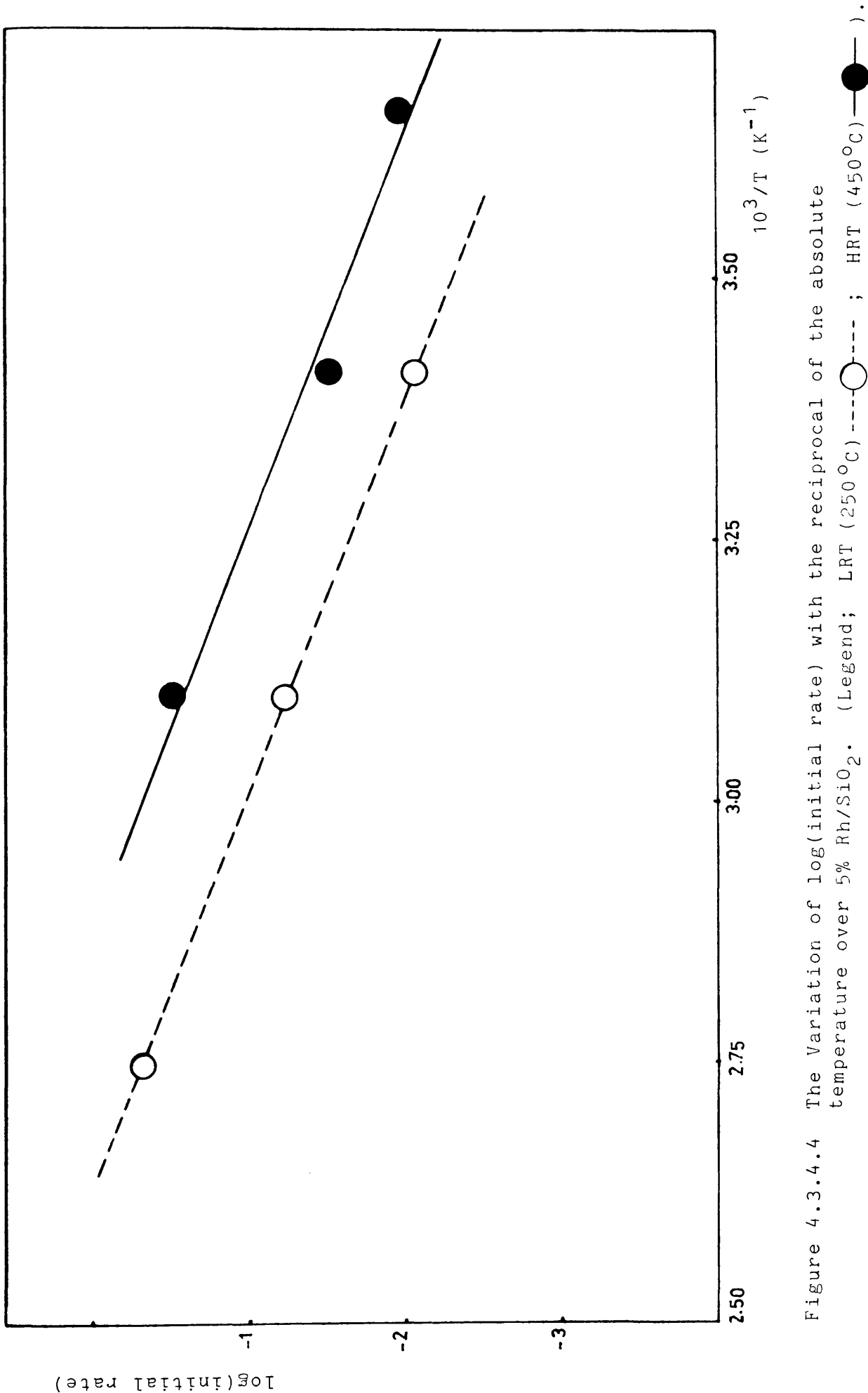


Figure 4.3.4.4 The Variation of  $\log(\text{initial rate})$  with the reciprocal of the absolute temperature over 5% Rh/SiO<sub>2</sub>. (Legend; LRT (250°C) ---○--- ; HRT (450°C) —●—).

Table 4.3.4.1

The Variation of Butene Distribution and Selectivity with Conversion over 5% Rh/SiO<sub>2</sub> reduced at LRT and at HRT at a reaction temperature of 20 ± 2°C; initial buta-1:3-diene pressure 25 torr; initial hydrogen pressure 75 torr.

Reaction	Conversion (%)	Reduction Temperature (°C)	Butene Distribution			Selectivity
			1-B	<u>t</u> -2-B	<u>C</u> -2-B	
3	23.7	250	57.3	25.6	17.1	0.913
5	39.6	"	57.7	25.7	16.6	0.921
2	62.9	"	52.4	29.8	17.8	0.902
4	79.5	"	52.2	29.4	18.4	0.902
1	101.0	"	38.4	36.3	25.3	0.828
3	24.1	450	55.3	29.5	15.2	0.900
5	37.9	"	54.7	28.7	16.6	0.895
2	55.4	"	53.7	30.4	15.9	0.901
4	75.7	"	51.7	31.5	16.8	0.885
1	91.8	"	47.1	33.6	19.3	0.879

Table 4.3.4.3

The Variation of Initial Rate and Butene Distribution with increasing Temperature over 5% Rh/SiO<sub>2</sub>

Reaction	Temperature (°C)	Butene Distribution			Initial Rate (torr/min)
		1-B	<u>t</u> -2-B	<u>C</u> -2-B	
Catalyst Reduction Temperature = 250°C					
1	20	53.0	27.7	19.3	0.51
3	50	51.0	29.1	19.9	3.45
2	90	33.5	41.9	24.6	28.57
Catalyst Reduction Temperature = 450°C					
5	0	48.8	30.2	21.0	0.63
1	20	55.9	30.2	13.9	1.79
3	50	44.6	30.4	25.0	18.18

#### 4.3.5 The Reaction of Butadiene with Hydrogen over 5% Rh/Al<sub>2</sub>O<sub>3</sub>

##### 4.3.5.1 The Pressure Fall against Time Curves for LRT and HRT Catalysts

(0.0109g) and (0.0050g) samples of catalyst were reduced respectively at low reduction temperature and at high reduction temperature. Figure 4.3.5.1 shows the pressure fall-time curves observed with each catalyst, from which it can be seen that the reaction occurred in two distinct stages. In each case the onset of the second stage was accompanied by an increase in rate. The acceleration point, denoted as  $-\Delta P_a$ , was obtained by extrapolating the first and the second stages of each reaction and finding the point of intersection. The acceleration occurred at a pressure fall of 24.5 torr and 25.0 torr respectively for the LRT and HRT catalysts.

##### 4.3.5.2 Deactivation Phenomena

A sample (0.0109g) of catalyst was reduced at 230°C. A series of hydrogenations were carried out consecutively at room temperature on the same catalyst sample. Between each reaction, the reaction vessel was evacuated for ten minutes to remove all the products of the previous hydrogenation. The variation of initial rate with reaction number is shown in figure 4.3.5.2.

##### 4.3.5.3 The Variation of Selectivity and Butene Distribution with Conversion at LRT and at HRT

Five successive hydrogenations, using a hydrogen:butadiene ratio of approximately 3 to 1 were carried out on two samples of catalyst. The results are shown in Table 4.3.5.1. From these

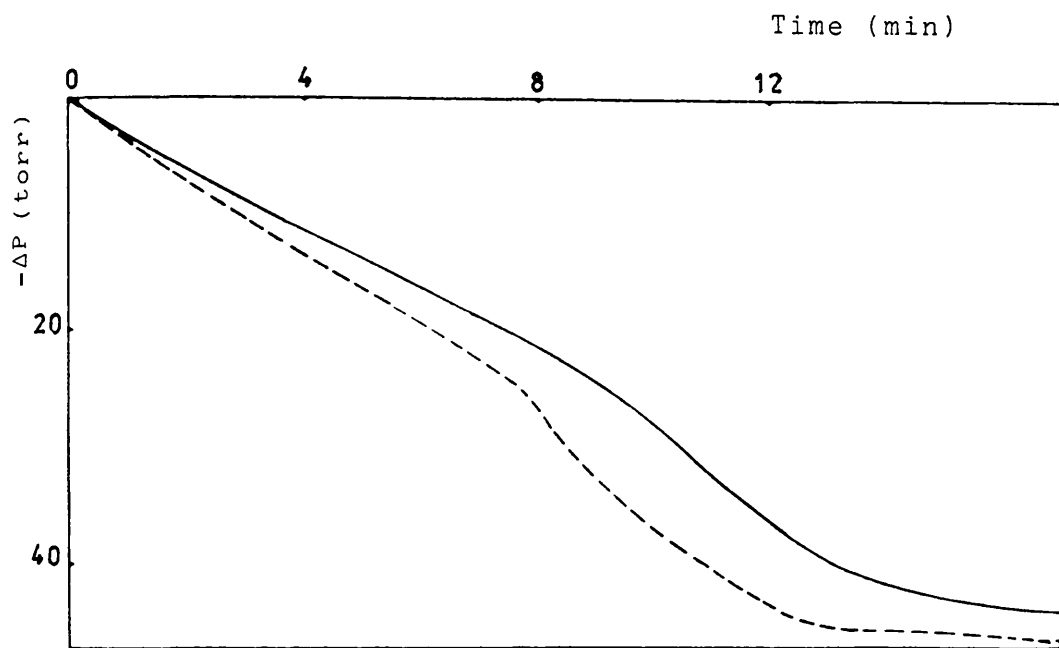


Figure 4.3.5.1 A typical pressure fall against time curve for the reaction of 25 torr of butadiene with 75 torr of hydrogen at  $20 \pm 2^\circ\text{C}$  over 5% Rh/Al<sub>2</sub>O<sub>3</sub>. (Legend; LRT (230°C) ----- ; HRT (450°C) ————— ).

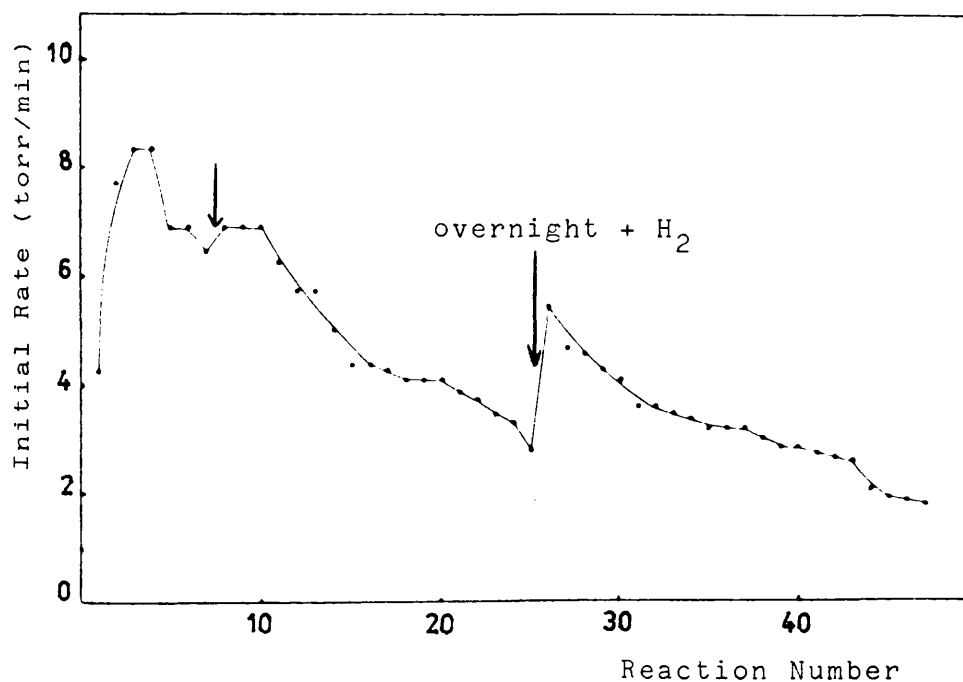


Figure 4.3.5.2 The Variation of Initial Rate with Reaction Number for the reaction of 25 torr of butadiene with 75 torr of hydrogen at  $20 \pm 2^\circ\text{C}$  over 5% Rh/Al<sub>2</sub>O<sub>3</sub> reduced at low temperature (230°C).

results, the selectivity and the initial distribution of butenes are obtained by extrapolation of figure 4.3.5.3 to zero conversion. The results are presented in Table 4.3.5.2.

Table 4.3.5.2

Catalyst Reduction Temperature ( $^{\circ}\text{C}$ )	Initial Butene Distribution (%)			Selectivity
	1-B	<u>t</u> -2-B	<u>C</u> -2-B	
230	57.5	29.0	13.5	0.932
450	60.0	25.1	14.9	0.893

#### 4.3.5.4 Dependence of Butene Distribution upon Temperature and the Activation Energies for LRT and HRT Catalysts

A series of reactions were carried out in the range  $20^{\circ}$  to  $90^{\circ}\text{C}$  (LRT) and  $20^{\circ}$  to  $90^{\circ}\text{C}$  (HRT) respectively using a standard 1:3::butadiene:hydrogen mixture. Each reaction was allowed to proceed to a percentage conversion of  $40 \pm 5\%$  and then analysed. The results are shown in Table 4.3.5.3. The activation energies were determined from the log (initial rate) versus  $(1/T)$  plots (figure 4.3.5.4) and were found to be  $42.22 \text{ KJ mole}^{-1}$  and  $37.39 \text{ KJ mole}^{-1}$  respectively for catalyst samples reduced at low and high temperature.

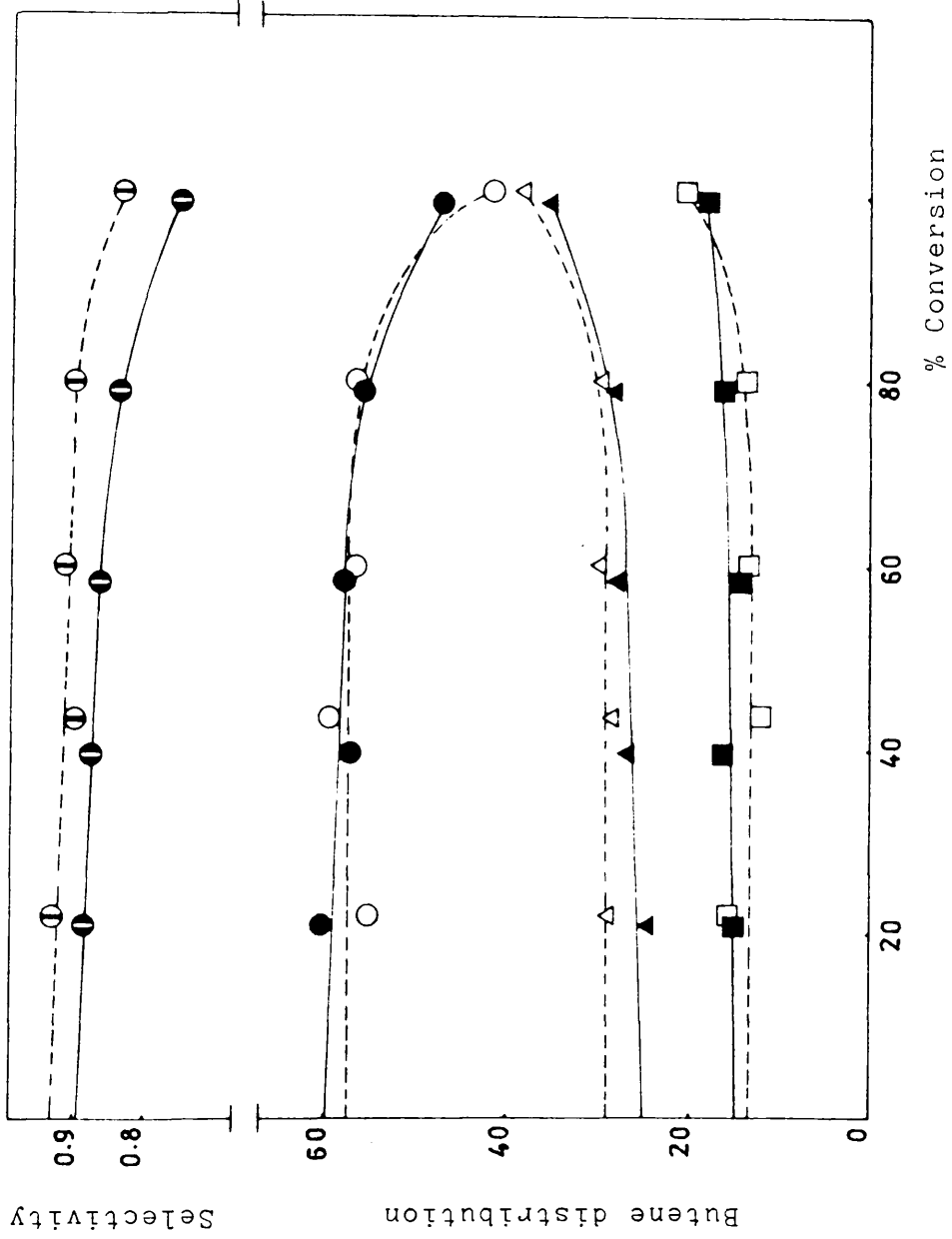


Figure 4.3.5.3 The Variation of Selectivity and Butene distribution with Conversion (%) at  $20 \pm 2^\circ\text{C}$  over 5% Rh/Al<sub>2</sub>O<sub>3</sub>.

(Legend; LRT (230°C))

- Selectivity; ---○--- 1-B
  - △--- t-2-B; ---□--- c-2-B
- HRT (450°C)
- Selectivity; ---●--- 1-B
  - ▲--- t-2-B; ---■--- c-2-B

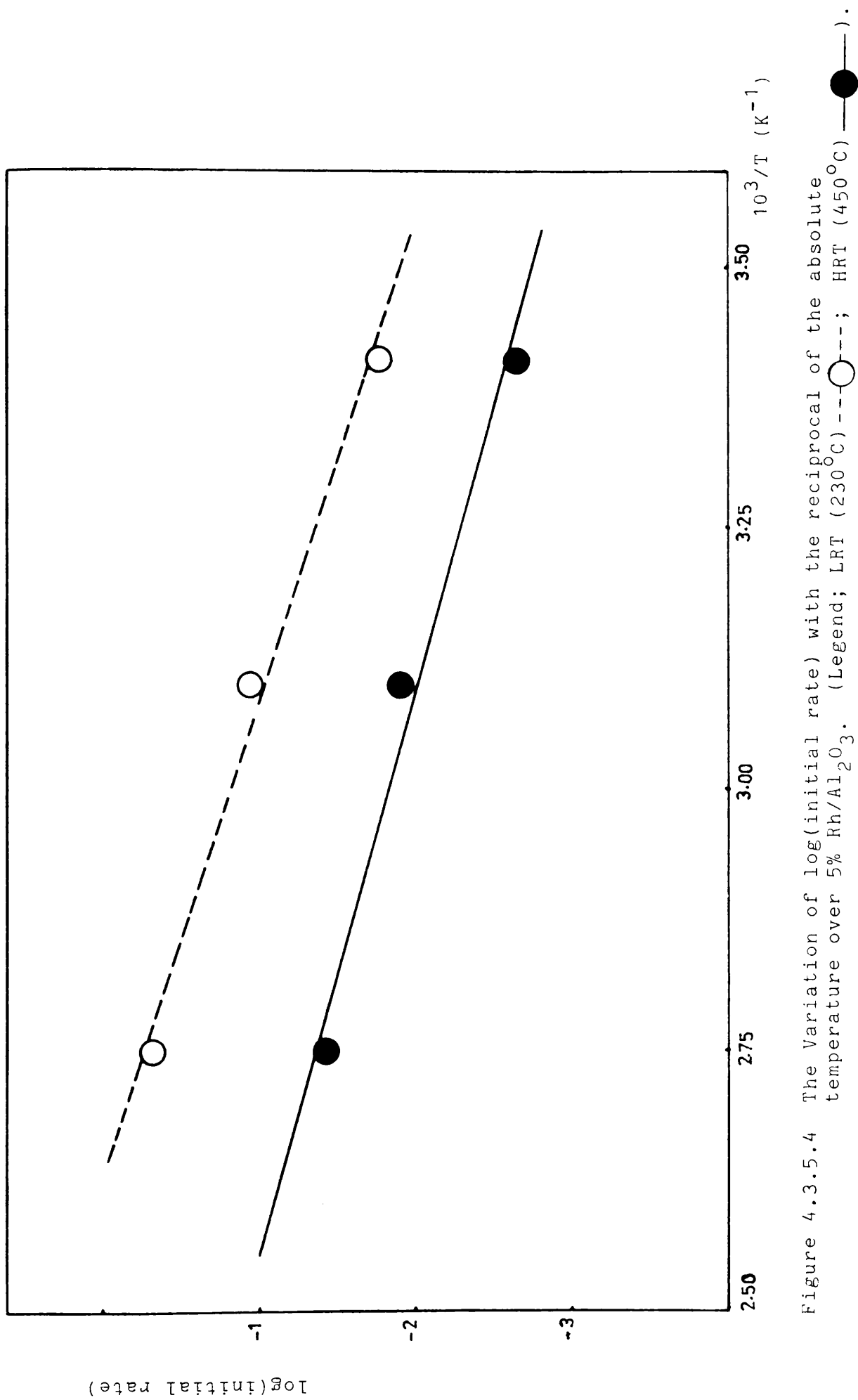


Figure 4.3.5.4 The Variation of  $\log(\text{initial rate})$  with the reciprocal of the absolute temperature over 5% Rh/Al<sub>2</sub>O<sub>3</sub>. (Legend; LRT (230°C) ---○---; HRT (450°C) —●—).

Table 4.3.5.1

The Variation of Butene Distribution and Selectivity with Conversion over 5% Rh/Al<sub>2</sub>O<sub>3</sub> reduced at LRT and at HRT at a reaction temperature of 20 ± 2°C; initial butadiene pressure 25 torr; initial hydrogen pressure 75 torr.

Reaction	Conversion (%)	Reduction Temperature (°C)	Butene Distribution			Selectivity
			1-B	t-2-B	c-2-B	
3	22.1	230	55.4	29.0	15.6	0.932
5	43.8	"	59.5	28.5	12.0	0.899
2	60.3	"	56.8	29.9	13.3	0.912
4	80.4	"	56.9	29.5	13.6	0.897
1	101.0	"	41.6	38.3	20.1	0.827
3	21.1	450	60.5	24.5	15.0	0.884
5	39.8	"	57.1	26.7	16.2	0.873
2	58.5	"	58.0	27.9	14.1	0.860
4	79.3	"	55.8	28.1	16.1	0.832
1	99.9	"	47.0	35.2	17.8	0.742

Table 4.3.5.3

The Variation of Butene Distribution and Initial Rate with  
Increasing Temperature over 5% Rh/Al<sub>2</sub>O<sub>3</sub>

Reaction	Temperature (°C)	Butene Distribution			Initial Rate (torr/min)
		1-B	<u>t</u> -2-B	<u>C</u> -2-B	
Catalyst Reduction Temperature = 230°C					
1	20	58.1	27.8	14.1	1.02
3	50	55.6	29.5	14.9	6.90
2	90	42.6	38.0	19.4	28.57
Catalyst Reduction Temperature = 450°C					
1	20	56.0	27.5	16.5	0.13
3	50	50.0	33.6	16.4	0.76
2	90	48.1	32.5	19.4	2.22

#### 4.3.6 The Reaction of Butadiene with Hydrogen over 5% Rh/TiO<sub>2</sub>

##### 4.3.6.1 The Pressure Fall against Time Curves for LRT and HRT Catalysts

(0.0178g) and (0.0199g) samples of catalyst were reduced respectively at low reduction temperature and at high reduction temperature. Figure 4.3.6.1 shows the pressure fall-time curves observed with each catalyst, from which it can be seen that the reaction occurred in two distinct stages. In each case the onset of the second stage was accompanied by an increase in rate. The acceleration point, denoted as  $-\Delta P_a$ , was obtained by extrapolating the first and the second stages of each reaction and finding the point of intersection. The acceleration occurred at a pressure fall of 29.0 torr and 34.0 torr respectively for the LRT and HRT catalyst.

##### 4.3.6.2 Deactivation Phenomena

A sample (0.0178g) of catalyst was reduced at 199°C. A series of hydrogenations were carried out consecutively at room temperature on the same catalyst sample. Between each reaction, the reaction vessel was evacuated for ten minutes to remove all the products of the previous hydrogenation. The variation of initial rate with reaction number is shown in figure 4.3.6.2.

##### 4.3.6.3 The Variation of Selectivity and Butene Distribution with Conversion at LRT and at HRT

Five successive hydrogenations, using a hydrogen:butadiene ratio of approximately 3 to 1 were carried out on two samples of catalyst. The results are shown in Table 4.3.6.1. From

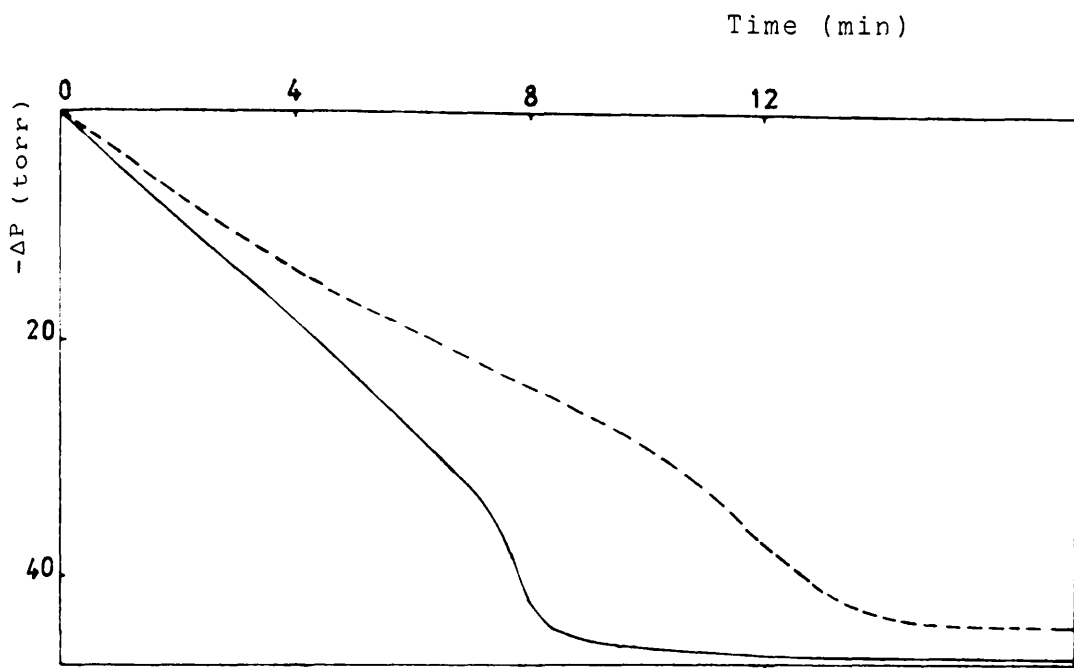


Figure 4.3.6.1 A typical pressure fall against time curve for the reaction of 25 torr of butadiene with 75 torr of hydrogen at  $20 \pm 2^\circ\text{C}$  over 5% Rh/TiO<sub>2</sub>. (Legend; LRT (199°C) ----- ; HRT (450°C) ——— ).

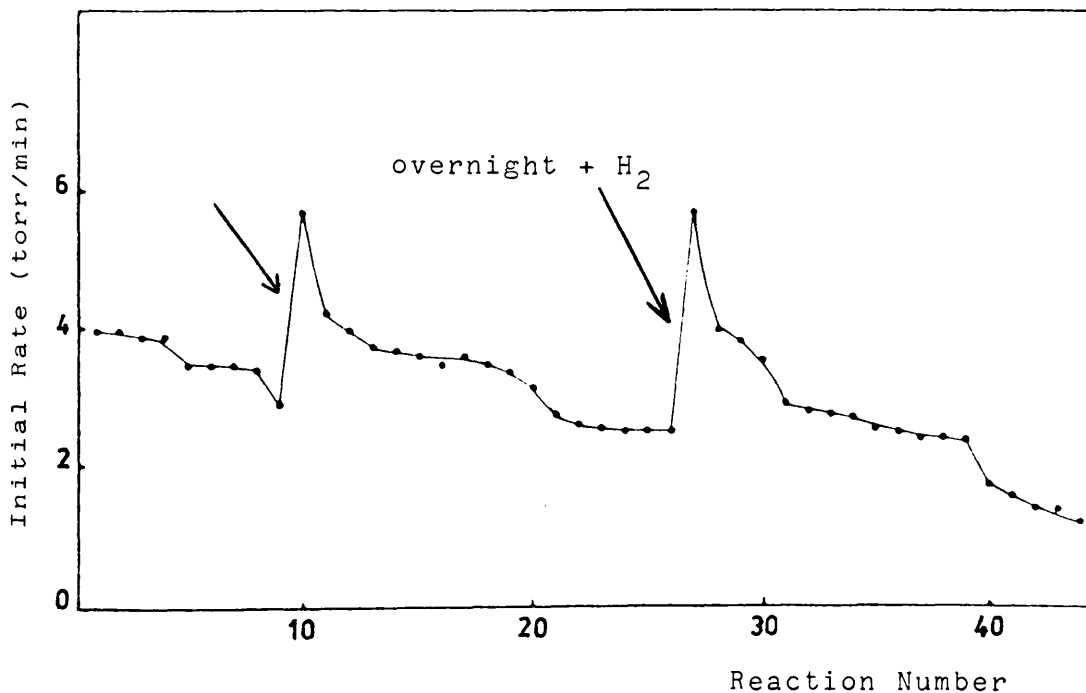


Figure 4.3.6.2 The Variation of Initial Rate with Reaction Number for the reaction of 25 torr of butadiene with 75 torr of hydrogen at  $20 \pm 2^\circ\text{C}$  over 5% Rh/TiO<sub>2</sub> reduced at low temperature (199°C).

these results, the selectivity and the initial distribution of butenes are obtained by extrapolation of figure 4.3.6.3 to zero conversion. The results are presented in Table 4.3.6.2.

Table 4.3.6.2

Catalyst Reduction Temperature ( $^{\circ}\text{C}$ )	Initial Butene Distribution (%)			Selectivity
	1-B	<u>t</u> -2-B	<u>c</u> -2-B	
199	52.5	32.5	15.0	0.865
450	54.5	29.5	16.0	0.890

4.3.6.4 Dependence of Butene Distribution upon Temperature and the Activation Energies for LRT and HRT Catalysts

A series of reactions were carried out in the range  $20^{\circ}$  to  $90^{\circ}\text{C}$  (LRT) and  $20^{\circ}$  to  $120^{\circ}\text{C}$  (HRT) respectively using a standard 1:3::butadiene:hydrogen mixture. Each reaction was allowed to proceed to a percentage conversion of  $40 \pm 5\%$  and then analysed. The results are shown in Table 4.3.6.3. The activation energies were determined from the log (initial rate) versus  $(1/T)$  plots (figure 4.3.6.4) and were found to be  $43.58 \text{ KJ mole}^{-1}$  and  $41.28 \text{ KJ mole}^{-1}$  respectively for catalyst samples reduced at low and high temperature.

Selectivity

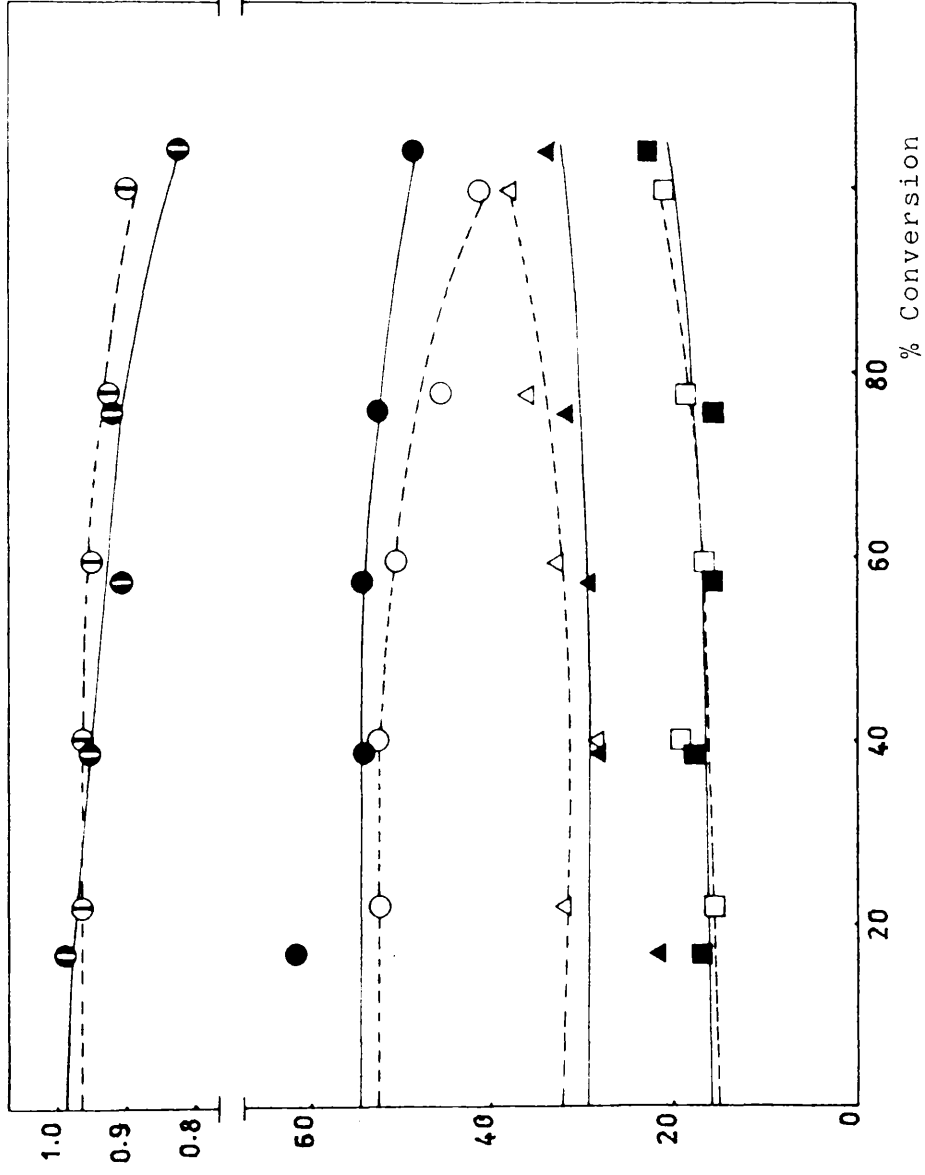


Figure 4.3.6.3 The Variation of Selectivity and Butene distribution with Conversion (%) at  $20 \pm 2^\circ\text{C}$  over 5% Rh/TiO<sub>2</sub>.

(Legend; LRT (199°C))

- Selectivity; 1-B;
- △ t-2-B;
- c-2-B;
- HRT (450°C)
- Selectivity; 1-B
- ▲ t-2-B;
- c-2-B).

Butene distribution

% Conversion

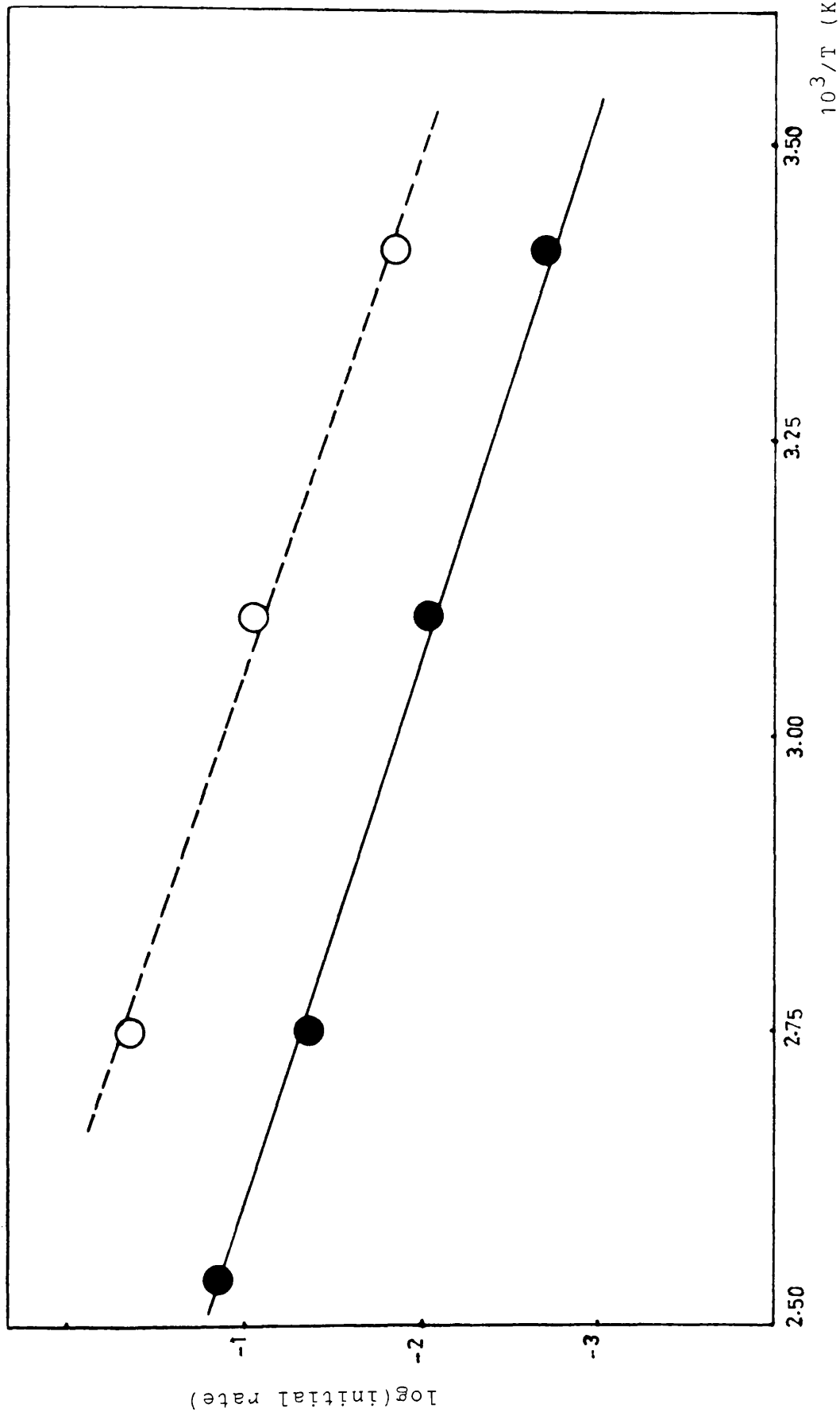


Figure 4.3.6.4 The Variation of  $\log(\text{initial rate})$  with the reciprocal of the absolute temperature over 5% Rh/TiO<sub>2</sub>. (Legend; LRT (199°C) ---○---; HRT (450°C) —●—).

Table 4.3.6.1

The Variation of Butene Distribution and Selectivity with Conversion over 5% Rh/TiO<sub>2</sub> reduced at LRT and at HRT at a reaction temperature of 20 ± 2°C; initial butadiene pressure 25 torr; initial hydrogen pressure 75 torr.

Reaction	Conversion (%)	Reduction Temperature (°C)	Butene Distribution			Selectivity
			1-B	t-2-B	c-2-B	
3	22.0	199	52.4	32.1	15.5	0.866
5	40.3	"	52.5	28.3	19.2	0.865
2	59.5	"	50.6	32.9	16.5	0.851
4	77.9	"	45.5	36.0	18.5	0.825
1	99.9	"	41.3	38.0	20.7	0.796
3	16.9	450	61.5	21.5	17.0	0.888
5	38.7	"	54.0	28.2	17.8	0.852
2	57.4	"	54.4	29.9	15.7	0.807
4	75.8	"	52.5	31.9	15.6	0.819
1	104.2	"	48.5	33.7	17.8	0.723

Table 4.3.6.3

The Variation of Butene Distribution and Initial Rate with  
Increasing Temperature over 5% Rh/TiO<sub>2</sub>

Reaction	Temperature (°C)	Butene Distribution			Initial Rate (torr/min)
		1-B	<u>t</u> -2-B	<u>c</u> -2-B	
Catalyst Reduction Temperature = 199°C					
1	20	50.3	30.4	19.3	0.85
3	50	46.3	32.6	21.1	5.40
2	90	27.3	46.6	26.1	25.43
Catalyst Reduction Temperature = 450°C					
1	20	52.7	29.7	17.6	1.71
3	50	52.6	29.9	17.5	10.00
2	90	52.1	31.0	16.9	43.48
4	120	48.8	33.5	17.7	50.00

#### 4.4 Electron Microscopic Examination of Catalysts

A rhodium metal catalyst supported on alumina was examined using a (JEOL 1200 Ex) Electron Microscope at 120 kV. This catalyst had been previously reduced in flowing hydrogen gas for 1 hour. Two catalyst samples reduced at different temperatures were examined. The micrographs of catalyst samples after carbon monoxide chemisorption are shown in Plates 4.4.1 and 4.4.2.

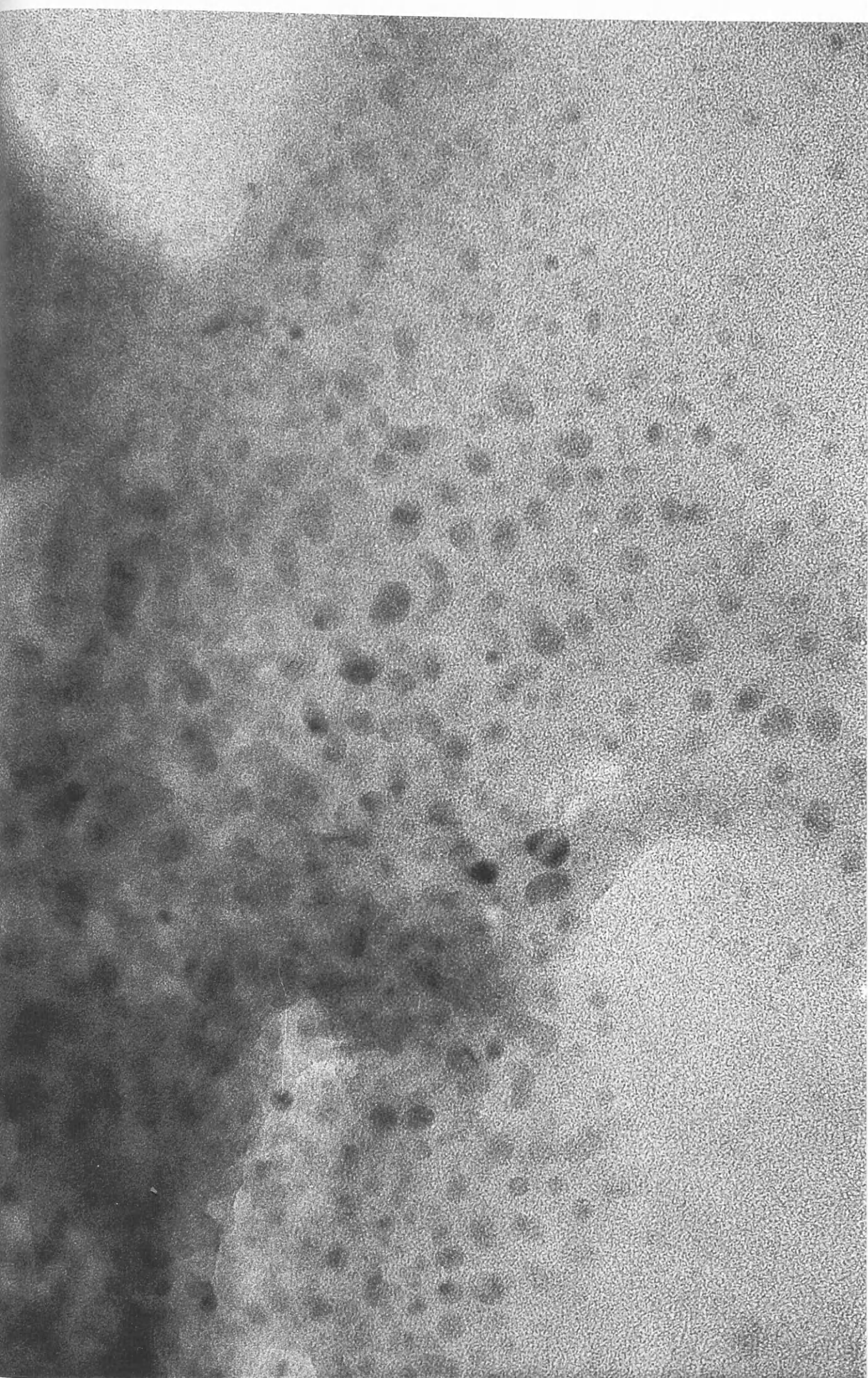
As seen on the micrograph of each catalyst sample, the metal particles can be observed and the average size of the metal particles, based on a particle count of 100, can be measured. The results are tabulated below.

Catalyst	Plate Number	Temperature Reduction (°C)	Average Size (Å)
Rh/Al <sub>2</sub> O <sub>3</sub>	4.4.1	200	10 - 20
Rh/Al <sub>2</sub> O <sub>3</sub>	4.4.2	450	20 - 40

Plate 4.4.1 Electron Micrograph of Rh supported on  $\text{Al}_2\text{O}_3$ ,  
which had been reduced at  $200^\circ\text{C}$ .  
(Magnification  $1.2 \times 10^6$ )



Plate 4.4.2 Electron Micrograph of Rh supported on  $\text{Al}_2\text{O}_3$ ,  
which had been reduced at  $450^\circ\text{C}$ .  
(Magnification  $1.2 \times 10^6$ )



## CHAPTER 5

## 5. Discussion

The results described in Chapter 4 will be discussed in detail in the ensuing sections of this Chapter.

### 5.1 Temperature Programmed Reduction Profiles

Temperature-programmed reduction was used to investigate the reducibility by hydrogen of the various catalysts.

Table 5.1 summarises the results reported in Chapter 4.

Table 5.1 Temperature Reduction Profiles for Various Supported Platinum and Rhodium Catalysts

(\* indicates major peaks)

Catalyst	Pt/SiO <sub>2</sub>	Pt/Al <sub>2</sub> O <sub>3</sub>	Pt/TiO <sub>2</sub>	Rh/SiO <sub>2</sub>	Rh/Al <sub>2</sub> O <sub>3</sub>	Rh/TiO <sub>2</sub>
Temp. max (°C)						
peak a	130	136	159*	204	135*	127
peak b	150	217*	209	227*		150*
peak c	202*	396	278	237*		178
peak d	384	500				
peak e	450					

The reduction profiles show that one of the supports used affects the absorption of hydrogen during TPR. However, Figures 4.1.1, 4.1.2 and 4.1.3 show that the consumption of hydrogen during TPR, the temperature-programmed reduction of

Pt on  $\text{TiO}_2$ , is less than for Pt on  $\text{Al}_2\text{O}_3$  or Pt on  $\text{SiO}_2$  catalysts. Also, Figures 4.1.4, 4.1.5 and 4.1.6 show that Rh on  $\text{Al}_2\text{O}_3$  or Rh on  $\text{SiO}_2$  absorb more hydrogen during TPR than the Rh on  $\text{TiO}_2$  catalyst.

TPR profiles for platinum supported on various supports show some common features, although there are also some notable differences. From Figures 4.1.1 and 4.1.2, it can be seen that both platinum on silica and platinum on alumina catalysts give similar values for the first reduction peaks, which are observed at  $T_{\text{max}} \text{ (a)} = 130^\circ\text{C}$  and  $T_{\text{max}} \text{ (a)} = 136^\circ\text{C}$  respectively. Also, a small peak ( $T_{\text{max}} \text{ (b)} = 150^\circ\text{C}$ ) is observed for platinum on silica (see Figure 4.1.1), following the first reduction peak.

It is important to note that the major reduction peak appears at different temperatures with platinum on the different supports. Thus, the major peak for platinum supported on titania appears in the profile as the first reduction peak at  $T_{\text{max}} \text{ (a)} = 159^\circ\text{C}$ , for platinum on alumina it appears as the second reduction peak at  $T_{\text{max}} \text{ (b)} = 217^\circ\text{C}$  and for platinum on silica catalyst it appears as the third reduction peak at  $T_{\text{max}} \text{ (c)} = 202^\circ\text{C}$ . Small peaks are also observed with platinum supported on titania catalyst, but following the major peak, indicating that a hydrogen consumption occurs at  $T_{\text{max}} \text{ (b)} = 209^\circ\text{C}$  and  $T_{\text{max}} \text{ (c)} = 278^\circ\text{C}$ . Higher temperature reduction peaks are observed with Pt on  $\text{SiO}_2$  at  $T_{\text{max}} \text{ (d)} = 384^\circ\text{C}$  and  $T_{\text{max}} \text{ (e)} = 450^\circ\text{C}$ , and with Pt on  $\text{Al}_2\text{O}_3$  at  $T_{\text{max}} \text{ (c)} = 396^\circ\text{C}$  and  $T_{\text{max}} \text{ (d)} = 500^\circ\text{C}$ . It

appears that the support plays an important role in determining the temperature at which the metal can be reduced.

The results presented in Table 5.1 concerning rhodium supported on various supports show that the temperatures corresponding to the peak maxima for each catalyst are close to each other and, in contrast to platinum, the highest temperature peak is below  $300^{\circ}\text{C}$ . Silica and alumina are known as the most important support for the metallic catalyst and give rise to a facile reduction of a Rh salt to Rh metal (46). It can be seen that the highest temperature TPR peaks for Rh on  $\text{Al}_2\text{O}_3$  and for Rh on  $\text{TiO}_2$  catalysts are below  $200^{\circ}\text{C}$ . Vis et al. (47) observed that the temperature for complete reduction of Rh salt to Rh metal is  $177^{\circ}\text{C}$  for Rh on  $\text{Al}_2\text{O}_3$  and Rh on  $\text{TiO}_2$  catalysts, in agreement with the results reported in Table 5.1. It was observed that the major peaks are better defined with platinum catalysts than with rhodium catalysts.

## 5.2 Determination of Metal Surface Area

The experimental results presented in the previous chapter clearly show that some interesting differences exist between platinum and rhodium supported on either silica, alumina or titania catalysts when used for the adsorption and desorption of carbon monoxide. The results presented in Tables 4.2.3 and 4.2.4 clearly show that carbon monoxide is adsorbed on all catalysts studied. A similar observation has

been reported by Bain et al. (24) for the interaction of carbon monoxide with Pt on  $\text{Al}_2\text{O}_3$  and Pt on  $\text{SiO}_2$  catalysts. They reported that both  $\text{Al}_2\text{O}_3$ - and  $\text{SiO}_2$ -supported Pt adsorb carbon monoxide.

For the high-temperature reduced catalysts ( $450^\circ\text{C}$ ), the number of molecules adsorbed differ widely from catalyst to catalyst compared with the low-temperature reduced catalysts ( $200^\circ\text{C}$ ). This decrease in the number of carbon monoxide molecules adsorbed is most clearly observed (see Tables 4.2.3 and 4.2.4) with Pt on  $\text{TiO}_2$ , Rh on  $\text{TiO}_2$  and Rh on  $\text{Al}_2\text{O}_3$  when these catalysts have been reduced at  $450^\circ\text{C}$ . However, it appears that both Pt on  $\text{SiO}_2$  and Rh on  $\text{SiO}_2$  catalysts show an increase of carbon monoxide molecules when the reduction temperature is increased from  $200^\circ\text{C}$  to  $450^\circ\text{C}$ . As silica is known to be an inert support, an interaction between metal and support would not be expected to exist in the region of high-temperature reduction used in the present work.

It is important to note that a method based on chemisorption of radioactive carbon monoxide has been used for surface metal area determinations. Table 5.2 summarises the results presented in Chapter 4 for the metal areas of all of the catalysts, reduced at low and high temperature.

Table 5.2 Metal Surface Areas of Various Supported Platinum and Rhodium Catalysts after Low- and High-Temperature Reduction

Catalyst	Pt/SiO <sub>2</sub>	Pt/Al <sub>2</sub> O <sub>3</sub>	Pt/TiO <sub>2</sub>	Rh/SiO <sub>2</sub>	Rh/Al <sub>2</sub> O <sub>3</sub>	Rh/TiO <sub>2</sub>
(a) Low-Temperature Reduction (200°C)						
metal area (m <sup>2</sup> g <sup>-1</sup> )	7.67	7.93	2.08	16.04	53.21	6.48
(b) High-Temperature Reduction (450°C)						
metal area (m <sup>2</sup> g <sup>-1</sup> )	9.85	6.30	0.87	22.89	25.71	3.91

The results show that, for the same support, the Rh surface areas are greater than the Pt surface areas, with both low-temperature (200°C) and high-temperature (450°C) reduced catalysts. They also show that the Pt surface area when the metal is supported on a transition-metal oxide (TiO<sub>2</sub>), is very much less than the Pt surface area when the platinum is supported on the non-transition-metal oxides (SiO<sub>2</sub> or Al<sub>2</sub>O<sub>3</sub>). With the Pt on TiO<sub>2</sub> catalyst, the Pt surface area obtained at low-temperature reduction (200°C) is 2.08 m<sup>2</sup>/g, whilst increasing temperature reduction to 450°C reduces the surface area to 0.87 m<sup>2</sup>/g. These effects may be due to the phenomenon of metal-metal interactions, in which the platinum atoms interact with the titanium ions of the support as suggested previously by Tauster et al. (25).

A similar effect is observed with rhodium catalysts. Table 5.2 shows that, Rh on  $\text{TiO}_2$  catalyst when reduced at  $200^\circ\text{C}$ , has a metal area of  $6.48 \text{ m}^2/\text{g}$ , whereas on increasing the temperature of reduction to  $450^\circ\text{C}$  the Rh surface area decreases to  $3.91 \text{ m}^2/\text{g}$ . A similar effect is observed in the results obtained with Rh on  $\text{Al}_2\text{O}_3$  catalyst which has a large surface Rh area of  $53.21 \text{ m}^2/\text{g}$  when reduced  $200^\circ\text{C}$ , but on increasing the reduction temperature to  $450^\circ\text{C}$ , the Rh surface area decreases to  $25.71 \text{ m}^2/\text{g}$ .

The changes in the metal surface area following the high temperature ( $450^\circ\text{C}$ ) reduction may be due to one or more of the following:-

- (i) incomplete reduction at the lower temperature ( $200^\circ\text{C}$ );
- (ii) sintering of the metal particles at the higher temperature and
- (iii) the existence of support effects.

(i) Would lead to an increase in area, (ii) to a decrease in metal area, and (iii) may lead to either an increase or a decrease depending on the nature of the effect.

Considering first the state of reduction of the catalysts, the temperature-programmed reduction results discussed in the previous section clearly show that, with both rhodium on alumina and rhodium on titania catalysts, reduction is complete at temperatures below  $200^\circ\text{C}$ . In consequence, no change in metal surface area would be expected with these catalysts when the pretreatment temperature is increased to  $450^\circ\text{C}$ . On the other hand, with

rhodium on silica and with platinum supported on either silica or alumina, further reduction does occur at temperatures above 200°C, and it might, therefore, be reasonable to expect an increase in the carbon monoxide adsorptive capacity. This is indeed the case with both rhodium and platinum when supported on silica, both of which show a significant increase in surface area after the high-temperature reduction. However, platinum on alumina shows a slight decrease in area as the reduction temperature is increased.

The second possibility is sintering of the metal particles, which may cause a loss of dispersion of the metal crystallites in a supported metal catalyst. Electron microscopy studies were used to examine the high area rhodium on alumina catalysts reduced at 200°C and at 450°C. The micrographs (plates 4.4.1 and 4.4.2) show clear variations in the average Rh particle sizes from 10 - 20Å at 200°C to 20 - 40Å at 450°C. This is consistent with the high metal area of this catalyst and with the observed decrease with increasing reduction temperature.

The third possibility which has to be considered is the occurrence of metal-support effects. The results obtained for Pt on SiO<sub>2</sub> catalyst, which are presented in Table 5.2, show that the Pt surface area increases from 7.67 m<sup>2</sup>/g to 9.85 m<sup>2</sup>/g when the reduction temperature is increased from 200°C to 450°C. Similarly with Rh on SiO<sub>2</sub>, the Rh surface area increases from 16.04 m<sup>2</sup>/g to 22.89 m<sup>2</sup>/g. It is known

that  $\text{SiO}_2$  is an inert support. Therefore, the increase in the Pt or Rh surface areas may be due to the incomplete, low-temperature, reduction as discussed above. It might be expected that silica has no effective interaction with the platinum or rhodium metal.

For Pt on  $\text{Al}_2\text{O}_3$ , a small decrease in the Pt surface area is observed from  $7.93 \text{ m}^2/\text{g}$  to  $6.30 \text{ m}^2/\text{g}$ . This may be due to a very weak interaction between the platinum and the alumina.

Incompletion of the low-temperature reduction can be disregarded as far as any effects with the alumina-supported catalysts are concerned. For the Pt on  $\text{TiO}_2$  catalyst (see Table 5.2), the Pt surface area after reduction at  $450^\circ\text{C}$  decreases to less than half its value when the catalyst is reduced at  $200^\circ\text{C}$ . This may be due to the interaction between Pt and  $\text{TiO}_2$  as was suggested by the Exxon Group (25). With Rh on  $\text{Al}_2\text{O}_3$ , the results for which are presented in Table 5.2, the Rh surface area after reduction at  $450^\circ\text{C}$  decreases to approximately half its initial value, whilst the Rh on  $\text{TiO}_2$  catalyst, a marked decrease of the Rh surface area is also observed. TPR profiles indicate that both Rh on  $\text{Al}_2\text{O}_3$  and Rh on  $\text{TiO}_2$  catalysts are reduced at low temperature. Therefore, these effects are indicative of the presence of a metal-support interaction, although its nature cannot be established from the present results.

### 5.3 Effects of the Support on the Behaviour of the Metal Catalysts in the Hydrogenation of Buta-1:3-diene

In this section the term 'butadiene' will be used to refer to buta-1:3-diene. The six catalysts used in this study were Pt/SiO<sub>2</sub>, Pt/Al<sub>2</sub>O<sub>3</sub>, Pt/TiO<sub>2</sub>, Rh/SiO<sub>2</sub>, Rh/Al<sub>2</sub>O<sub>3</sub> and Rh/TiO<sub>2</sub>. Each catalyst was reduced before use at either 200°C (LRT) or 450°C (HRT).

The reactions of butadiene with hydrogen were carried out using a reactant ratio of hydrogen:butadiene of 3:1. From (Figure 4.3.1.1 to Figure 4.3.6.1) the pressure fall against time curves it can be seen that the reaction proceeded in two distinct stages. The analysis of the reaction products showed that this type of pressure-time curve arose as a result of the high selectivity for butene formation shown by each catalyst. The pressure fall against time curves showed a close resemblance to the so-called type (C) curves obtained for the metal-catalysed hydrogenation of acetylene (31).

From Figures 4.3.2.1 and 4.3.5.1 it can be seen that with both platinum and rhodium, when supported on alumina, the initial reaction rates were greater when the catalyst was reduced at low temperature than when reduced at high temperature. However, with both silica- and titania-supported platinum and rhodium the converse is true. Furthermore, both rhodium-titania and platinum-titania, when reduced at high temperature (450°C) showed a sharper acceleration point than the other catalysts reduced at a similar temperature. These observations, together with those summarised in Table 5.2

indicate that there is no direct correlation between the initial activity and the metal area, as determined by carbon monoxide chemisorption, at least with the silica- and titania-supported metals.

When successive butadiene hydrogenations were performed on the same catalyst sample, the pressure fall against time curves show that, both first and second stages of the hydrogenation reaction underwent deactivation with catalyst use. Figures 4.3.1.2, 4.3.2.2. and 4.3.3.2 show the initial rates for butadiene hydrogenation upon reaction numbers observed during two periods of use. Figures 4.3.4.2, 4.3.5.2 and 4.3.6.2 were observed during three periods of use. Between each period, each catalyst was left in hydrogen for 14 hours as indicated by an arrow on these diagrams.

With all of the catalysts a progressive deactivation was observed from reaction to reaction and with each catalyst, except platinum on alumina, storage in hydrogen at the reaction temperature for 14 hours resulted in a partial restoration of activity over a short period of usage, although the activity-reaction number curves rapidly reverted to their original shape in spite of this slight reactivation, until eventually a steady state activity was attained. Similar observations have been made with a variety of supported metal catalysts when used for the hydrogenation of acetylene (48) and propa-1:2-diene (45), where it was shown that the activation corresponded to a progressive build-up of hydrocarbonaceous residues on the catalyst surface. With platinum

on alumina no reactivation was observed when the catalysts were stored under hydrogen.

It is of particular interest to note that with each platinum catalyst the initial rate of reaction progressively decreased (Figures 4.3.1.2, 4.3.2.2 and 4.3.3.2), whereas with each rhodium catalyst (Figures 4.3.4.2, 4.3.5.2 and 4.3.6.2) the initial activity increased with catalyst usage to a maximum value, before following the expected deactivation curve. This is particularly the case with the Rh on  $\text{TiO}_2$  catalyst (see Figure 4.3.6.2) where the initial rates at the commencement of the second and the third periods are significantly higher than the initial rate of the reaction immediately after reduction.

There is a distinct difference between platinum and rhodium catalysts in the rate of deactivation. Figures 4.3.4.2, 4.3.5.2 and 4.3.6.2 show that, the initial rates observed with rhodium decrease slowly when compared with the initial rates of the reactions over platinum catalysts (see Figures 4.3.1.2, 4.3.2.2. and 4.3.3.2). This is consistent with the general observation that, in hydrogenation reactions, rhodium metal is more active than platinum metal. In general, it is agreed that platinum and rhodium catalysts are selective for butene formation (31). The initial butene distributions and selectivities obtained by extrapolation of figures 4.3.1.3, 4.3.2.3, 4.3.3.3, 4.3.4.3, 4.3.5.3 and 4.3.6.3, which were tabulated in Chapter 4, are summarised in Table 5.3.

Table 5.3 Initial Butene Distributions and Selectivity  
Observed in Butadiene Hydrogenation over Various  
Supported Platinum and Rhodium Catalysts

Catalyst	Temperature Reduction (°C)	Initial Butene Distribution (%)			Selectivity
		1-B	<u>t</u> -2-B	<u>c</u> -2-B	
5% Pt/SiO <sub>2</sub>	220	71.0	19.7	9.3	0.720
	450	73.8	17.6	8.6	0.751
5% Pt/Al <sub>2</sub> O <sub>3</sub>	230	73.0	18.4	8.6	0.710
	449	70.0	19.5	10.5	0.746
5% Pt/TiO <sub>2</sub>	200	77.3	12.6	10.1	0.698
	450	75.0	14.0	11.0	0.667
5% Rh/SiO <sub>2</sub>	250	58.4	25.7	15.9	0.920
	450	56.5	27.6	15.9	0.905
5% Rh/Al <sub>2</sub> O <sub>3</sub>	230	57.5	29.0	13.5	0.932
	450	60.0	25.1	14.9	0.893
5% Rh/TiO <sub>2</sub>	199	52.5	32.5	15.0	0.865
	450	54.5	29.5	16.0	0.890

From these results it can be seen that over both the platinum and rhodium catalysts all three isomeric n-butenes, as well as n-butane, were formed as initial products. However, both the butene distribution and the selectivity appear to be independent of the catalyst reduction temperature for all the catalysts. The only variation, which is apparent, is the difference between platinum and rhodium. This suggests that, with regard to the nature of the reaction products formed, any

SMSI effects which may be present, particularly with the titania-supported catalysts, are of no significance.

The results presented in Figure 4.3.1.3 - Figure 4.3.6.3 also show that the butene distributions are almost independent of the extent of hydrogenation until most of the butadiene has reacted but are quite different from the expected equilibrium distributions. This is in agreement with previous results reported for rhodium and platinum catalysts (34). From Tables 4.3.1.3, 4.3.2.3, 4.3.3.3, 4.3.4.3, 4.3.5.3 and 4.3.6.3 it can be seen that the butene distributions are dependent on the reaction temperature. It can be clearly seen that over all six catalyst studies above 50°C, the yield of but-1-ene progressively decreases, whilst the yield of trans-but-2-ene correspondingly increases.

From Table 5.3, it is observed that the selectivities for butene formation are high over all catalysts studied. The selectivity values observed in the first stage of the reaction over platinum supported on either silica, alumina or titania are less than those observed with rhodium supported on the same support materials. The observations regarding the variation of selectivity with conversion over each catalyst, presented in Figures 4.3.1.3 - 4.3.6.3, show that the selectivities are initially independent of conversions. However, as the first stage of the reaction progresses, the selectivities become conversion dependent. From these figures, the shapes of selectivity-conversion plots are very similar when each catalyst was reduced at the two different temperatures. As a result, the selectivity values presented

in Table 5.3 show that, over each catalyst, the reduction temperature does not affect either the selectivity of the butene formation, as noted above, or the variation of selectivity as the reaction proceeds. Over all the catalyst studies, the activations energies for butadiene hydrogenation reactions were determined experimentally from the initial rate measurements. The values are summarised on Table 5.4.

Table 5.4 Activation Energies for Butadiene Hydrogenation over Various Supported Platinum and Rhodium Catalysts after Low- and High-Temperature Reductions

Catalyst	Temperature Reduction (°C)	Activation Energy (KJ mol <sup>-1</sup> )	Temperature range (°C)
5% Pt/SiO <sub>2</sub>	220	58.61	0 - 90
	450	57.84	20 - 120
5% Pt/Al <sub>2</sub> O <sub>3</sub>	230	49.19	0 - 90
	449	50.49	20 - 120
5% Pt/TiO <sub>2</sub>	200	42.33	20 - 90
	450	59.57	20 - 120
5% Rh/SiO <sub>2</sub>	250	51.07	20 - 90
	450	50.11	0 - 50
5% Rh/Al <sub>2</sub> O <sub>3</sub>	230	42.22	20 - 90
	450	37.39	20 - 90
5% Rh/TiO <sub>2</sub>	199	43.58	20 - 90
	450	41.28	20 - 120

These results show that, although there is quite a marked variation from support to support, the catalyst reduction temperature had little or no effect on the value of the activation energy for any particular catalyst, with the exception of platinum on titania, which showed a significantly higher value when reduced at the higher temperature. This may be due either to the occurrence of sintering or to the incompleteness of the low-temperature reduction. The former has been reviewed by Hughes (49) who has suggested that sintering may produce a high value of activation energy. The extent of the low-temperature reduction has already been discussed in Section 5.2.

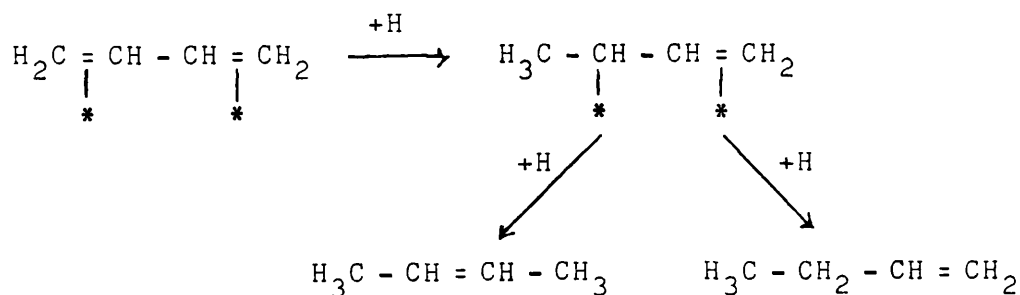
The experimental determinations of the activation energies for butadiene hydrogenation (see Figures 4.3.1.4 - 4.3.6.4) over rhodium supported on either silica or alumina were more difficult than over the other catalysts. This was due to the higher inherent activities of these two catalysts, which resulted in the reaction becoming diffusion-controlled at relatively low reaction temperatures. In consequence, as can be seen from Table 5.4, the temperature range over which the activation energies could be determined was more limited than with the other catalysts.

In general, the activation energies for the supported platinum catalyst were slightly higher than those observed with the corresponding supported rhodium catalysts.

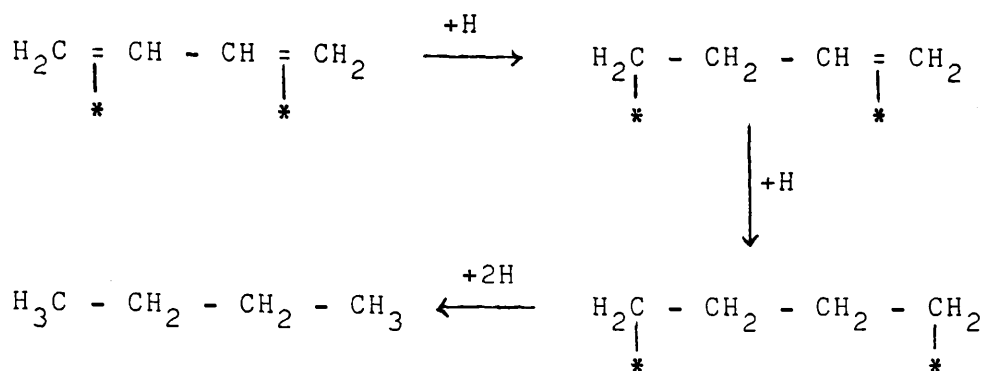
Detailed examination of the variation of the butene distributions with conversion shows that, with the exception of rhodium on titania, there is no apparent effect of the

temperature of hydrogen reduction pretreatment on the butene distribution or selectivity. The only effect of changing the support on the butene distribution is in determining the conversion at which the second stage of the reaction, involving the further isomerisation of the n-butenes and a decrease in olefin selectivity, becomes important. Thus, with titania-supported platinum and rhodium this occurs at ca. 60% reaction, with rhodium on silica and alumina at ca. 80% reaction and with alumina- and silica-supported platinum at ca. 100% conversion.

These results are consistent with the mechanism proposed previously (34) in which each n-butene is formed directly from adsorbed butadiene, the but-1-ene resulting from 1:2-addition of hydrogen; the but-2-enes by direct 1:4-addition:-



Since the selectivity is less than unity, that is n-butane is produced as an initial product, and there is no evidence of butene isomerisation during the initial stages of the reaction, it appears likely that the n-butane is formed from adsorbed butadiene via a route not involving adsorbed butene as an intermediate. Such a route may be one involving an 1:4-adsorbed intermediate:-



A similar conclusion has been reached for the formation of ethane in the initial stages of acetylene hydrogenation (48).

#### 5.4 General Conclusions

The results of the studies presented in this thesis show that, with titania-supported platinum and rhodium, to a lesser extent, alumina-supported platinum and rhodium catalysts, a metal-support interaction may be induced by high-temperature reduction of these catalysts in hydrogen. Whilst this interaction has an effect on the extent of chemisorption of carbon monoxide, it appears to have no effect upon the activity, selectivity or butene distribution observed in the hydrogenation of butadiene. The only effects which are apparent are small changes from support to support, which are consistent with changes in the extent of dispersion of each metal on the different supports. It may, therefore, be concluded that SMSI effects are of no real significance in catalytic hydrogenation reactions.

REFERENCES

1. G.C. Bond and R. Burch (Specialist Periodical Report) the Royal Society of Chemistry, London, 1983, 27 - 60.
2. S.J. Thomson and G. Webb, Heterogeneous Catalysis. (Oliver and Boyd), 1 - 18.
3. J.H. Sinfelt, Catal. Rev., 1969, 3, 180.
4. D. Briggs, J. Dewing, A.G. Burden, R.B. Moyes and P.B. Wells, J. Catal., 1980, 65, 31.
5. F. Solymosi, Catal. Rev., 1967, 1, 233.
6. G.M. Schwab, Adv. Catal., 1978, 27, 3.
7. S.D. Worley, C.A. Rice, G.A. Mattson, C.W. Curtis, J.A. Guin and A.R. Tarrer, J. Phys. Chem., 1982, 86, 2714.
8. J.R. Katzer, G.C.A. Schuit and J.H.C. Van Hooff, J. Catal., 1979, 59, 278.
9. M.J. Yacaman, S. Fuentes and J.M. Dominguez, Surf. Sci., 1981, 106, 472.
10. F. Solymosi, A. Erdöhelyi and T. Bansagi, J. Catal., 1981, 68, 371.
11. F. Solymosi, L. Völgyesi and T. Bansagi, J. Chem. Soc. Faraday Trans. 1, 1981, 77, 2645.
12. P.C. Flynn, S.E. Wanke and P.S. Turner, J. Catal., 1974, 33, 233.
13. R.T.K. Baker, E.B. Prestridge and R.L. Garten, J. Catal., 1979, 59, 293.
14. G.J. Den Otter and F.M. Dautzenberg, J. Catal., 1978, 53, 116.

15. B.H. Isaacs and E.E. Peterson, J. Catal., 1982, 77, 43.
16. S.D. Robertson, B.D. McNicol, J.H. De Bass and S.C. Kloet, J. Catal., 1975, 37, 424.
17. R.R. Ford, Adv. Catal., 1970, 21, 103.
18. A.C. Yang and C.W. Garland, J. Phys. Chem., 1957, 61, 1504.
19. N. Sheppard and T.T. Nguyen, Advances in Infrared and Raman Spectroscopy, 1978, 5, 67.
20. S.J. Thomson and G. Webb, Heterogenous Catalysis, (Oliver and Boyd), 44.
21. R.P. Eischens and W.A. Pliskin, Adv. Catal., 1958, 10, 233.
22. G. Blyholder, J. Phys. Chem., 1975, 79, 756.
23. D.J.C. Yates and J.H. Sinfelt, J. Catal., 1967, 8, 348.
24. F.T. Bain, S.D. Jackson, S.J. Thomson, G. Webb and E. Willocks, J. Chem. Soc. Faraday Trans. I, 1976, 72, 2516.
25. S.J. Tauster, S.C. Fung and R.L. Garten, J. Am. Chem. Soc., 1978, 100, 170.
26. S.J. Tauster and S.C. Fung, J. Catal., 1978, 55, 29.
27. J.G. Dickson, L. Kats and R. Ward, J. Am. Chem. Soc., 1961, 83, 3026.
28. J.A. Horsley, J. Am. Chem. Soc., 1979, 101, 2870.
29. C. Ocal and S. Ferrer, J. Chem. Phys., 1986, 84, 6474.
30. F.J. Schepers, J.G. Van Senden, E.H. Van Broekhoven and V. Ponec, J. Catal., 1985, 94, 400.
31. G. Webb in Comprehensive Chem. Kinetics, 1978, Vol. 20.

32. J.J. Phillipson, P.B. Wells and G.R. Wilson, J. Chem. Soc. A, 1969, 1351.
33. A.J. Bates, Z.K. Leszczynski, J.J. Phillipson, P.B. Wells and G.R. Wilson, J. Chem. Soc. A, 1970, 2435.
34. G.C. Bond, G. Webb, P.B. Wells and J.M. Winterbottom, J. Chem. Soc., 1965, 3218.
35. S.J. Thomson and G. Webb, Heterogeneous Catalysis, (Oliver and Boyd), 131 - 144.
36. N.R. Avery, J. Catal., 1970, 19, 15.
37. G.C. Bond and P.B. Wells, Adv. Catal., 1964, 15, 91.
38. G. Webb, Thesis, Univ. of Hull, Hull, England, 1963.
39. W.G. Young, R.L. Meier, J. Vinograd, H. Bollinger, L. Kaplan and S.L. Linden, J. Am. Chem. Soc., 1947, 69, 2046.
40. A. Rieche, A. Grimm and H. Albecht, Brennstoff Chem., 1961, 42, 5.
41. E.F. Meyer and R.L. Burwell, J. Am. Chem. Soc., 1963, 85, 2881.
42. P.B. Wells and A.J. Bates, J. Chem. Soc. A.1968, 3064.
43. J. Grant, R.B. Moyes, R.G. Oliver and P.B. Wells, J. Catal., 1976, 42, 213.
44. R.B. Bernstein and T.I. Taylor, Science (1947), 106, 498.
45. N.C. Kuhnen, S.J. Thomson and G. Webb, J. Chem. Soc., Faraday Trans. 1, 1983, 79, 2195.
46. S.D. Worley, C.A. Rice, G.A. Mattson, C.W. Curtis, J.A. Guin and A.R. Tarrer, J. Phys. Chem. 1982, 86, 2714 - 2717.

47. J.C. Vis, H.F.J. Van't Blik, T. Huizinga, J. Van Grondelle and R. Prins, *J. Catal.*, 1985, 95, 333 - 345.
48. Asad S. Al-Ammar and Geoffrey Webb, *J. Chem. Soc.*, *Faraday Trans. I*, 1979, 75, 1900.
49. R. Hughes, *Deactivation of Catalysts*, 1984, pp.22.

